MD-17-SHA/UM/3-20

MARYLAND DEPARTMENT
OF TRANSPORTATION
STATE HIGHWAY
ADMINISTRATION

Larry Hogan
Governor
Boyd K. Rutherford
Lt. Governor
Pete K. Rahn
Secretary
Gregory Slater
Administrator

MARYLAND DEPARTMENT OF TRANPORTATION
STATE HIGHWAY ADMINISTRATION

RESEARCH REPORT

STANDARDIZING LIGHTWEIGHT DEFLECTOMETER MODULUS MEASUREMENTS FOR COMPACTION QUALITY ASSURANCE

**Dr. Charles W. Schwartz, Zahra Afsharikia,
Dr. Sadaf Khosravifar**

**UNIVERSITY OF MARYLAND
COLLEGE PARK**

APPENDICES

SEPTEMBER 2017

The contents of this report reflect the views of the author who is responsible for the facts and the accuracy of the data presented herein. The contents do not necessarily reflect the official views or policies of the Maryland Department of Transportation. This report does not constitute a standard, specification, or regulation.

Table of Contents

APPENDIX 1. OTHER DOTS' FINDINGS **1**
- 1.1. MINNESOTA DOT 1
- 1.2. INDIANA DOT 3
- 1.3. FLORIDA DOT 4
- 1.4. NEBRASKA DEPARTMENT OF ROADS 5
- 1.5. EUROPEAN UNION 6
- 1.6. UNITED KINGDOM 7
- 1.7. NCHRP 10-84 STUDY 8

APPENDIX 2. EQUIPMENT MODELING **10**
- 2.1. FORCE VERSUS HEIGHT ASSUMPTIONS FOR ZORN LWD 10
- 2.2. LWD TESTING ON FOUR-PINT STEEL BEAM 11
  - *2.2.1. Frequency domain analysis* *18*
  - *2.2.2. Conclusion* *23*

APPENDIX 3. RESILIENT MODULUS TESTING **24**
- 3.1. TEST PITS MATERIAL CHARACTERISTICS 24
- 3.2. SOIL WATER CHARACTERISTIC CURVE (SWCC) 27
- 3.3. RESILIENT MODULUS SAMPLE PREPARATION AND TESTING 29
- 3.4. EVALUATED UNSATURATED RESILIENT MODULUS CONSTITUTIVE MODELS 38
- 3.5. COMPARISON OF EVALUATED M_R PREDICTIVE MODELS 41

APPENDIX 4. FIELD VALIDATION TESTING **48**
- 4.1. PROJECTS LOCATIONS AND DETAILS 51
  - *4.1.1. Virginia* *51*
  - *4.1.2. Maryland* *52*
  - *4.1.3. New York* *56*
  - *4.1.4. Missouri* *57*
  - *4.1.5. Indiana* *59*
  - *4.1.6. Florida* *61*
- 4.2. SUMMARY OF LWD FIELD MODULI, MEASURED WATER CONTENT, AND NDG RESULTS 63
- 4.3. DEVELOPING CORRELATION BETWEEN MODULI AT FIRST AND SECOND HALF-HEIGHTS DROPS 68
- 4.4. REGRESSION ANALYSIS 75

List of Tables

Table 1-1. LWD Target Values for Granular Material (Siekmeier et al. 2009) 1
Table 1-2. LWD Target Values for Fine Grained Soil (Siekmeier et al. 2009)................................ 2
Table 1-3. Maximum LWD deflection for Florida stablized subgrade 5
Table 1-4. Maximum LWD deflection for Florida limerock base.. 5
Table 1-5. NDOR max allowable LWD deflection values for different NGI 6
Table 1-6. UK specification. Target pavement foundation surface modulus 8
Table 2-1. True static stiffness of the 4-point beam as measured by Instron 13
Table 2-2. Peak stiffness (k_p) from Olson LWD testing on 4 point beam. 15
Table 2-3. Peak stiffness (k_p) from Zorn LWD testing on 4 point beam....................................... 16
Table 2-4. Peak stiffness (k_p) from Dynatest LWD testing on 4 point beam. 17
Table 3-1. Material description.. 24
Table 3-2. OMC, MDD and Specific gravity of the test material.. 25
Table 3-3. Testing plan for M_R testing according to AASHTO T-307.. 32
Table 3-4. The mold dimensions, number of layers and drops per layer for Proctor molds and M_R molds for standard and modified compaction energy.. 33
Table 3-5. Testing sequence for subgrade soils 34
Table 3-6. Testing sequence for base soils 35
Table 3-7. ALF M_R test results 36
Table 3-8. HPC M_R test results.. 37
Table 3-9. VA21a M_R test results 37
Table 3-10- Soil Type and Description (From Andrei, 2003) 38
Table 3-11. Overall RMSE of the evaluated models for each soil. 44
Table 3-12. Overall relative bias of the evaluated Models for each soil. 45
Table 4-1. LWD field evaluation testing date.. 48
Table 4-2. Quantities of field tests performed at each site with different devices........................ 49
Table 4-3. Material characteristics for evaluated field soils 50
Table 4-4. Summary of field water content measured by NDG 63
Table 4-5. Summary of field water content obtained by oven drying method 64
Table 4-6. Summary of Percent Compaction values measured by NDG in the field 65
Table 4-7. Summary of Olson LWD moduli on the field sites... 66
Table 4-8. Summary of Zorn LWD moduli on the field sites.. 67
Table 4-9. Summary of Dynatest LWD moduli on the field sites 68
Table 4-10. Regression coefficients and statistics for MD 5 subgrade.. 75
Table 4-11. Regression coefficients and statistics for NY embankment soil 76
Table 4-12. Regression coefficients and statistics for MD 337 GAB.. 76
Table 4-13. Regression coefficients and statistics for MD 404 GAB.. 77
Table 4-14. Regression coefficients and statistics for FL base material...................................... 78

List of Figures

Figure 1-1. Comparison between LWD on gyratory mold target values, MNDOT target modulus, and in-situ LWD values (from White et. al, 2009) 3
Figure 2-1. Similified schematic of LWD- soil motion as a one DOF mass-spring system 10
Figure 2-2. Schematic of the BVT 11
Figure 2-3. Dynatest LWD test performed on BVT 12
Figure 2-4. k_p as a function of beam span for the all the evaluated devices. 13
Figure 2-5. Measurement of BVT static stiffness (k_s) with the Instron machine. 14
Figure 2-6. SDOF analog for the BVT: (a) four-point beam testing configuration; (b) corresponding SDOF analog (after Hoffmann, 2004). 19
Figure 2-7. Spectral analysis on Dyantest LWD 21
Figure 2-8. Spectral analysis on Olson LWD 22
Figure 2-9. k_s from spectral analysis versus k_p of conventional peak method 23
Figure 3-1. Gradation of the materials used in this study 24
Figure 3-2. Moisture-Density relationships for (A) VA21a, (B) ALF, and (C) HPC 26
Figure 3-3. Schematic of the 3 zones of SWCC (Fredlund and Xing, 1994) 27
Figure 3-4. SWCC for the material used in this study 29
Figure 3-5. Resilient Modulus Terms: contact stress, cyclic axial stress (σ_{cyclic}), and maximum resilient vertical stress (σ_{max}) (AASHTO T-307) 30
Figure 3-6. Stress-strain relationship in M_R test 31
Figure 3-7. UTM- 100 apparatus and sample 31
Figure 3-8. The bounds of pore suction for Lytton (1995). 41
Figure 3-9. RMSE of evaluated models at different moisture and compaction energy condition for (a) Plastic, and (b) Non-plastic soils. 42
Figure 3-10. Average RE of evaluated models at different moisture and compaction energy condition for (a) Plastic, and (b) Nonplastic soils 43
Figure 3-11. $M_{R\text{-predicted}}$ VS. $M_{R\text{-measured}}$ - Model M2 for Soil PVSG. 44
Figure 3-12. (a) RMSE and (b) RE at different moisture and compaction energy conditions for Model 8. 45
Figure 3-13. $M_{R\text{-predicted}}$ from model M8 VS. $M_{R\text{-measured}}$ for GMAB and PVSG soils 46
Figure 4-1. Aerial view of the virgina Tola road evaluation site and test locations 51
Figure 4-2. Gradation Curve of Virginia site geomaterials 52
Figure 4-3. Gradation Curve of MD5 site geomaterials 52
Figure 4-4. Aerial view of the MD5 field evaluation site 53
Figure 4-5. Aerial view of the MD337 field evaluation site 54
Figure 4-6. Gradation Curve of MD337 site geomaterials 54
Figure 4-7. Aerial view of the MD404 field evaluation site 55
Figure 4-8. Gradation Curve of MD404 site geomaterials 56
Figure 4-9. Gradation Curve of New York site geomaterials 56
Figure 4-10. Aerial view of the New York Luther Forest Boulevard evaluation site 57
Figure 4-11. Aerial view of the Missouri I-64 evaluation site 58
Figure 4-12. Gradation Curve of Missouri site geomaterials 59
Figure 4-13. Aerial view of the Indiana Graham road evaluation site 60
Figure 4-14. Gradation Curve of Indiana site geomaterials 61
Figure 4-15. Gradation Curve of Florida site geomaterials 61

Figure 4-16. Aerial view of the Florida SR23 field evaluation site 62
Figure 4-17. Comparison of moduli at first half-height drop and moduli at second half-height drop for Zorn LWD. 70
Figure 4-18. Comparison of moduli at first half-height drop and moduli at second half-height drop for Dynatest LWD. 72
Figure 4-19. Comparison of moduli at first half-height drop and moduli at second half-height drop for Olson LWD. 74

APPENDIX 1. OTHER DOTS' FINDINGS

1.1. Minnesota DOT

The MNDOT specification for using LWD for QA of geomaterials suggests defining the target LWD deflection based on the grading number (GN) (see Equation 1-1 below) and field moisture content for granular materials and on the plastic limit and field moisture content for fine-grained soils. The MNDOT specification requires testing immediately after compaction. Table 1-1 and Table 1-2 provide the target LWD deflection and modulus for granular materials and fine soils, respectively. The specification is provided in the following link: http://www.dot.state.mn.us/materials/gblwd.html

$$GN(\%\text{passing}) = \frac{25mm + 19mm + 9.5mm + 4.75mm + 2.00mm + 425\mu m + 75\mu m}{100} \quad \textbf{Equation 1-1}$$

Table 1-1. LWD Target Values for Granular Material (Siekmeier et al. 2009)

GN	Moisture Content	Target LWD Modulus		Target LWD Deflection
		Keros/Dynatest	Zorn	
	%	MPa	MPa	mm
3.1 – 3.5	5 -7	120	80	0.38
	7- 9	100	67	0.45
	9 - 11	75	50	0.60
3.6 – 4.0	5 -7	120	80	0.38
	7- 9	80	53	0.56
	9 - 11	63	42	0.71
4.1 – 4.5	5 -7	92	62	0.49
	7- 9	71	47	0.64
	9 - 11	57	38	0.79
4.6 – 5.0	5 -7	80	53	0.56
	7- 9	63	42	0.71
	9 - 11	52	35	0.86
5.1 – 5.5	5 -7	71	47	0.64
	7- 9	57	38	0.79
	9 - 11	48	32	0.94
5.6 – 6.0	5 -7	63	42	0.71
	7- 9	50	33	0.90
	9 - 11	43	29	1.05

Table 1-2. LWD Target Values for Fine Grained Soil (Siekmeier et al. 2009)

Plastic Limit	Estimated Optimum Moisture	Field Moisture as a % of Optimum Moisture	Zorn Deflection Target at Field Moisture	
			Minimum	Maximum
%	%	%	mm	mm
Non-plastic	10-14	70 – 74	0.5	1.1
		75 - 79	0.6	1.2
		80 - 84	0.7	1.3
		85 - 89	0.8	1.4
		90 - 94	1.0	1.6
15 – 19	10 - 14	70 – 74	0.5	1.1
		75 - 79	0.6	1.2
		80 - 84	0.7	1.3
		85 - 89	0.8	1.4
		90 - 94	1.0	1.6
20 – 24	15 - 19	70 – 74	0.8	1.4
		75 - 79	0.9	1.6
		80 - 84	1.0	1.7
		85 - 89	1.2	1.9
		90 - 94	1.4	2.1
25 – 29	20 - 24	70 – 74	1.0	1.7
		75 - 79	1.2	1.9
		80 - 84	1.4	2.1
		85 - 89	1.6	2.3
		90 - 94	1.8	2.6
30 – 34	25 - 29	70 – 74	1.3	2.0
		75 - 79	1.5	2.2
		80 - 84	1.7	2.4
		85 - 89	1.9	2.7
		90 - 94	2.2	3.0

White et al. (2009) in the study *Implementation of Intelligent Compaction Performance Based Specifications in Minnesota* developed and evaluated a new approach for LWD target value determination in the lab. Samples were compacted using a gyratory compaction (150 mm diameter x 150 mm high), since this is thought to simulate field compaction characteristics better than impact/Proctor compaction method. Samples were prepared using both granular and non-granular soil at various moisture and dry unit weights. LWD testing using a Zorn LWD with a 100-mm plate diameter was performed on the specimens while in the gyratory mold. The results were used to evaluate the moisture content-dry unit weight-LWD modulus relationship. Target values were then calculated based on reaching a 95% to 110% standard Proctor maximum density on the contour plots of multiple regression relationships.

Additionally, acceptance specification for the field projects in this study required constructing a control strip for each type of material used for grading. Optimum compaction is reached when additional compactor passes do not result in significant increase in stiffness. The acceptable moisture content range was set between 65% to 95% of standard Proctor optimum moisture content. The LWD target value was defined as the average of three LWD tests performed on the control strip.

Overall, the LWD on gyratory mold method's target values were within the range of MNDOT suggested target modulus (Figure 1-1). Additional research was recommended to: (1) better simulate the field boundary conditions, (2) evaluate this mold method for a variety of soil types, and (3) obtain a cost-efficient test set up.

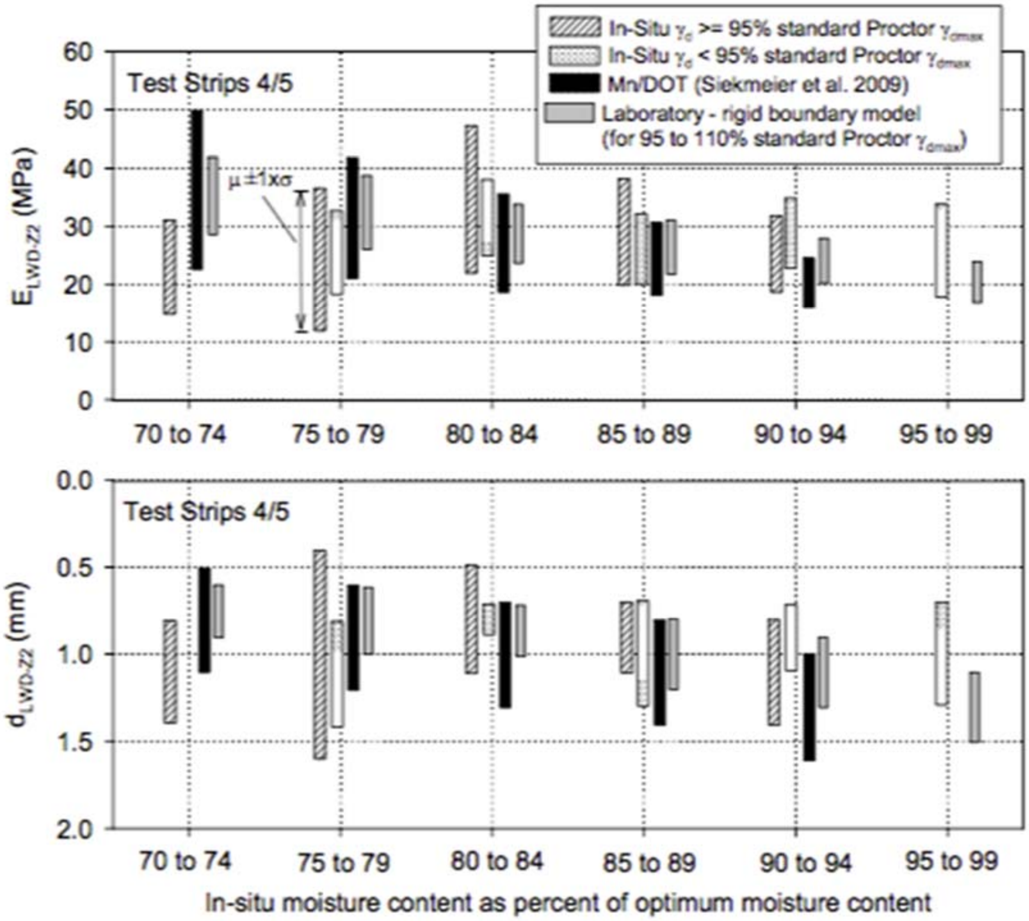

Figure 1-1. Comparison between LWD on gyratory mold target values, MNDOT target modulus, and in-situ LWD values (from White et. al, 2009)

1.2. Indiana DOT

The INDOT also developed a test method for *Field Determination of Deflection Using Light Weight Deflectometer (ITM No. 508-12T)*. The INDOT specification can be used on granular soils, coarse aggregates and chemically modified soils. Specification link: http://www.in.gov/indot/div/mt/itm/pubs/508_testing.pdf

The INDOT specification provides two options to determine the LWD target deflection value: (1) Control strip and (2) Comparison. In the first method, the specification requires: (a) construction of a control strip to meet the specified requirements; (b) LWD testing during the control strip construction at specified intervals; and (c) plotting the average LWD deflection against the roller pass count. The minimum deflection is set as the target value. The deflection measured in the LWD test on the compacted layer should not exceed 1.1 time the LWD target value.

In the second method, the target value is selected based on comparisons with Dynamic Penetration Index (DPI) for granular base or the INDOT-specified density method for fine-grained soils. The LWD target value is defined as the average LWD deflection at which minimum DPI or density values pass their respective criteria.

1.3. Florida DOT

Glagola et al (2015) proposed a specification for measuring deflection using a portable impulse plate load device in the *Performance-Based Quality Assurance/Quality Control (QA/QC) Acceptance Procedures for In-Place Soil Testing Phase 3* study. The specification requires LWD testing to be performed concurrently with the nuclear density testing so that both the density and modulus requirements are satisfied. There are two methods of obtaining the target maximum allowable deflection using LWDs: (1) correlations between LWD measurements and laboratory resilient modulus values (Table 1-3 and Table 1-4) for stabilized subgrade and limerock base material, and (2) direct measurement on a test strip for other type of geomaterial.

The test strip is constructed using the contractor’s material and roller compactor. Ten LWD deflection measurements are conducted after four passes of roller on vibratory mode. Then an additional pass is made and another round of ten LWD deflection measurements taken. If the difference between average deflections are less than 0.02 mm, then the LWD average deflection values after fifth pass will be the target maximum deflection, else this procedure should continue until the average difference is less than 0.02 mm.

In case the average deflection after LWD testing in the field is more than the maximum allowable deflection (i.e., failing compaction), a moisture test should be performed. LWD testing is then repeated after 24 hours at the same location and if the deflections then are equal to or less than the maximum allowable deflection, then the compaction will be accepted.

It is recommended to conduct moisture content testing in the field with a Calcium Carbide gas pressure moisture tester. For lime rock, cemented coquina, and shell-rock base material, moisture content is measured with a NDG per Florida’s sampling and testing methods.

Table 1-3. Maximum LWD deflection for Florida stablized subgrade

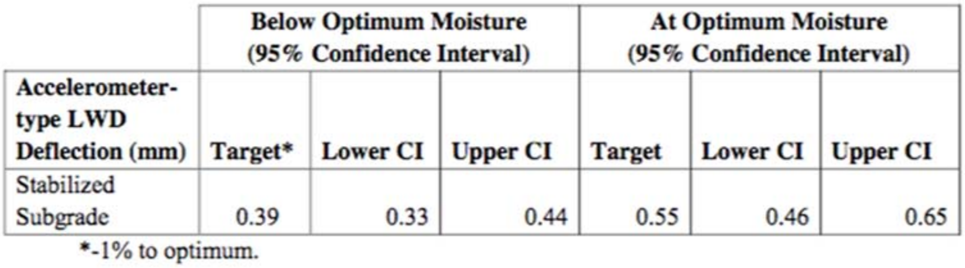

	Below Optimum Moisture (95% Confidence Interval)			At Optimum Moisture (95% Confidence Interval)		
Accelerometer-type LWD Deflection (mm)	**Target***	**Lower CI**	**Upper CI**	**Target**	**Lower CI**	**Upper CI**
Stabilized Subgrade	0.39	0.33	0.44	0.55	0.46	0.65

*-1% to optimum.

Table 1-4. Maximum LWD deflection for Florida limerock base

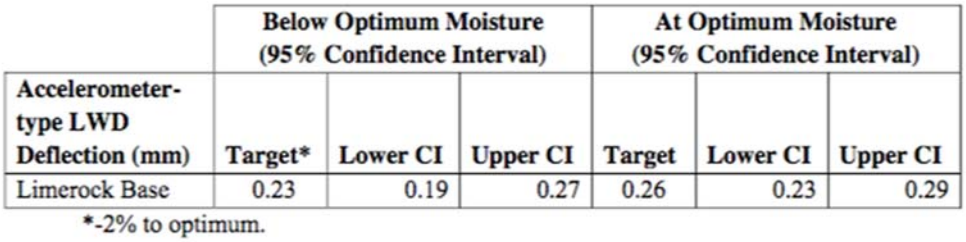

	Below Optimum Moisture (95% Confidence Interval)			At Optimum Moisture (95% Confidence Interval)		
Accelerometer-type LWD Deflection (mm)	**Target***	**Lower CI**	**Upper CI**	**Target**	**Lower CI**	**Upper CI**
Limerock Base	0.23	0.19	0.27	0.26	0.23	0.29

*-2% to optimum.

1.4. Nebraska Department of Roads

Nebraska department of roads (NDOR) uses LWD deflection plus moisture testing for QA of embankment, subgrade, foundation course, granular fill, and granular backfills according to NDOR *Lightweight Deflectomer (LWD) Field Testing – Quick Reference Guide*. Two methods of LWD target value determination are provided: (1) Based on resilient modulus correlations to Nebraska group index (NGI), and (2) Direct measurement from a test strip or calibration area. In the first method, the specification requires the moisture content to be within the specification limit, then the LWD target deflection should pass the values in the Table 1-5, depending on the unbound material location (under concrete or asphalt pavement, and for the top 3 feet or below 3 feet under the pavement).

When the deflection data for a specific soil type is not available, a 200-foot test strip must be compacted in two 8-inch lifts. Moisture content testing is required to confirm it is within the acceptable limits. Three LWD tests are conducted after each pass of the roller until the average deflection for three consecutive passes does not change significantly with any additional pass (less than 10% change). This final deflection value becomes the LWD target value. The field LWD deflections after compaction must not surpass 1.1 time the LWD target value.

Further research is recommended to complete the NGI vs LWD deflections for all soil types and conditions. Another recommendation was to search for a reliable field moisture content measurement device.

Table 1-5. NDOR max allowable LWD deflection values for different NGI

Nebraska Group Index	Concrete Upper 3'	Concrete Below 3'	Asphalt Upper 3'	Asphalt Below 3'
	Max Deflection (mm)	Max Deflection (mm)	Max Deflection (mm)	Max Deflection (mm)
-2	0.5	0.5	0.5	0.5
-1	0.5	0.5	0.5	0.5
0	0.5	0.5	0.5	0.5
1	1	1.5	0.5	1.5
2	1	1.5	0.5	1.5
3	2	3	1	3
4	2	3	1	3
5	2	3	1	3
6	2	3	1	3
7	1.5	3	0.75	3
8	1.5	3	0.75	3
9	1.5	3	0.75	3
10	2	4	1	4
11	2	4	1	4
12	2	4	1	4
13	2	4	1	4
14	3	5	2	5
15	3	5	2	5
16	3	5	2	5
17	4	6	3	6
18	4	6	3	6
19	5	8	4	8
20	5	8	4	8
21	5	8	4	8
22	6	9	5	9
23	6	9	5	9
24	6	9	5	9

1.5. European Union

The European Union (EU) also has developed a specification for LWD implementation (*CEN ICS 93.020*). In this specification two parameters are determined through LWD testing: (1) LWD modulus, which the EU specification terms the dynamic modulus, calculated based on the Boussinesq equation; and (2) dynamic compactness (T_{rd}), which shows the quality of the compaction. T_{rd} is computed as:

$$T_{rd} = T_{rE} \times T_{rw}$$

Equation 1-2

where T_{rE} is site relative compaction at a given water content and T_{rw} is the moisture correction coefficient to adjust for differences between the measured moisture content and optimum moisture content. T_{rw} is calculated as:

$$T_{rw} = \frac{\rho_{di}}{\rho_{d\max}}$$

Equation 1-3

In which ρ_{dmax} is the maximum dry density value obtained in the modified Proctor test and ρ_{di} is the dry density value from compaction curve of the modified Proctor tests corresponding to the in situ moisture content.

The testing process to obtain T_{rw} involves six sequences of LWD testing, each consisting of three LWD drops (total of 18 drops) on the loose, non-compacted material at the site. The average deformation of the second sequence is used to determine the initial dynamic modulus. The final dynamic modulus is calculated from the sixth testing sequence. According to the standard, the work imparted on the material during the six LWD sequences is equivalent to that applied in the modified Proctor test.

The EU specification determines the relative compaction T_{rE} at the field moisture content from the compaction curve using the following equation:

$$\%T_{rE} = 100 - \Phi_0 \times D_m$$

Equation 1-4

where Φ_0 is a linear coefficient calculated from the Proctor-test results, typically assumed to be 0.365 ± 0.025, and D_m is the deformation index, calculated from sum of the elements of the data line formed from the difference of the subsequent deflections up to the drop.

A similar approach was pursued by MNDOT (White et al., 2009) to compact the loose material in the field with multiple LWD drops so that the measured LWD modulus would asymptotically determine the target modulus. However, the target obtained by this method was lower than the average modulus measured after roller compaction at about the same moisture content. This was hypothesized to be due to the higher (by a factor of 3 to 4) compaction stresses under the roller as compared to the imparted stress under the 200 mm LWD plate.

1.6. United Kingdom

The *UK specification* defines four foundation classes according to the long term in-service foundation surface modulus values, as follows:

- Class 1 $\geq$ 50MPa
- Class 2 $\geq$ 100MPa
- Class 3 $\geq$ 200MPa

– Class 4 ≥ 400MPa

For construction QC, the target mean and minimum modulus values are specified for the four foundation classes as shown in Table 1-6. The moving mean of five consecutive in-situ foundation surface modulus measurements must equal or exceed the target mean foundation surface modulus. All individual in-situ foundation surface modulus measurements must equal or exceed the target minimum foundation surface modulus.

Table 1-6. UK specification. Target pavement foundation surface modulus

Long-Term In-Service Modulus (MPa)			Class I	Class II	Class III	Class IV
			≥50	≥100	≥200	≥400
Target Mean Modulus (MPa)	Unbound		40	80	…	…
	Bound	Fast Curing	50	100	300	600
		Slow Curing	40	80	150	300
Target Minimum Modulus (MPa)	Unbound		25	50	…	…
	Bound	Fast Curing	25	50	150	300
		Slow Curing	25	50	75	150

1.7. NCHRP 10-84 Study

The NCHRP 10-84 (2014) study proposed a framework for modulus based specification using LWD. The suggested procedure is to calculate the LWD effective modulus (E_{eff}) from the Boussinesq equation after conducting the test in the field. Then, E_{eff} is adjusted using the following formula:

$$E_{adj} = E_{eff} \times K_{lab-field} \times K_{moist}$$ **Equation 1-5**

In this equation, $K_{lab\text{-}field}$ is an adjustment factor that accounts for differences between lab and field moduli at the same moisture content and density:

$$K_{lab-field} = (F_{env})^{\lambda}$$ **Equation 1-6**

where λ= -0.36 and F_{env} = the relationship proposed by Cary and Zapata (2010) simplified by replacing wPI with zero:

$$\log(F_{env}) = \left(-.40535 + \frac{1.20693}{1 + e^{\left(0.68184 + 1.33194\left(\frac{S - S_{opt}}{100}\right)\right)}} \right)$$

Equation 1-7

In this equation, S_{opt} = degree of saturation at optimum moisture content and S = degree of saturation at compaction moisture content.

K_{moist} is an adjustment factor for differences in the compaction and testing moisture contents:

$$K_{moist} = e^{\eta(w_c - w_T)}$$

Equation 1-8

where η=0.18 for fine-grained soils and 1.19 for unbound aggregates, w_T is moisture content at time of testing (in percent); and w_C is moisture content at time of compaction (in percent).

The specification suggests direct measurement of the resilient modulus of the geomaterial per AASHTO T-307 for target modulus determination. The pavement section is then modeled in a nonlinear structural pavement algorithm that simulates the center deflection under the LWD load the Boussinesq equation and using that to calculate the E_{target}.

The evaluation of the proposed specification showed that achieving adequate layer modulus is weakly associated with achieving density. Changes in the assumed Poisson's ratio will highly affect the acceptance rate. Different LWDs estimate different moduli at the same test spot, suggesting the necessity for LWD specific specification. NCHRP 10-84 also found that it is very important to consider the properties of the underlying layers in setting the LWD target values, which is in line with findings from Khosravifar et al. (2013). A common concern regarding the modulus-based devices was the variability of the measurements. Based on tests on 20 independent specimens, Nazarian et al. (2014) found that the repeatability of the LWD devices is more than 15% and their reproducibility is more than 12%. Above 70% of variability in the LWD devices measurements was attributed to the variation in the materials properties.

Nazarian et al. (2013) only performed small scale testing in which specimens were compacted in a 90-cm diameter PVC pipe to a thickness of less than 0.55 m; these are much different conditions than in the field. Grasmick (2013) performed LWD testing on a large free-standing soil box structure with inside dimensions of 2.4m x 2.4m x 1.2m constructed out of timber. One significant issue reported in this work was the reflection of the LWD induced waves off the wood/soil box.

The online survey circulated among state Departments of Transportation (DOTs) as part of the NCHRP 10-84 project revealed that, while DOTs are interested in implementing a practical modulus-based specification, the incorporation of laboratory resilient modulus tests is not desirable.

Finally, NCHRP 10-84 recommended modulus-based acceptance tests to be implemented in conjunction with moisture measurements. Ironically, the nuclear density gauge was determined as the most reasonable moisture measurement tool in this study.

APPENDIX 2. EQUIPMENT MODELING

2.1. Force Versus Height Assumptions for Zorn LWD

The load of Zorn LWD at drops other than the full height was estimated based on a single DOF mechanical model assumption illustrated in Figure 2-1.

A linear relationship can be derived between the square root of the drop height and the impact force. Upon releasing the falling weight, the gravitational potential energy (E) stored in the falling weight transforms to kinetic energy and then to elastic potential energy in the spring when the mass hits the spring, as shown in the following equations:

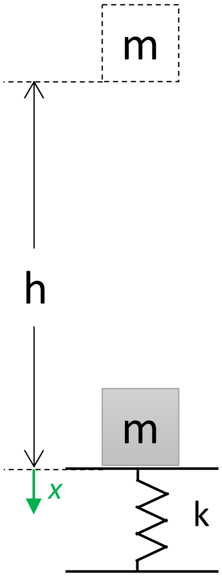

Figure 2-1. Similified schematic of LWD- soil motion as a one DOF mass-spring system.

$$\boldsymbol{E = m.g.h = \frac{1}{2}k.\Delta x^2} \qquad \textbf{Equation 2-1}$$

$$\boldsymbol{F = k.\Delta x} \qquad \textbf{Equation 2-2}$$

therefore:

$$\boldsymbol{F = \sqrt{2.m.g.h.k}} \qquad \textbf{Equation 2-3}$$

Error! Reference source not found. was used to estimate the impact force of Zorn LWD at h eights other than the full height when necessary.

2.2. LWD Testing on Four-Pint Steel Beam

The performance of the three LWD devices was examined with the beam verification tester (BVT) developed by Hoffman et al. (2004). The BVT is a simply supported steel beam under two symmetric loads, also known as a four-point beam. The schematic of the beam is shown below:

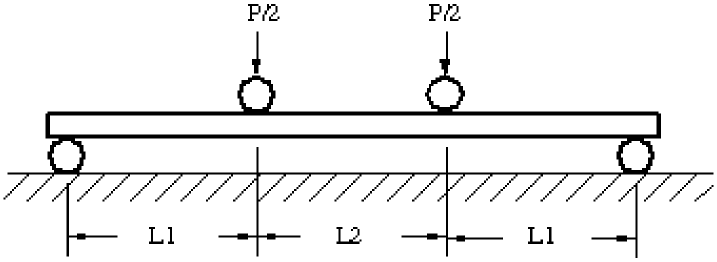

Figure 2-2. Schematic of the BVT

L2 was 10 cm while 2L1+L2 was varied from 40 cm to 70 cm in 10 cm intervals to produce a linear elastic structure with different stiffness values. The static stiffness of the beam (k_s) was measured by applying a ramp load at a slow rate of 0.2 mm/sec using an Instron Machine (Figure 2-5). The k_s was subsequently compared to the peak stiffness derived from LWD testing on the beam ($k_{p\text{-LWD}}$). Figure 2-3 shows the Dynatest LWD on the beam as an example.

Using the LWD test data, the beam stiffness was calculated through two methods:

a) Peak stiffness ($k_{p\text{-LWD}}$) based on the ratio of peak load (F_{peak}) to peak deflection (d_{peak}) as reported by LWD ($k_{p\text{-LWD}}= F_{peak}/d_{peak}$).

b) Static Stiffness ($k_{s\text{-LWD}}$). Based on the frequency response function and assumption of a single-degree-of-freedom mechanical model.

The most important objective of the BVT tests were to (1) verify the calibration and reliability of the three test devices on a linear elastic structure with known stiffness properties; and (2) assess the necessity to perform a full frequency domain analysis of the load and deflection signals for future LWD testing on soil. This study was based on work performed by Hoffmann et al. (2004), who found significant systematic errors of up to 278% between the $k_{p\text{-LWD}}$ calculated from a Prima-100 LWD and the true stiffness of the beam (k_s).

Tests were performed using the 300-mm diameter plate and the drop heights listed in Table 2-2, Table 2-3, and Table 2-4 for the Olson, Zorn, and Dynatest LWD respectively. Figure 2-4 presents the $k_{p\text{-LWD}}$ versus the beam span for the evaluated LWDs. Tests were highly repeatable with coefficients of variation (CV) of less than 3% for all devices. The $k_{p\text{-LWD}}$ for all three devices was overall in the same ballpark of the true stiffness of the beam, contrary to the finding of Hoffmann et al. (2004).

For Zorn and Olson, the $k_{p\text{-LWD}}$ results were in line with true k_s of the beam at beam spans of 60 and 70 cm. As the beam span decreased, the $k_{p\text{-LWD}}$ underestimated the stiffness. In case of the Dynatest LWD, k_p was close to the true stiffness of the beam at beam spans 40 and 50 cm and only slightly underestimated at higher beam spans.

The underestimation of the beam stiffness by Olson and Zorn in this experiment could be justified by the fact that these two LWDs measure the deflection of the plate whereas the

Dynatest LWD measures the deflection of the beam in the center of the plate. The underestimation was more significant for Zorn, which could be attributed to the error from assuming the peak load and different plate thickness.

Moreover, the Zorn and Olson devices are measuring the deflections of the quarter load points. Under static loading, the load point deflections are expected to be less than the centerline deflections. This would result in even higher errors for the Zorn and Olson stiffness than given here. However, under dynamic conditions it is conceivable that the centerline deflections during the initial portion of the response (i.e., at peak load and deflection) may be less than the load point deflections because of inertial lag.

Another explanation is that the deformations of the bearing cylinders at the load points (especially indentation effects) are included in the Zorn and Olson's deflections but not for the Dynatest's. This would cause the Zorn and Olson devices to overestimate deflections and thus underestimate stiffness, consistent with results shown in Figure 2-4.

Table 2-1 provides the k_s measured by the Instron machine. Table 2-2, Table 2-3, and Table 2-4 present $k_{p\text{-}LWD}$ and the $k_{p\text{-}LWD}/k_s$ ratio for the Olson, Zorn, and Dynatest LWDs, respectively.

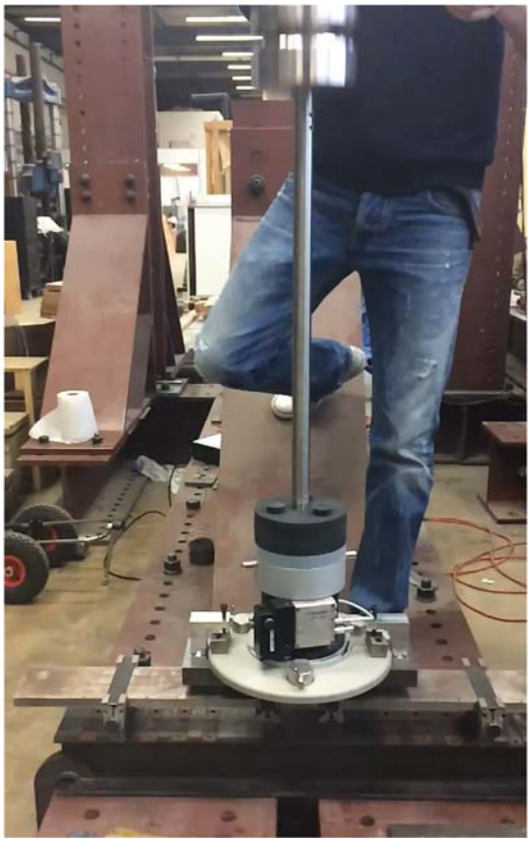

Figure 2-3. Dynatest LWD test performed on BVT

Table 2-1. True static stiffness of the 4-point beam as measured by Instron

Span [cm]	ks-true [MN/m]
30	7.92
40	5.01
50	2.42
60	1.45
70	0.91

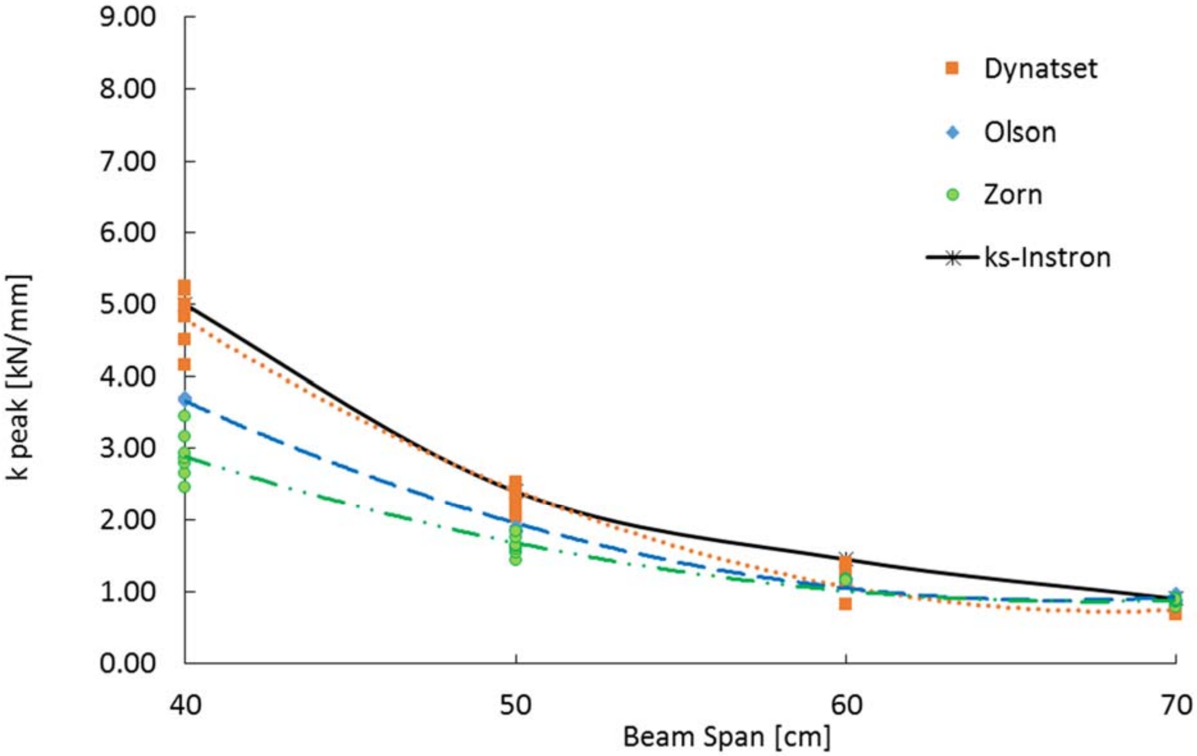

Figure 2-4. k_p **as a function of beam span for the all the evaluated devices.**

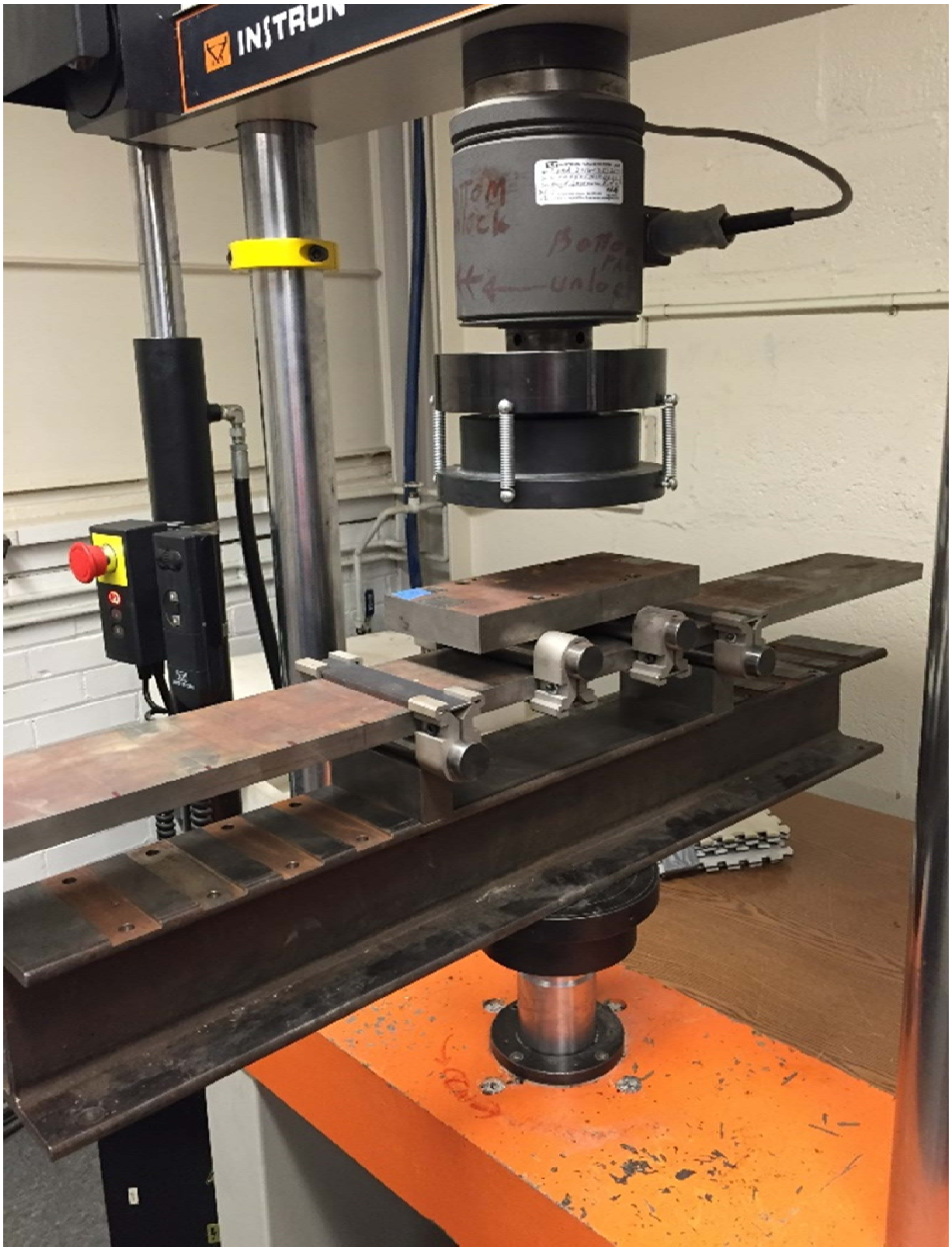

Figure 2-5. Measurement of BVT static stiffness (k_s) with the Instron machine.

Table 2-2. Peak stiffness (k_p) from Olson LWD testing on 4 point beam.

Span [cm]	**Drop height** [cm]	**Force** [kN]	**d** [mm]	**$k_{p\text{-}LWD}$** [MN/m]	**$k_{p\text{-}LWD}/k_s$** [-]
40	2.5	1.70	0.463	3.68	0.7
40	5.1	2.20	0.594	3.70	0.7
40	7.6	2.80	0.752	3.72	0.7
40	10.2	3.09	0.837	3.69	0.7
40	12.7	3.38	0.923	3.66	0.7
40	21.6	4.72	1.268	3.72	0.7
50	2.5	1.51	0.814	1.86	0.8
50	5.1	1.96	1.075	1.82	0.8
50	7.6	2.37	1.285	1.85	0.8
50	10.2	2.80	1.503	1.86	0.8
50	12.7	3.17	1.680	1.89	0.8
50	21.6	4.13	2.162	1.91	0.8
60	2.5	1.47	1.311	1.12	0.8
60	5.1	1.88	1.620	1.16	0.8
60	7.6	2.23	1.925	1.16	0.8
60	10.2	2.58	2.214	1.17	0.8
60	12.7	2.90	2.453	1.18	0.8
60	21.6	3.85	2.861	Deflection sensor overload	
70	2.5	1.45	1.705	0.85	0.9
70	5.1	1.81	2.108	0.86	0.9
70	7.6	2.22	2.489	0.89	1.0
70	10.2	2.48	2.818	0.88	1.0
70	12.7	2.77	2.837	0.98	1.1
70	21.6	3.65	2.899	Deflection sensor overload	

Table 2-3. Peak stiffness (k_p) from Zorn LWD testing on 4 point beam.

Span	Drop height	Force	d	$k_{p\text{-LWD}}$	$k_{p\text{-LWD}}/k_s$
[cm]	[cm]	[kN]	[mm]	[MN/m]	[-]
40	2.54	1.32	0.537	2.47	0.5
40	5.08	1.87	0.707	2.65	0.5
40	7.62	2.29	0.818	2.80	0.6
40	10.16	2.65	0.922	2.87	0.6
40	12.7	2.96	1.011	2.93	0.6
40	31.75	4.68	1.482	3.16	0.6
40	72.4	7.07	2.028	3.46	0.7
50	2.54	1.32	0.918	1.44	0.6
50	5.08	1.87	1.215	1.54	0.6
50	7.62	2.29	1.436	1.60	0.7
50	10.16	2.65	1.616	1.64	0.7
50	12.7	2.96	1.804	1.64	0.7
50	31.75	4.68	2.666	1.76	0.7
50	72.4	7.07	3.792	1.85	0.8
60	31.75	4.68	4.011	1.17	0.8
60	72.4	7.07	3.253	1.16	0.8
70	2.54	1.32	1.683	0.79	0.9
70	5.08	1.87	2.179	0.86	0.9
70	7.62	2.29	2.643	0.87	1.0
70	10.16	2.65	3.049	0.87	1.0
70	12.7	2.96	3.288	0.90	1.0
70	31.75	4.68	5.228	0.90	1.0
70	72.4	7.07	8.406	0.83	0.9

Table 2-4. Peak stiffness (k_p) from Dynatest LWD testing on 4 point beam.

Span	**Drop height**	**Force**	**d**	**$k_{p\text{-LWD}}$**	**$k_{p\text{-LWD}}/k_s$**
[cm]	[cm]	[kN]	[mm]	[MN/m]	[-]
40	2.54	0.78	0.150	5.25	1.0
40	5.08	1.15	0.229	5.00	1.0
40	7.62	1.58	0.303	5.20	1.0
40	10.16	1.95	0.403	4.82	1.0
40	12.7	2.27	0.503	4.51	0.9
40	17.78	2.86	0.687	4.16	0.8
50	2.54	0.80	0.315	2.53	1.0
50	5.08	1.17	0.490	2.39	1.0
50	7.62	1.64	0.666	2.45	1.0
50	10.16	1.97	0.863	2.28	0.9
50	12.7	2.28	1.037	2.20	0.9
50	17.78	2.77	1.362	2.04	0.8
60	2.54	0.82	0.586	1.40	1.0
60	5.08	1.22	0.929	1.31	0.9
60	7.62	1.51	1.222	1.24	0.9
60	10.16	1.82	1.589	1.15	0.8
60	12.7	2.08	1.889	1.10	0.8
70	2.54	0.75	0.923	0.81	0.9
70	5.08	1.11	1.616	0.69	0.8
70	7.62	1.41	1.986	0.71	0.8
70	10.16	1.65	2.439	0.68	0.7
70	12.7	1.97	2.825	0.70	0.8

2.2.1. Frequency domain analysis

To account for the transient load and displacement data recorded on the BVT, the response was analyzed in the frequency domain using the Fast Fourier transform (FFT) algorithm in MATLAB. The technique has already been used by several researchers e.g. Hoffmann (2004).

In a linear system with y(t) and u(t) as the output and input of the system, respectively, the transient response of the linear system can be analyzed by the Frequency Response Function (FRF) defined as the ratio of the Fourier transform of the output, Y(f) and the Fourier transform of the input, U(f):

$$FRF(f) = \frac{Y(f)}{U(f)}$$

Equation 2-4

where *f* is the frequency in Hz.

Assuming a linear model, the FRF of the dynamic stiffness, K(f) and mobility, M(f) are defined as follows:

$$K(f) = \frac{F(f)}{X(f)}$$

Equation 2-5

$$M(f) = \frac{\dot{X}(f)}{F(f)}$$

Equation 2-6

where F(f), X(f), and $\dot{X}(f)$ are the respective Fourier transforms of the force f(t), the displacement x(t), and the velocity $\dot{x}(t)$.

The static stiffness, k_s, of this linear model can therefore be computed as the magnitude of the dynamic stiffness, K(f), at zero frequency. The geophone or accelerometer measurements are not reliable at low frequencies and thus the static stiffness cannot directly be calculated from the measurements (Hoffmann, 2004). Alternatively, the experimental data corresponding to the FRF of the dynamic stiffness at higher frequencies can be extrapolated to zero frequency. To get a more accurate extrapolation to zero frequency, the single degree of freedom (SDOF) mass (m), spring (with stiffness k), and damper (with damping coefficient c) linear system was considered to explain the LWD-beam movement. The ordinary differential equation (ODE) of motion for the SDOF mass-spring-damper system is as follows:

$$m\ddot{x}(t) + c\dot{x}(t) + kx(t) = f(t)$$

Equation 2-7

where $\ddot{x}(t)$ is the acceleration, m is summation of the mass of the LWD, including the receptacle and any other part on top of the verification beam, c represents the damping of the beam, and stiffness k is equal to the static stiffness of the verification beam (k_s).

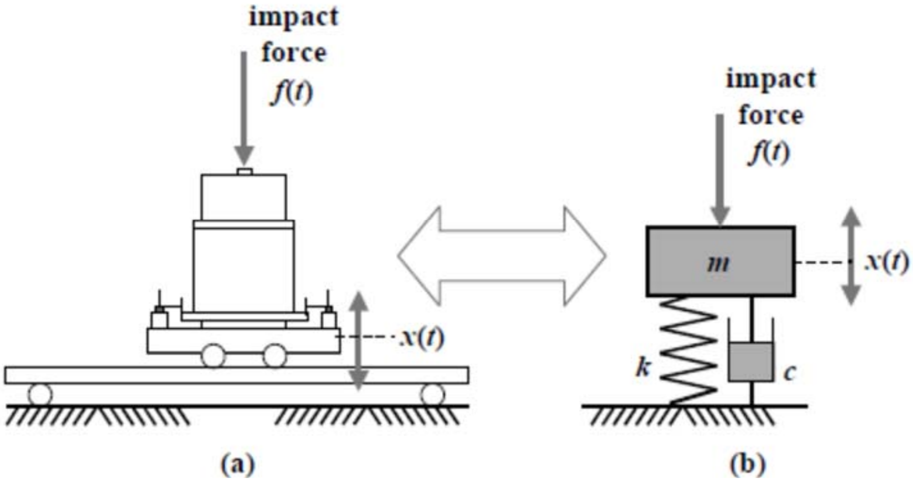

Figure 2-6. SDOF analog for the BVT: (a) four-point beam testing configuration; (b) corresponding SDOF analog (after Hoffmann, 2004).

The K(f) and M(f) functions can be derived by taking the Fourier transform from Equation 2-7 in the time domain. The functions as shown in Equation 2-8 and Equation 2-9 for K(f) and M(f), respectively, can be used for curve fitting and extrapolation of the experimental data to zero frequency. Since the force and deflection data were readily available in the tested LWDs, the spectral analysis using the dynamic stiffness function, K(f), was utilized.

$$K(f)=k\left[\left(1-\beta^{2}\right)+2i\xi\beta\right]$$ **Equation 2-8**

$$M(f)=\frac{1}{k}\frac{2i\pi f}{(1-\beta^{2})+2i\xi\beta}$$ **Equation 2-9**

Where $\beta=\frac{f}{f_n}$ is the tuning ratio, $\xi=\frac{c}{4\pi m f_n}$ is the damping ratio, and $f_n=\frac{1}{2\pi}\sqrt{\frac{k}{m}}$ is the undamped natural frequency.

To reduce the effects of experimental noise and minimize the errors, a spectral average technique was used. This technique was effectively used by Bendat and Piersol (2011) and Guzina and Osburn (2002) for back calculating the FWD modulus on layered systems and by Hoffmann (2004) for the spectral analysis of the Prima-100 LWD impact load on the BVT. In the averaging technique, the dynamic stiffness function is estimated as:

$$K(f) = \frac{G_{xf}(f)}{G_{xx}(f)}$$ **Equation 2-10**

where G_{xf} (f) is the one-sided cross-spectral density function of the deflection and force records and G_{xx} (f) is the one-sided auto-spectral density function of the deflection record. G_{xf} (f) and G_{xx} (f) were calculated using the built-in functions in MATLAB. The spectral averaging approach also allows for assessing the quality of the measurements and validity of the linearity assumption via the coherence function:

$$\gamma^2(f) = \frac{\left|G_{xf}(f)\right|^2}{G_{ff}(f)G_{xx}(f)}$$ **Equation 2-11**

where G_{ff} (f) is the one-sided auto-spectral density function of the force record. The coherence function ranges from 0 to 1, where a value of zero shows no correlation between the input and output and a value of 1 shows the system is perfectly linear and noise free. The spectral analysis was not possible for the Zorn LWD since the load is not measured and a fixed load is assumed. An example of the spectral analysis on the Dynatest and Olson LWDs is shown in Figure 2-7 and Figure 2-8, respectively. Figure 2-9 depicts the strong agreement of the $k_{p\text{-}LWD}$ and k_s values from the spectral analysis for the Dynatest LWD.

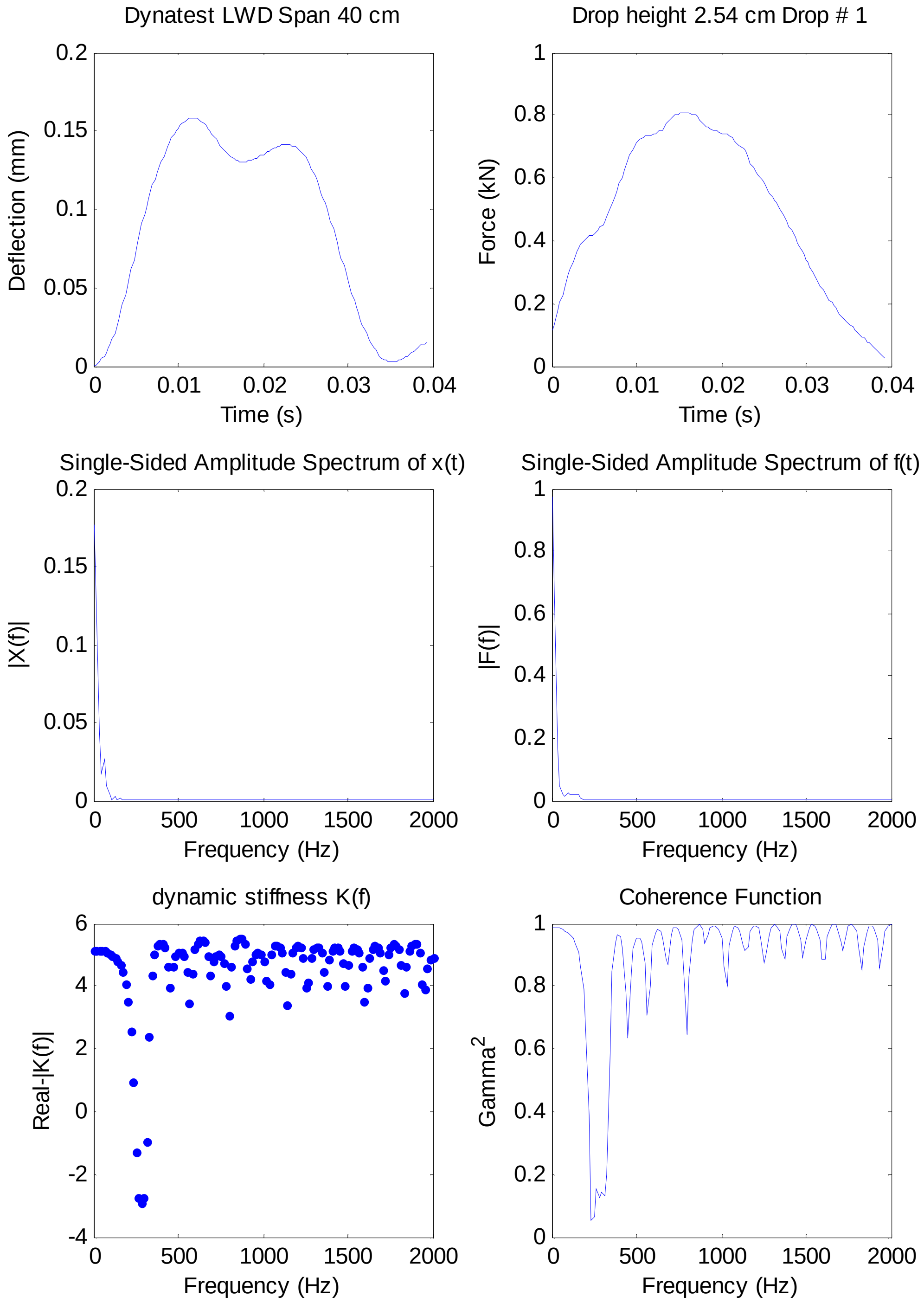

Figure 2-7. Spectral analysis on Dyantest LWD

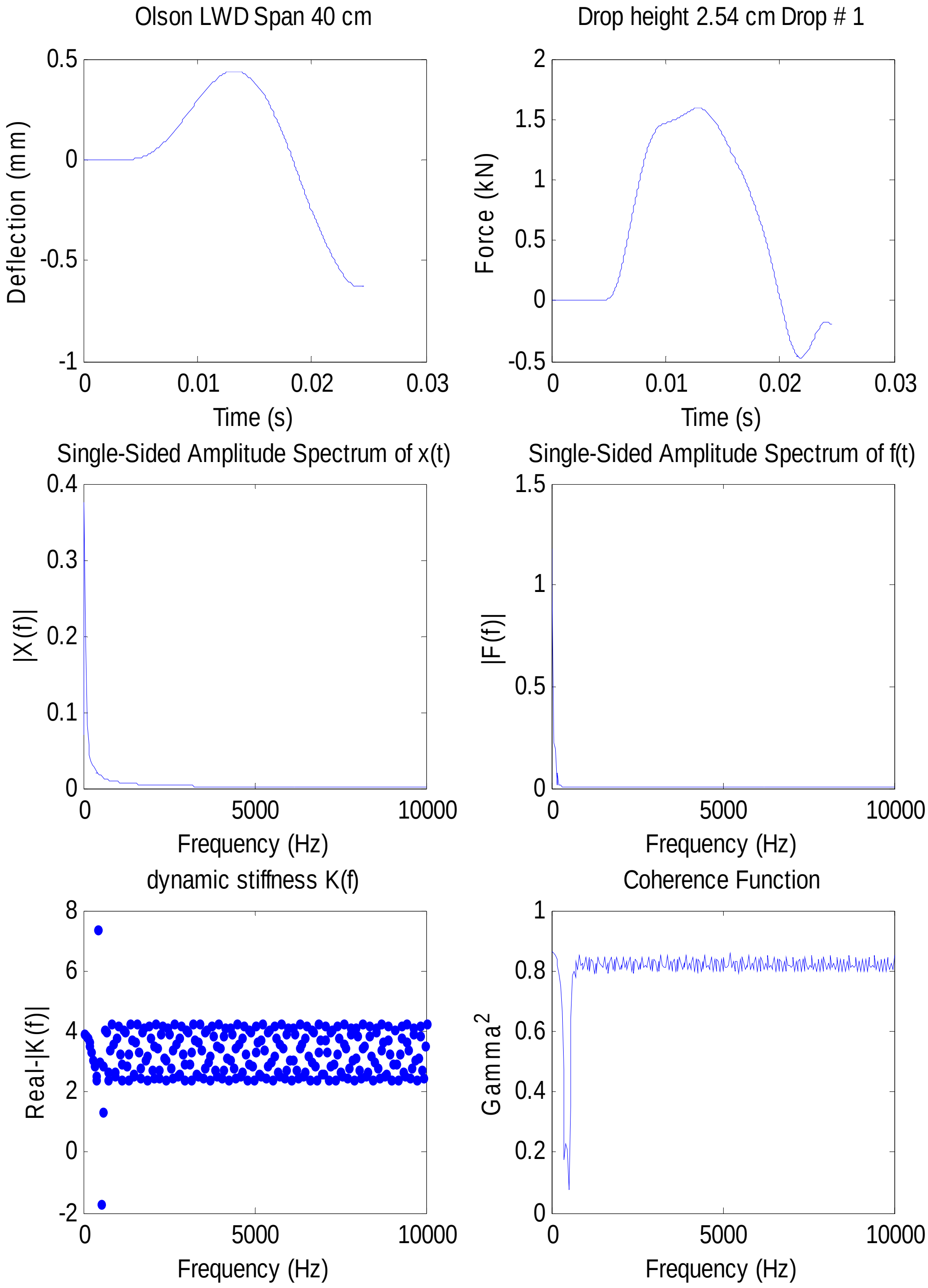

Figure 2-8. Spectral analysis on Olson LWD

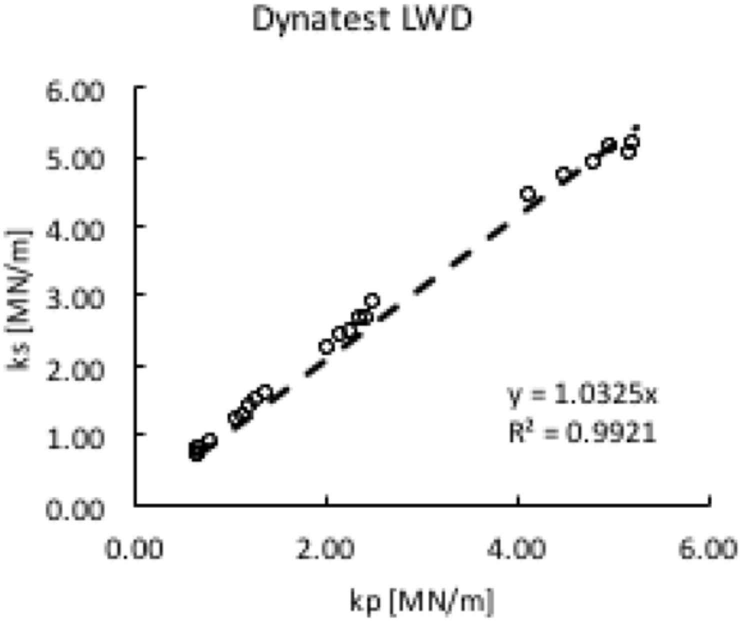

Figure 2-9. k_s from spectral analysis versus k_p of conventional peak method

2.2.2. Conclusion

The objective was to distinguish the inherent differences in the LWD devices. To accomplish this task, LWD testing was performed on a four-point linear elastic steel beam with known stiffness properties. The stiffness from LWD was measured from (1) conventional peak method (k_{peak}), by normalizing the peak force by peak deflection; and (2) through frequency domain spectral analysis to find the static k (k_s). The results showed that the LWDs provide a good estimate of the beam stiffness through peak method and spectral analysis can only slightly improve the results.

APPENDIX 3. RESILIENT MODULUS TESTING

3.1. Test Pits Material Characteristics

In this section, the properties of the materials used in the test pits are described. The ALF soil used in the study was excavated from a hill at TFHRC and the VA21a stone and HPC were donated by the Luck Stone Company. The Unified Soil Classification and Atterberg Limits (AASHTO T-89 and T-90) of the studied soils are summarized in Table 3-1.

Table 3-1. Material description

Material	Soil classification	PL	LL	PI	D_{90}	D_{60}	D_{30}	D_{20}	D_{10}	P_{200}	C_U	C_C
[-]	[-]	[%]	[%]	[%]						[%]		
VA21a	GW	-	-	-	13.8	6.6	1.7	0.8	0.3	3.3	25.1	1.7
ALF	SM	27	31	5		0.2				41.6		
HPC	CH-MH	38	65	27						81.7		

Figure 3-1 shows the gradation of the materials. The gradations were obtained per AASHTO T-27 for VA21a and per AASHTO T-11 and T-27 (wet and dry sieve analysis) for the ALF and HPC soils. The gradations were monitored throughout all phases of the project to ensure uniformity.

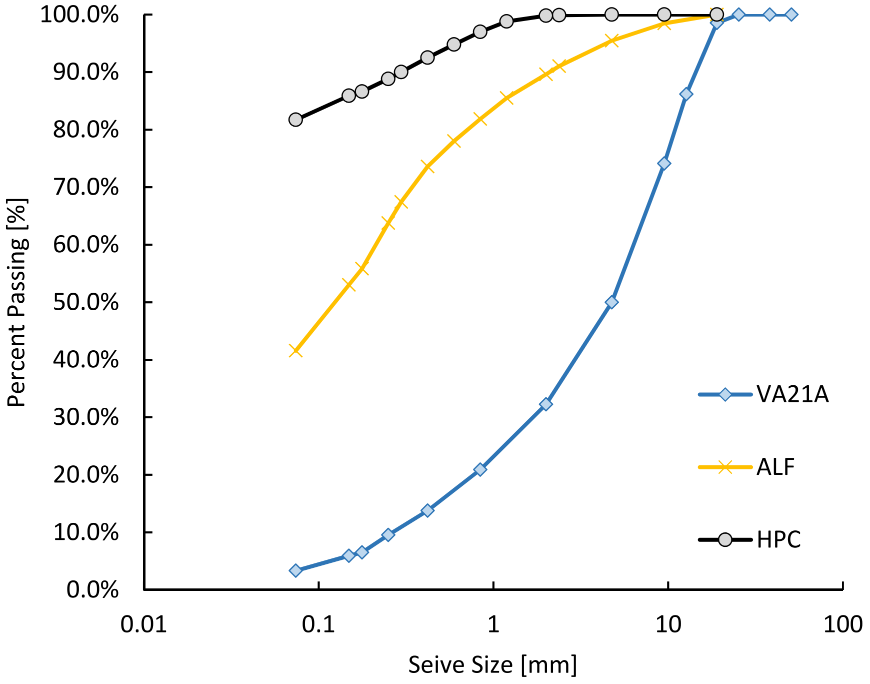

Figure 3-1. Gradation of the materials used in this study

The moisture-density relationships were determined for all three materials. Table 3-2 presents the optimum moisture content (OMC), maximum dry density (MDD) and bulk specific gravity of the test material. Figure 3-2 presents the moisture- density curves for all soils.

Table 3-2. OMC, MDD and Specific gravity of the test material

Soil Type	AASHTO Procedure	Method	Compaction energy	MDD	OMC	Specific Gravity[1]
[-]	[-]	[-]	[-]	kg/m^3 (pcf)	[%]	[-]
VA21a	T-99	D	Standard	2307.7 (144.0)	5.0	2.77
VA21a	T-180	D	Modified	2435.9 (152.0)	4.5	
ALF	T-99	C	Standard	1923.1 (120.0)	11.5	2.71
ALF	-	C	Semi Modified[2]	2003.2 (125.0)	10.5	
ALF	T-180	C	Modified	2083.3 (130.0)	9.5	
HPC	T-99	A	Standard	1522.4 (95.0)	24.0	2.66

(1) Specific gravity test per AASHTO T-84 and T-85

(2) Customized compaction energy: 3 layers, 25 drops per layer using a 4.54 kg rammer and a 457-mm drop

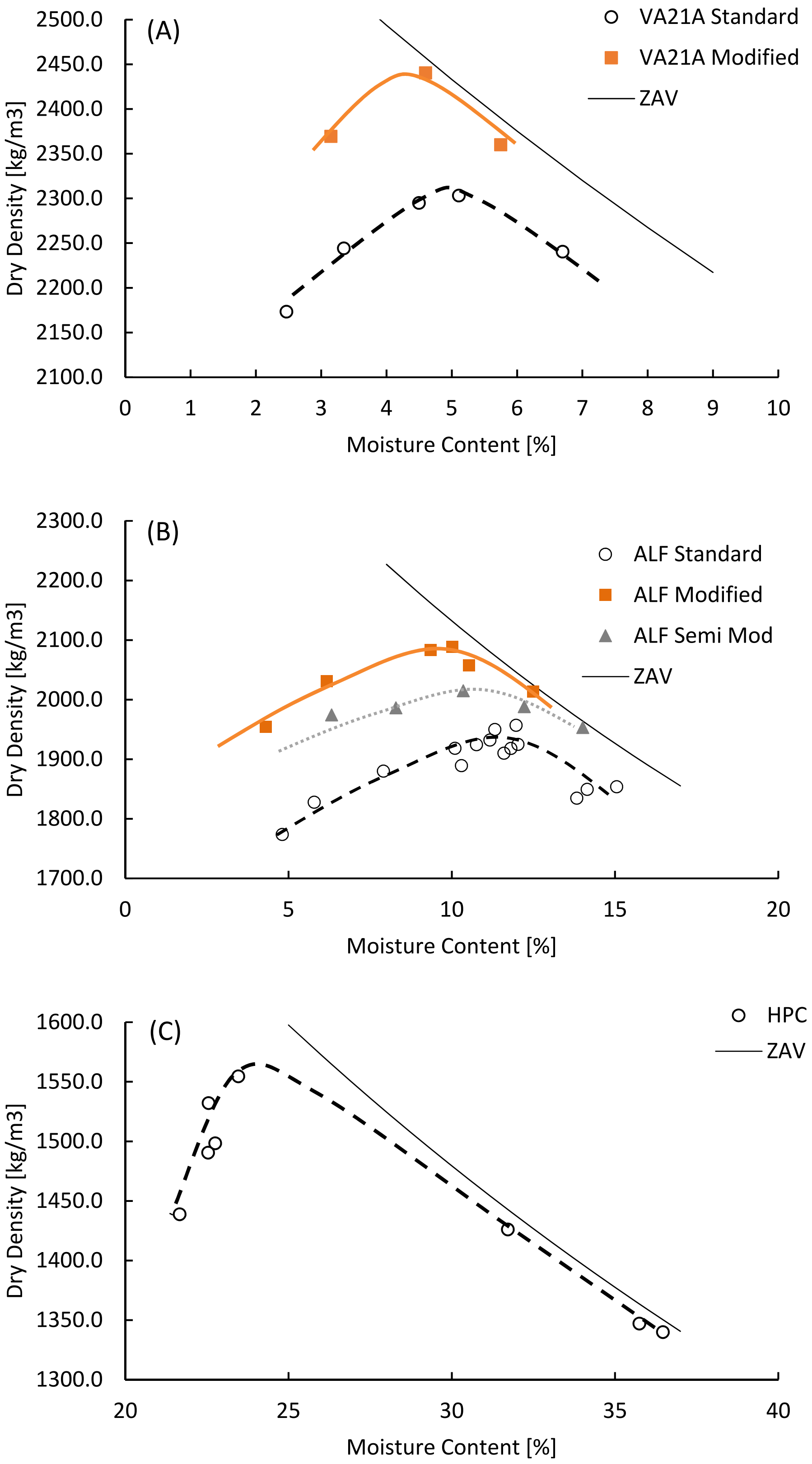

Figure 3-2. Moisture-Density relationships for (A) VA21a, (B) ALF, and (C) HPC.

3.2. Soil Water Characteristic Curve (SWCC)

The SWCC is the constitutive relationship existing between the degree of saturation of a soil (S) or volumetric water content and the associated matric suction. The degree of saturation is expressed by:

$$S = \frac{V_w}{V_v}$$ **Equation 3-1**

The SWCC is an important constitutive relationship for unsaturated soils. The typical shape of the soil-water characteristic curve is showed in Figure 3-3. The suction (usually in logarithmic scale) increases as the degree of saturation (S) decreases. SWCC consists of three different zones as shown in Figure 3-3.

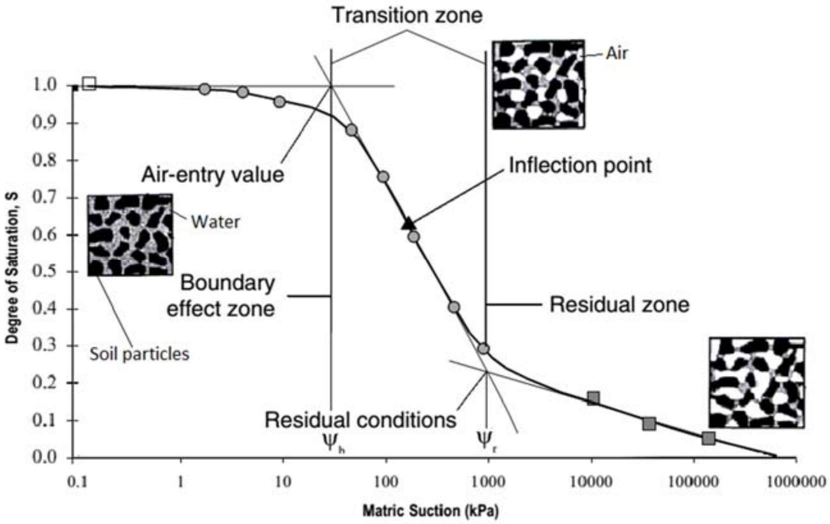

Figure 3-3. Schematic of the 3 zones of SWCC (Fredlund and Xing, 1994)

In the first zone, known as the boundary effect zone, the suction is low and the soil is in a completely saturated condition. An increment of reduction in degree of saturation (S) does not generate a substantial increase in suction. This situation continues until some air bubbles start to appear in the soil skeleton. The suction associated with this point is known as air-entry value, indicated as $(u_a\text{-}u_w)_b$ or ψ_b.

The second part of SWCC is called the transition zone. It starts at the air-entry value. In this zone, an increment of reduction in degree of saturation is associated with a considerable increase in suction.

In the third part of curve, called the residual zone, a very significant reduction in degree of saturation is required for any further increase of suction. The suction value at the start of the third zone is marked as ψ_r and the associated S is known as the residual degree of saturation (S_r).

The SWCC is commonly formulated as a nonlinear sigmoid function using the four-parameter equation proposed by Fredlund and Xing (1994):

$$\theta_w = c(h) \times \left[\frac{\theta_{sat}}{\left[\ln \left[\exp(1) + \left(\frac{h}{a_f} \right)^{b_f} \right] \right]^{c_f}} \right]$$ **Equation 3-2**

$$c(h) = \left[1 - \frac{\ln\left(1 + \frac{h}{h_r}\right)}{\ln\left(1 + \frac{10^6}{h_r}\right)} \right]$$ **Equation 3-3**

where: θ_w = volumetric water content,
h = matric suction in kPa,
a_f = fitting parameter, which is primarily a function of the air entry value of the soil,
b_f = fitting parameter, which is primarily a function of the rate of water extraction from the soil, once the air entry value has been exceeded,
c_f = fitting parameter, which is primarily a function of the residual water content,
h_{rf} = fitting parameter, which is primarily a function of the suction at which residual water content occurs, and

C(h) = correction factor which is a function of matric suction.

While SWCC can be directly measured in the lab, there are several studies that predict the SWCC parameters based on the gradation and soil index properties. In this study, the empirical model in the Mechanistic-Empirical Pavement Design Guide (MEPDG) was used to obtain the fitting parameters of the Fredlund and Zing SWCC equation. These equations are as follows:

(i)

$$\begin{aligned} &\text{if } P_{200}PI > 0 \\ &a_f = 0.00364\left(P_{200}PI\right)^{3.35} + 4\left(P_{200}PI\right) + 11, \text{ kPa} \\ &\frac{b_f}{c_f} = -2.313\left(P_{200}PI\right)^{0.14} + 5 \\ &c_f = 0.0514\left(P_{200}PI\right)^{0.465} + 0.5 \\ &\frac{h_r}{a_f} = 32.44e^{0.0186\left(P_{200}PI\right)} \end{aligned}$$ **Equation 3-4**

(ii)

$$
\begin{aligned}
&\text{if } P_{200}PI = 0\\
&a_f = 0.8627\left(D_{60}\right)^{-0.751}, \text{ kPa}\\
&\bar{b}_f = 7.5\\
&c_f = 0.1772\ln\left(D_{60}\right) + 0.7734\\
&\frac{h_r}{a_f} = \frac{1}{D_{60} + 9.7e^{-4}}
\end{aligned}
$$

Equation 3-5

The predicted SWCC for the test soils is shown in Figure 3-4.

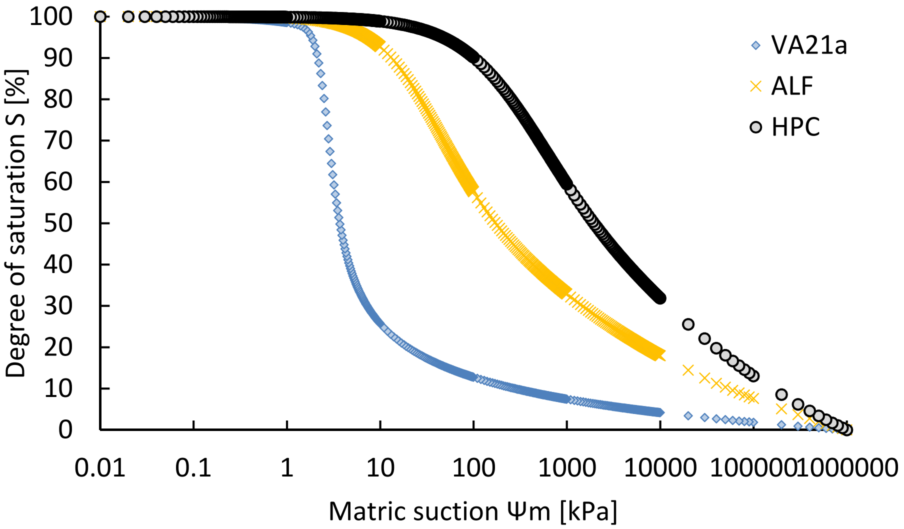

Figure 3-4. SWCC for the material used in this study

3.3. Resilient Modulus Sample Preparation and Testing

The Resilient Modulus (M_R) of unbound materials is determined by repeated load triaxial compression tests per the AASHTO T-307 in the laboratory. Table 3-3 summarizes the testing plan for the M_R tests performed in the lab.

Each cycle of the axial stress is a haversine shape pulse with the duration of 0.1 second and the rest period of 0.9 second. During the rest period, a contact stress equal to 10% of the maximum axial stress (σ_{max}) is maintained. The cyclic stress (σ_{cyclic}) is therefore equal to σ_{max}- $\sigma_{contact}$= 90% σ_{max}.

M_R is defined as the ratio of the amplitude of the repeated axial cyclic stress (σ_{cyclic}) to the amplitude of the resultant recoverable axial strain (ε_r). Figure 3-5 and Figure 3-6 show the terms of a load pulse in M_R test, and the stress- strain relation for a given cycle in the test, respectively.

The tests were performed using a 100 kN Servo Hydraulic Dynamic Universal Testing Machine (UTM-100) from IPC Global in the University of Maryland Pavement Materials Laboratory (Figure 3-7). The original 100 kN capacity load cell of the machine was replaced with a smaller and hence more delicate load cell with a 6 kN capacity. Two external linear variable differential transformers (LVDT)s were used to record the deformations under the cyclic dynamic haversine load.

The samples were prepared in molds with a height to diameter ratio of 2 using the Proctor hammer. These molds are taller than those used in a conventional Proctor compaction test (Figure 3-7). The number of layers and drops per layer were adjusted for the tall M_R molds to achieve the densities like that of the Proctor test. Table 3-4 lists the adjusted numbers of layers and drops per layer used in compaction of the M_R samples unless otherwise stated (i.e., for the case of less than standard compaction for ALF Pit 1 material).

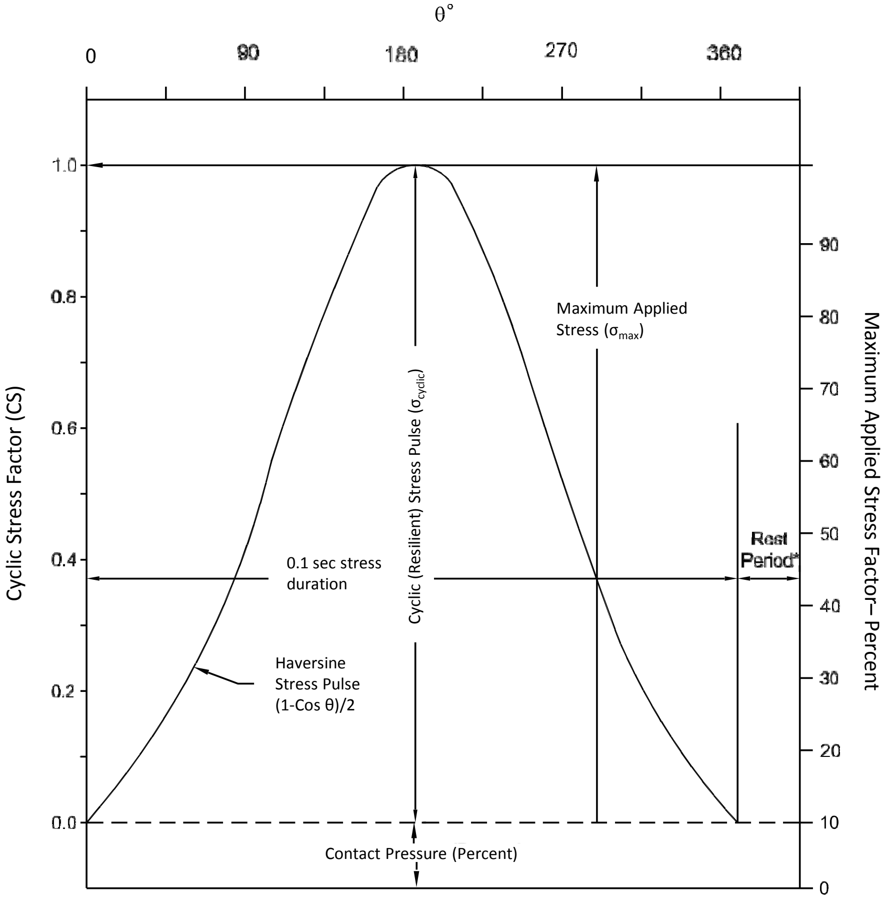

* The rest period will be 0.9 s for hydraulic loading devices

Figure 3-5. Resilient Modulus Terms: contact stress, cyclic axial stress (σ_{cyclic}), and maximum resilient vertical stress (σ_{max}) (AASHTO T-307)

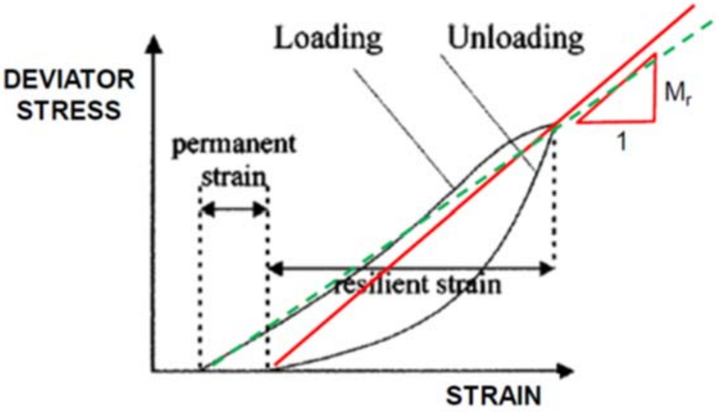
DEVIATOR STRESS
Loading
Unloading
M_r
1
permanent strain
resilient strain
STRAIN

Figure 3-6. Stress-strain relationship in M_R test

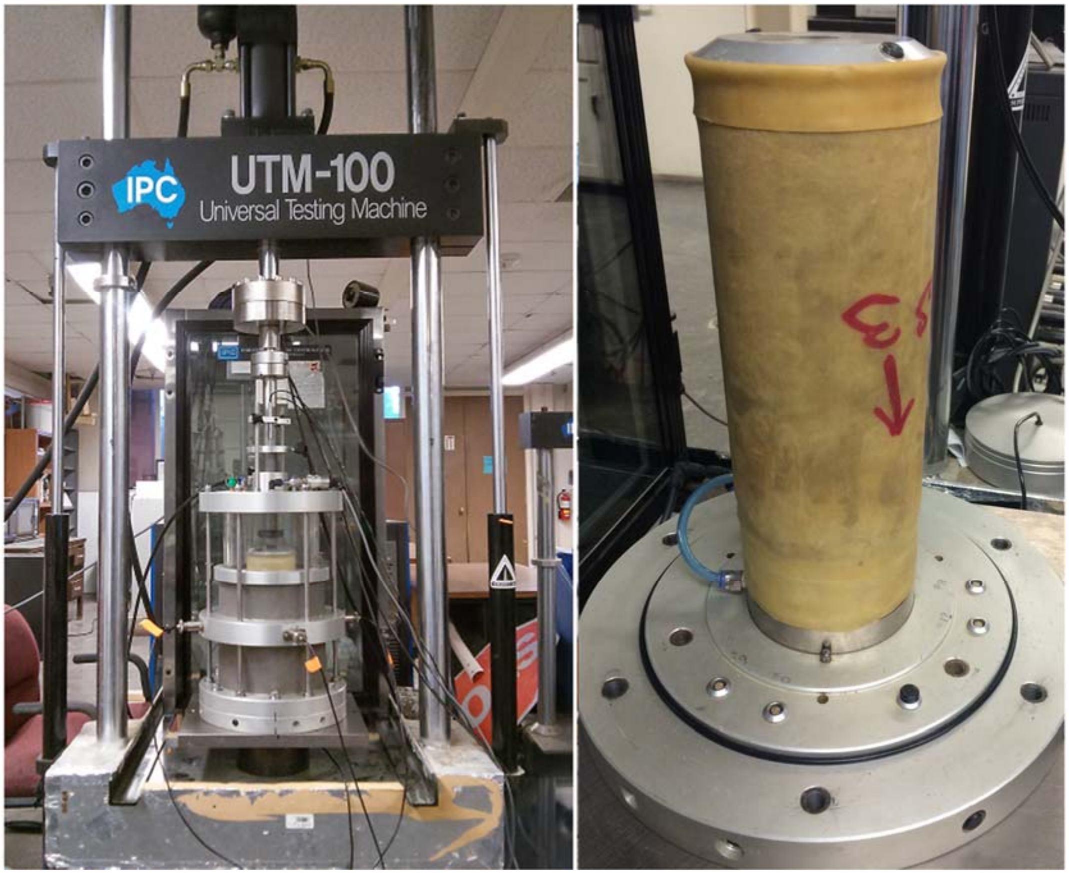
IPC
UTM-100
Universal Testing Machine
35

Figure 3-7. UTM- 100 apparatus and sample

Table 3-3. Testing plan for M_R testing according to AASHTO T-307

Soil Type	**Target MC**	**Target DD**	**Mold diameter**	**Compaction energy**	**Condition**	**# of Replicate**	**Base or Subgrade Procedure**
[-]	[%]	[kg/m^3 (pcf)]	[mm]	[-]	[-]	[-]	[-]
VA21a	4.5	2435 (152)	150	Modified	Optimum-Pit 2, Pit 3	2	Base
ALF	11.5	1922.2 (120.0)	100	Standard	Optimum	3	Subgrade+Base
ALF	15.3	1837.3 (114.7)	100	Standard	Pit 2	2	Subgrade+8 cycles of Base
ALF	10.0	1771.2 (110.6)	100	<standard[1]	~Pit 1	2	Subgrade+Base
HPC	24.0	1521.8 (95.0)	100	Standard	Optimum	2	Subgrade+Base
HPC	29.0	1457.7 (91.0)	100	Standard	Pit 3	2	Subgrade+8 cycles of Base

(1) 3 layers- 15 drops per layer

Table 3-4. The mold dimensions, number of layers and drops per layer for Proctor molds and M_R molds for standard and modified compaction energy

Proctor Mold		**Standard (T-99)**		**Modified (T-180)**	
		100 mm mold	150 mm mold	100 mm mold	150 mm mold
Weight of the hammer	[kg]	2.495	2.495	4.54	4.54
Height of drop	[m m]	305	305	457	457
Number of drops per layer	[-]	25	56	25	56
Number of layers	[-]	3	3	5	5
Diameter of mold	[mm]	101.6	152.4	101.6	152.4
Height of mold	[mm]	116.3	116.3	116.3	116.3
Volume of mold	[cm^3]	0.94	2.12	0.94	2.12
Compaction energy/volume	[kNm/m^3]	594	591	2698	2686
M_R Mold		**Standard**		**Modified**	
		100 mm mold	150 mm mold	100 mm mold	150 mm mold
Weight of the hammer	[kg]	2.495	2.495	4.54	4.54
Height of drop	[mm]	305	305	457	457
Number of drops per layer	[-]	26	48	31	59
Number of layers	[-]	5	9	7	12
Diameter of mold	[mm]	101.6	152.4	101.6	152.4
Height of mold	[mm]	203.2	295.02	203.2	295.02
Volume of mold	[cm^3]	1.65	5.38	1.65	5.38
Compaction energy/volume	[kNm/m^3]	589	599	2681	2678

The load combinations are chosen based on the location of the material in the pavement structure—whether it is a subgrade or base, and Table 3-6 present the test sequences for subgrade and base soils, respectively.

Table 3-5. Testing sequence for subgrade soils

Sequence No.	Confining Pressure, σ_3		Max. Axial Stress, σ_{max}		Cyclic Stress, σ_{cyclic}		Constant Stress, $0.1\ \sigma_{max}$		No. of Load Applications
-	kPa	psi	kPa	psi	kPa	psi	kPa	psi	-
0	41.4	6	27.6	4	24.8	3.6	2.8	0.4	500–1000
1	41.4	6	13.8	2	12.4	1.8	1.4	0.2	100
2	41.4	6	27.6	4	24.8	3.6	2.8	0.4	100
3	41.4	6	41.4	6	37.3	5.4	4.1	0.6	100
4	41.4	6	55.2	8	49.7	7.2	5.5	0.8	100
5	41.4	6	68.9	10	62.0	9.0	6.9	1.0	100
6	27.6	4	13.8	2	12.4	1.8	1.4	0.2	100
7	27.6	4	27.6	4	24.8	3.6	2.8	0.4	100
8	27.6	4	41.4	6	37.3	5.4	4.1	0.6	100
9	27.6	4	55.2	8	49.7	7.2	5.5	0.8	100
10	27.6	4	68.9	10	62.0	9.0	6.9	1.0	100
11	13.8	2	13.8	2	12.4	1.8	1.4	0.2	100
12	13.8	2	27.6	4	24.8	3.6	2.8	0.4	100
13	13.8	2	41.4	6	37.3	5.4	4.1	0.6	100
14	13.8	2	55.2	8	49.7	7.2	5.5	0.8	100
15	13.8	2	68.9	10	62.0	9.0	6.9	1.0	100

Table 3-6. Testing sequence for base soils

Sequence No.	Confining Pressure, σ_3		Max. Axial Stress, σ_{max}		Cyclic Stress, σ_{cyclic}		Constant Stress, 0.1 σ_{max}		No. of Load Applications
-	kPa	psi	kPa	psi	kPa	psi	kPa	psi	-
0	103.4	15	103.4	15	93.1	13.5	10.3	1.5	500–1000
1	20.7	3	20.7	3	18.6	2.7	2.1	0.3	100
2	20.7	3	41.4	6	37.3	5.4	4.1	0.6	100
3	20.7	3	62.1	9	55.9	8.1	6.2	0.9	100
4	34.5	5	34.5	5	31.0	4.5	3.5	0.5	100
5	34.5	5	68.9	10	62.0	9.0	6.9	1.0	100
6	34.5	5	103.4	15	93.1	13.5	10.3	1.5	100
7	68.9	10	68.9	10	62.0	9.0	6.9	1.0	100
8	68.9	10	137.9	20	124.1	18.0	13.8	2.0	100
9	68.9	10	206.8	30	186.1	27.0	20.7	3.0	100
10	103.4	15	68.9	10	62.0	9.0	6.9	1.0	100
11	103.4	15	103.4	15	93.1	13.5	10.3	1.5	100
12	103.4	15	206.8	30	186.1	27.0	20.7	3.0	100
13	137.9	20	103.4	15	93.1	13.5	10.3	1.5	100
14	137.9	20	137.9	20	124.1	18.0	13.8	2.0	100
15	137.9	20	275.8	40	248.2	36.0	27.6	4.0	100

The MEPDG universal constitutive model was fit to the experimental data.

$$M_R = k_1 . p_a \left(\frac{\theta}{p_a}\right)^{k_2} . \left(\frac{\tau_{oct}}{p_a} + 1\right)^{k3}$$ **Equation 3-6**

where:

M_R = resilient modulus;
$\theta = \sigma_1 + \sigma_2 + \sigma_3 = \sigma_1 + 3 \cdot \sigma_3$ = bulk stress;
$\tau_{oct} = \frac{1}{3} \cdot \sqrt{(\sigma_1 - \sigma_2)^2 + (\sigma_1 - \sigma_3)^2 + (\sigma_2 - \sigma_3)^2}$ = octahedral shear stress;
p_a = atmospheric pressure used to normalize the equation;
k_1, k_2, k_3 = regression constants determined from the laboratory tests.

The regression coefficient k_1 in MEPDG model is a positive number that is directly proportional to the modulus. The coefficient k_2 is a positive value and is known as the stress hardening term;

this is most significant in granular material. The coefficient k_3 is a negative value, known as the stress softening term. The k_3 coefficient is more significant in clay, showing a reduction of modulus with an increase of the octahedral shear stress.

Table 3-7, Table 3-8, and Table 3-9 summarize the average test results and the coefficients of the M_R universal constitutive model for the ALF, HPC, and VA21a soils, respectively. For individual results for each test specimen please refer to Khosravifar (2015).

Table 3-7. ALF M_R test results

Sample ID	**[-]**	**OPT**	**Pit 2**	**~Pit 1**
Achieved MC	[%]	11.9%	14.6%	9.4%
Achieved DD	[pcf]	118.9	116.5	110.6
	[kg/m3]	1904.3	1867.0	1771.2
Pa	[kPa]	101.3	101.3	101.3
k1	[-]	1437.4	177.6	793.9
k2	[-]	0.429	0.485	0.601
k3	[-]	-3.717	0.000	-2.023
SSE	[MPa^2]	131.6	384.1	1635.8
Sqr(SSE)	[MPa]	11.5	19.60	40.44
R^2	[MPa^2]	98.1%	58.7%	66.2%
R^2_adj	[MPa^2]	97.6%	52.8%	61.4%
Max Sample-to-Sample COV of M_R at different stress states	[%]	32.5%	27.9%	5.0%
Average Sample-to-Sample COV of M_R at different stress states	[%]	16.2%	13.2%	1.8%

Table 3-8. HPC M_R test results

Test Condition/ Material	[-]	OPT	Pit 3
Achieved MC	[%]	24.5	30.8
Achieved DD	[pcf]	93.6	89.4
	[kg/m3]	1499.2	1432.1
Pa	[kPa]	101.3	101.3
k1	[-]	888.8	583.4
k2	[-]	0.378	0.095
k3	[-]	-0.843	-1.789
SSE	[MPa^2]	2261.6	259.0
Sqr(SSE)	[MPa]	47.56	16.09
R^2	[MPa^2]	26.8	81.0
R^2_adj	[MPa^2]	16.4	78.3
Max Sample-to-Sample COV of M_R at different stress states	[%]	6.4	18.7
Average Sample-to-Sample COV of M_R at different stress states	[%]	2.4	5.3

Table 3-9. VA21a M_R test results

Sample ID	[-]	VA21a__Ave OMC
Achieved MC	[%]	3.7
Achieved DD	[pcf]	153.4
	[kg/m3]	2458.0
Pa	[kPa]	101.3
k1	[-]	590.6
k2	[-]	0.824
k3	[-]	0.000
SSE	[MPa2]	2765.0
Sqr(SSE)	[MPa]	52.58
R2	[MPa2]	96.6
R2_adj	[MPa2]	95.7
Max Sample-to-Sample COV of MR at different stress states	[%]	47.9
Average Sample-to-Sample COV of MR at different stress states	[%]	17.6

3.4. Evaluated Unsaturated Resilient Modulus Constitutive Models

Four types of subgrade and four types of granular base soil data from Andrei (2003) were used to evaluate the models. The soil type and description for each material is presented in

Table 3-10. All base materials and one of the subgrade soils were non-plastic. More information about the volumetric and mechanical properties of the soils can be found in Andrei (2003).

The soil water characteristic curves, which were key inputs to the evaluated models, were predicted from the gradation and soil indices using the Fredlund and Xing (1994) procedure as implemented in the MEPDG. The unconfined compression (U_C), which was input to one of the predictive models, was estimated from CBR values according to Black (1962).

For all the soils, the M_R tests were performed on specimens compacted with standard and modified Proctor energies at their corresponding optimum moisture content as well as above and below optimum. This resulted in a total of 6 scenarios for each soil.

Table 3-10- Soil Type and Description (From Andrei, 2003)

	Soil Types	**Description**
Subgrade	Phoenix Valley Subgrade (PVSG)	Clayey Sand, SC
	Yuma Sand Subgrade (YSSG)	Poorly Graded Gravel with Sand, GP, Non Plastic
	Flagstaff Clay Subgrade (FCSG)	Clayey Sand, SC
	Sun City Subgrade (SCSG)	Clayey Sand, SC
Base	Grey Mountain Base (GMAB2)	Well Graded Gravel with Sand, GW, Non Plastic
	Salt River Base (SRAB2)	Poorly Graded Sand with Gravel, SP, Non Plastic
	Globe Base (GLAB2)	Poorly Graded Sand with Silt and Gravel, SP-SM, Non Plastic
	Prescott Base (PRAB2)	Poorly Graded Sand with Silt and Gravel, SP-SM, Non Plastic

The 9 following models were selected for evaluation. The parameters of the following models were calibrated—except for M4 and M6 predictive models—based on the measured data at optimum moisture content and maximum dry density of the standard Proctor compaction test scenario. The models where subsequently used to predict the M_R at the other moisture-density conditions. The evaluated models are explained below:

M1 is the general nonlinear model implemented in the MEPDG and is a function of total bulk stresses. This model does not consider the effect of suction *u*.

M1: $$\boldsymbol{M_R = K_1 P_a \left(\frac{\sigma_{bulk}}{P_a}\right)^{K_2} \left(\frac{\tau_{oct}}{P_a} + 1\right)^{K_3}}$$ **Equation 3-7** in which $\sigma_{bulk} = \sigma_1 + \sigma_2 + \sigma_3 = \sigma_d + 3\sigma_c$, $\sigma_1, \sigma_2, \sigma_3$ = three principal stresses, σ_d= deviatoric stress, σ_c= confining stress, τ_{oct}= octahedral shear stress = $\frac{\sqrt{3}}{2}\sigma_d$, and the coefficients K_1, K_2, and K_3 are regression coefficients.

M2, the second evaluated model, is similar to M1, with the bulk effective stress ($\sigma_{bulk} + 3u$) replacing σ_{bulk}. The reason for the multiplication of suction by 3 is that suction adds to each of the three principal effective stresses.

M2: $\boldsymbol{M_R = K_1 P_a \left(\frac{\sigma_{bulk}+3u}{P_a}\right)^{K_2} \left(\frac{\tau_{oct}}{P_a} + 1\right)^{K_3}}$ **Equation 3-8**

M3, proposed by Liang et al (2008) adds a suction dependency term (χ) to the effective stress term. The suction dependency term was proposed by Khalili and Khabbaz (1998). In this model the suction term (u) is not multiplied by 3.

M3: $\boldsymbol{M_R = K_1 P_a \left(\frac{\sigma_{bulk}+\chi u}{P_a}\right)^{K_2} \left(\frac{\tau_{oct}}{P_a} + 1\right)^{K_3}}$ **Equation 3-9**

$\boldsymbol{\chi = \left(\frac{(u_a - u_w)_b}{u_a - u_w}\right)^{0.55} = \frac{u_{air-entry}}{u}}$ **Equation 3-10**

The $u_{air-entry}$ term is the suction at air entry level where air starts to enter the largest pores in the soil. The upper limit of χ is equal to 1.

M4, proposed by Siekmeier (2011), has been found a suitable predictive model for subgrade and fine soils. The K_1-K_3 coefficients are also predicted as a function of suction and volumetric moisture content from SWCC of the soils. The equations are as follows:

M4: $\boldsymbol{M_R = K_1 P_a \left(\frac{\sigma_{bulk}+\theta_w f u}{P_a}\right)^{K_2} \left(\frac{\tau_{oct}}{P_a} + 1\right)^{K_3}}$ **Equation 3-11**

in which $K_1 = 800 \times \left(\frac{1}{5\theta_{sat}}\right)^{1.5} \times \left(\frac{1}{log_{10}(u)}\right)$, $K_2 = log_{10}(u) - 1$, $K_3 = -8\theta_{sat}$,

$f = \theta_w^{10\theta_{sat}^3}$, θ_w= volumetric water content, θ_{sat}= volumetric water content at saturation, and $\chi = \theta_w f$.

The χ in M4 model is not bracketed by the upper bound of 1. The M4 predictive model was re-evaluated as model M5, in which the K values were calibrated for each soil through nonlinear regression. The formula for *f* was kept the same.

Yan et al. (2013) proposed two predictive models for subgrade soils based on gene expression programming (GEP) to correlate M_R with routine properties of subgrade soils and state of stress. GEP I was computationally unstable for non-plastic soils and was found erroneous for plastic soil and has thus been excluded from the comparisons. The GEP II model, selected for evaluation as model M6—is displayed below:

Equation 3-12

$$\text{M6: } M_R = \text{atan}\left\{\gamma_d * \left[\frac{\gamma_d - U_c}{PI}\right]\right\} + \left\{2 * \left[\frac{sqrt(PI)}{P_{200}}\right]\right\} + \sigma_d + \left\{2 * \sin\left[\frac{\gamma_d * \exp\{\text{atan}[\sin(P_{200})]\}}{P_{200}}\right]\right\} + (\sigma_d * \text{atan}\{sqrt(P_{200}) - [(\sigma_d * P_{200})/\gamma_d]\}) + \{\text{atan}[sqrt(U_c) - \gamma_d] + \text{atan}(\gamma_d)\}$$

in which *Uc* = unconfined compressive strength, *PI* = Plasticity Index, *P200* = percentage passing the No. 200, γ_d= dry density, and σ_d= deviatoric stress.

Recently, Gu et al. (2014) evaluated a model proposed by Lytton (1995) and reported satisfactory predictions for base course aggregates. The model is:

$$\boldsymbol{M_R = K_1 P_a \left(\frac{\sigma_{bulk} - 3\theta_w f u}{P_a}\right)^{K_2} \left(\frac{\tau_{oct}}{P_a}\right)^{K_3}}$$ **Equation 3-13**

The *f* parameter in this model is a function of θ_a and θ_u, which are the volumetric water contents of the soil at air entry and unsaturation, respectively. The parameter *f* is bracketed by the upper and lower bounds below:

$$\boldsymbol{f_{upper\ bound} = \left[\left(\frac{\theta_a - \theta_w}{\theta_a - \theta_u}\right) + \frac{1}{\theta_w}\left(\frac{\theta_w - \theta_u}{\theta_a - \theta_u}\right)\right]}$$ **Equation 3-14**

$$\boldsymbol{f_{lower\ bound} = \left[\frac{1}{\left(\frac{\theta_a - \theta_w}{\theta_a - \theta_u}\right) + \theta_w\left(\frac{\theta_w - \theta_u}{\theta_a - \theta_u}\right)}\right]}$$ **Equation 3-15**

Three *f* values were evaluated in the Lytton model to predict the resilient modulus, resulting in the following models. $\chi = \theta_w f$ ranges from $\theta_u$to 1 and therefore is theoretically sound.

M7 based on $f = \frac{f_{upper\ bound} + f_{lower\ bound}}{2}$, **M8** based on $f = f_{upper\ bound}$, and **M9** based on $f = f_{lower\ bound}$. Figure 3-8 shows the bounds of the pore suction for Lytton (1995) model.

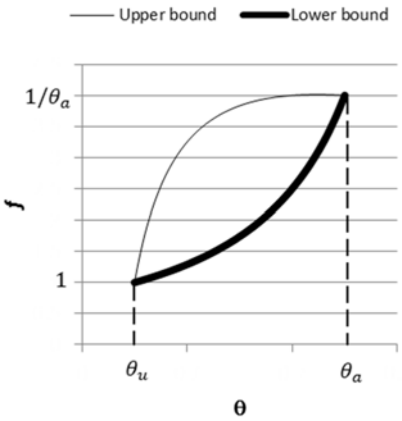

Figure 3-8. The bounds of pore suction for Lytton (1995).

3.5. Comparison of Evaluated M$_R$ Predictive Models

Least squares analysis was applied to the measured data at optimum moisture content and maximum standard dry density for all models except for the M4 and M6 predictive models to find the best model. To evaluate the performance of the models, the root mean square error (RMSE) and average relative error (RE) of model prediction were calculated at each moisture condition (wet, dry, optimum), each compaction energy effort (standard and modified Proctor compaction effort), and overall for each soil and every model. RMSE, a measure of model accuracy, reflects both systematic and nonsystematic error variation and has the same units as M$_R$, here reported in ksi. RE measures the systematic error or bias of the models. The definitions of these evaluation criteria are given as follows:

$$\mathbf{RMSE} = \sqrt{\frac{1}{n}\sum_{i=1}^{n}\left((M_{R-predicted} - M_{R-measured})^2\right)} \qquad \textbf{Equation 3-16}$$

$$\mathbf{RE} = \frac{\frac{1}{n}\sum_{i=1}^{n}(M_{R-predicted} - M_{R-measured})}{\frac{1}{n}\sum_{i=1}^{n}(M_{R-measured})} = \bar{e}/\overline{M_R} \qquad \textbf{Equation 3-17}$$

Figure 3-9 shows the distribution of RMSE of the evaluated models at different moisture and compaction energy conditions. As expected, all the models performed well at the optimum moisture and density, the condition at which was the model parameters were calibrated. Prediction errors were the highest at dry of optimum at both compaction efforts. Figure 3-10 presents the prediction bias of the models for the plastic and non-plastic soils. Overall, all models underpredicted at dry of optimum for non-plastic soils.

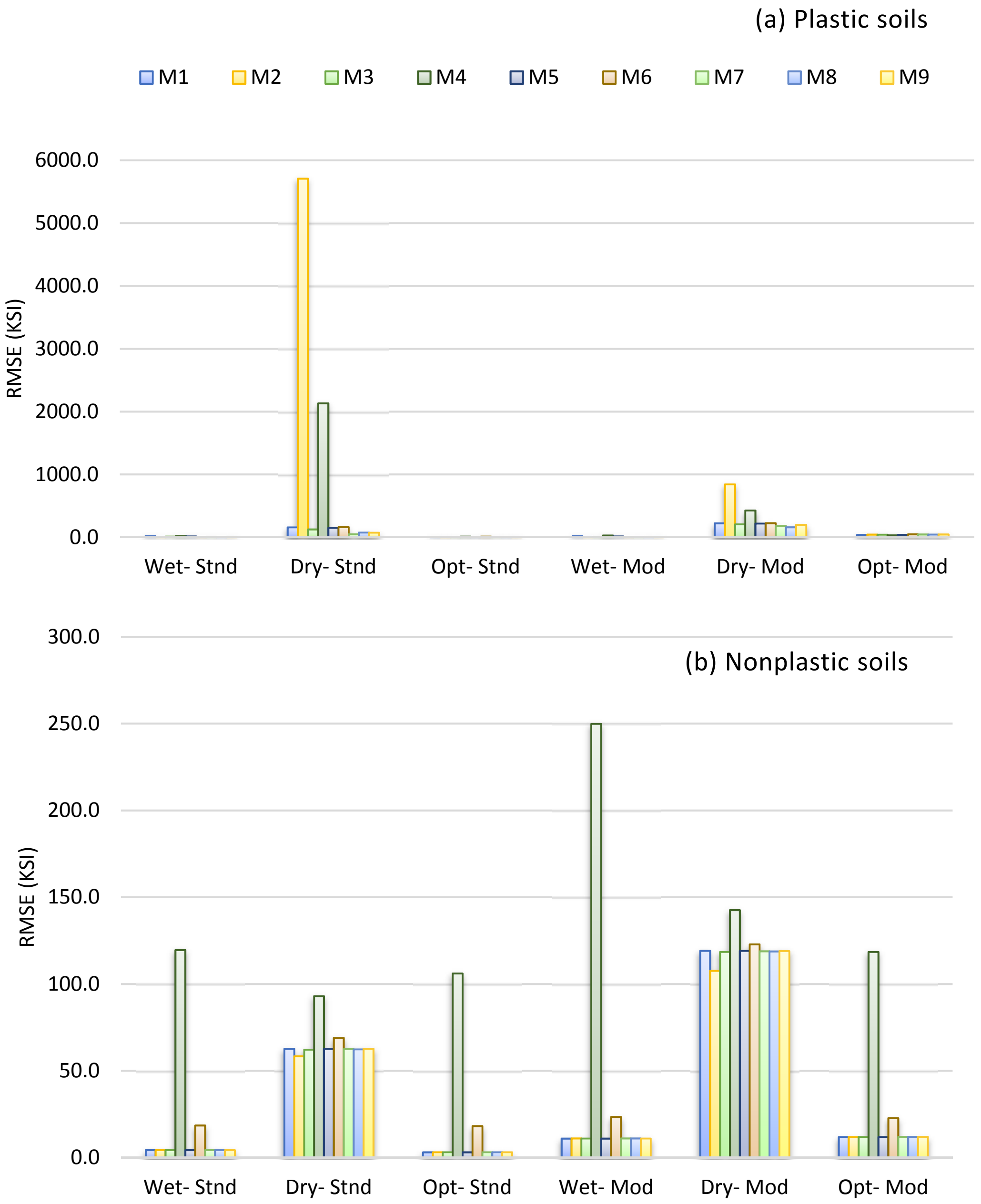

Figure 3-9. RMSE of evaluated models at different moisture and compaction energy condition for (a) Plastic, and (b) Non-plastic soils.

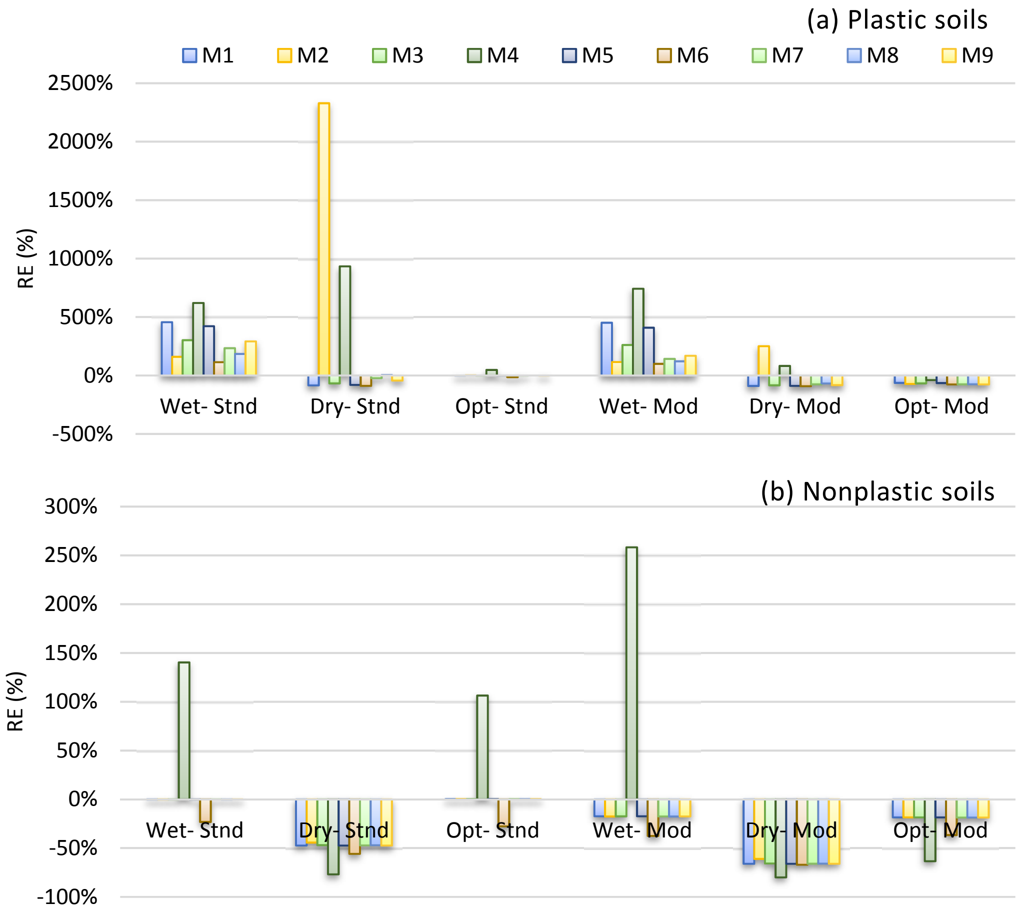

Figure 3-10. Average RE of evaluated models at different moisture and compaction energy condition for (a) Plastic, and (b) Nonplastic soils.

The overall RMSE of prediction of the models per soil is shown in

Table 3-11. The shaded cells in the table present the most accurate model. Overall, model M8—Lytton (1995) with $f_{\text{upper bound}}$—outperformed the other models for both plastic and neoplastic soils. The M2 model, which in fact is the effective stress model with f=1, performed very well for non-plastic soils but did not provide an acceptable prediction accuracy for plastic soils.

An example of the measured vs. predicted M_R by M2 for a plastic soil (PVSG) is shown in Figure 3-11 shows the RE for each model and soil type. Again, model M8 was overall the most consistent model for both plastic and non-plastic soils. Model M4 and M2, while outperformed in several soil types, were erroneous in several others and did not provide a consistent prediction over the range of the evaluated soils.

Figure 3-12 presents the RMSE and RE for model M8 at different moisture and compaction effort conditions. M8, although better than the other models, under predicted the moduli at dry of optimum and optimum moisture at the modified compaction condition for all soils and over predicted at wet of optimum for the standard and modified compaction conditions of the plastic soils.

Figure 3-13 shows the measured vs. predicted M_R for GMAB and PVSG for the M8 model. These two soils provided the most and least accurate predictions, respectively.

Table 3-11. Overall RMSE of the evaluated models for each soil.

RMSE (ksi)	M1	M2	M3	M4	M5	M6	M7	M8	M9
1.PVSG	143.0	3452.0	129.8	292.4	139.8	141.9	99.9	90.3*	118.0
2.YSSG	88.0	67.9	87.1	268.4	87.9	96.8	87.5	87.4	87.5
3.FCSG	49.6	49.6	49.2	46.2	49.7	55.0	51.4	50.9	52.1
4.SCSG	107.7	2964.4	86.9	2138.2	102.7	110.4	57.8	60.4	64.9
5.GMAB	26.9	26.8	26.9	196.0	26.9	37.5	26.9	26.9	26.9
6.SRAB	48.3	44.5	48.0	81.6	48.3	50.3	48.3	48.1	48.4
7.GLAB	41.1	39.9	40.9	67.3	41.1	43.3	41.0	40.9	41.1
8.PRAB	47.0	46.0	46.9	208.7	47.0	47.7	47.0	47.0	47.1
Plastic	100.1	2155.3	88.6	825.6	97.4	102.4	69.7	67.2	78.3
NonPlastic	50.3	45.0	49.9	164.4	50.2	55.1	50.1	50.1	50.2
All	69.0	836.4	64.5	412.3	67.9	72.9	57.5	56.5	60.8

* The shaded cells show the model yielded the lowest RMSE of prediction for each Soil type.

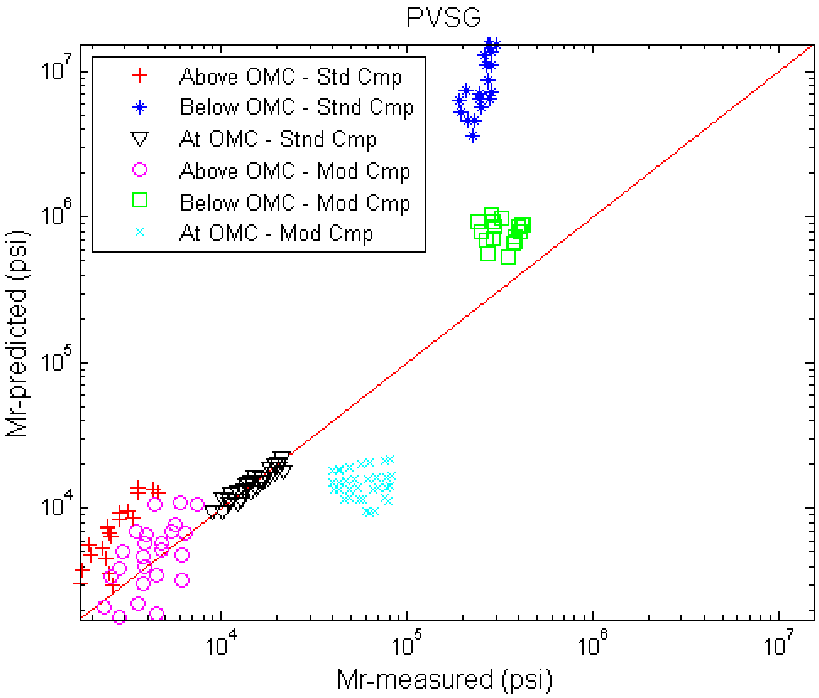

Figure 3-11. $M_{R\text{-predicted}}$ VS. $M_{R\text{-measured}}$ - Model M2 for Soil PVSG.

Table 3-12. Overall relative bias of the evaluated Models for each soil.

RE, %	M1	M2	M3	M4	M5	M6	M7	M8	M9
1.PVSG	-83%	1310%	-76%	85%	-81%	-86%	-53%	-30%	-68%
2.YSSG	-55%	-43%	-55%	127%	-55%	-80%	-55%	-55%	-55%
3.FCSG	-58%	-66%	-65%	-51%	-60%	-75%	-70%	-69%	-71%
4.SCSG	-71%	1789%	-58%	1240%	-67%	-83%	-21%	-5%	-35%
5.GMAB	-23%	-23%	-23%	16%	-23%	-40%	-23%	-23%	-23%
6.SRAB	-36%	-34%	-36%	-28%	-36%	-41%	-36%	-36%	-36%
7.GLAB	-32%	-31%	-32%	-36%	-32%	-38%	-32%	-32%	-32%
8.PRAB	-35%	-34%	-35%	-50%	-35%	-41%	-35%	-35%	-35%

* The shaded cells show the model yielded the lowest RMSE of prediction for each Soil type.

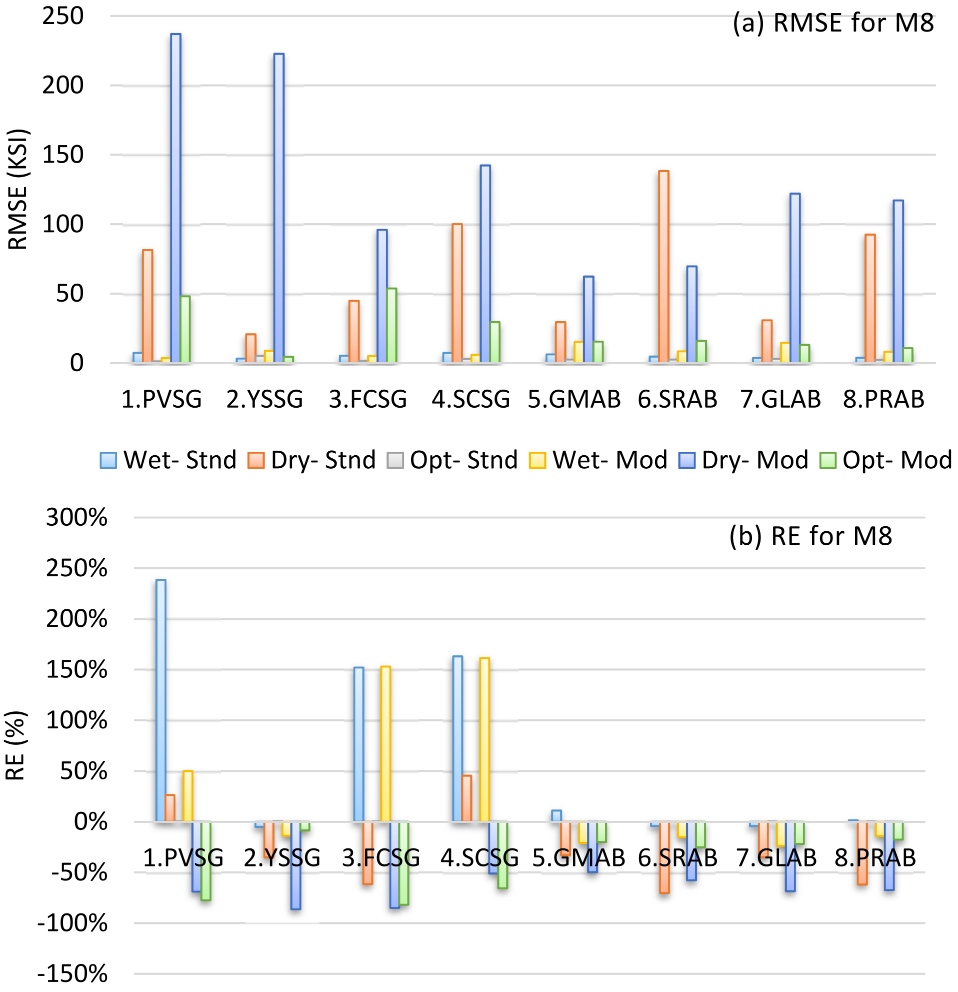

Figure 3-12. (a) RMSE and (b) RE at different moisture and compaction energy conditions for Model 8.

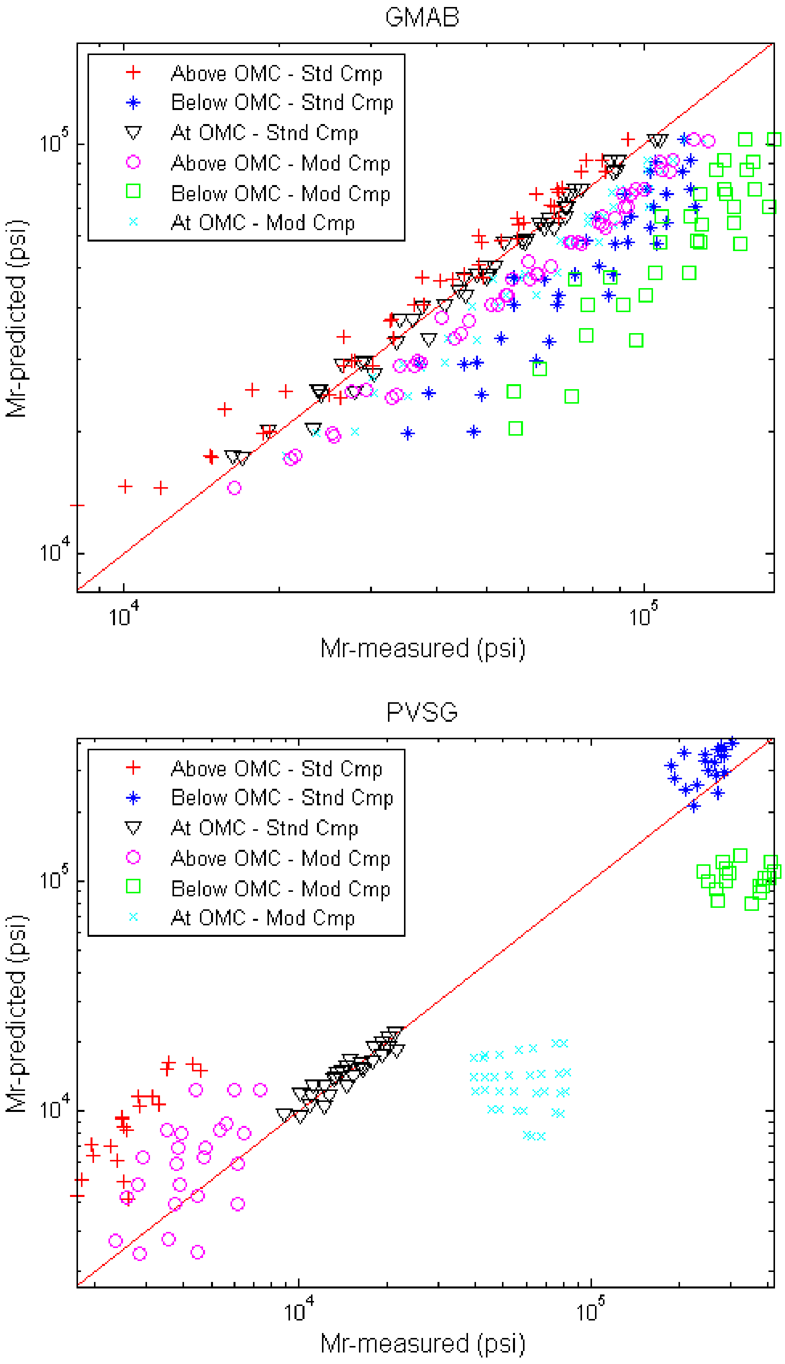

Figure 3-13. M$_{\text{R-predicted}}$ from model M8 VS. M$_{\text{R-measured}}$ for GMAB and PVSG soils.

Overall, model M8—the model proposed by Lytton (1995) using the upper bound of the suction resistance factor ($\theta_{w}f$)—was found to be the most accurate model over a wide range of fine and coarse and plastic and nonplastic soils used in pavements subgrades and bases. However, the

RMSE for all models were high and far from acceptable. Local biases existed in all the evaluated models. The models tended to systematically under predict the moduli at dry of optimum.

APPENDIX 4. FIELD VALIDATION TESTING

LWD test dates at each site is presented in Table 4-1. Also Table 4-2 summarizes the quantity of tests performed (NDG, LWD devices and oven drying moisture test -AASHTO T 265) at each test site.

Gradation test (AASHTO T27-11), Atterberg limits (AASHTO T89-13, and T90-00), and Specific Gravity (AASHTO T85-10, T84-10, and ASTM D854-14) testing was performed in the lab on the soil samples collected from each test site.

The basic soil parameters: uniformity coefficient (Cu), coefficient of gradation (Cc), the soil particle diameter corresponding to 30% finer in the particle-size distribution (D30), the diameter corresponding to 60% finer in the particle-size distribution (D60), and the diameter in the particle-size distribution curve corresponding to 10% finer also defined as the effective size (D10) are exhibited in Table 4-3 for each soil type at test sites evaluated in this project.

The gradation curve in plotted for each site in Section 4.1. Also, the aerial views of projects locations, and any important field condition or limitation description are presented in Section 4.1.

Table 4-1. LWD field evaluation testing date

	State Location	Material Type	Testing Date
1	Virginia	Phenix subgrade	7/30/15
2	Maryland	MD 5 waste contaminated (WC) embankment	8/5/15
3		MD 5 subgrade	8/13/15
4		MD 337, deep GAB layer	8/14/15
5		MD404 sand overlaying subgrade	10/15/15
6		MD 404 subgrade	
7		MD 404 GAB	10/15/15
8	New York	Embankment (local subgrade)	8/20/15
9	Indiana	Cement modified subgrade	8/25/15
10		GAB	8/27/15
11	Missouri	Subgrade	-
12		GAB	8/26/15
13	Florida	Subgrade	10/20/15
14		Base	10/20/15

Table 4-2. Quantities of field tests performed at each site with different devices

	Location	Soil Type	NDG	Zorn LWD	Dynatest LWD	Olson LWD	Oven Moisture Content
1	Virginia	Phenix subgrade	15	30	30	30	10
2	Maryland	MD 5 waste contaminated embankment	20	60	60	0	40
3		MD 5 subgrade	30	90	90	90	60
4		MD 337, deep GAB layer	2	60	60	60	20
5		MD404 sand overlaying subgrade	10	30	30	30	10
6		MD 404 subgrade	10				10
7		MD 404 GAB	10	30	30	30	10
8	New York	Embankment (local subgrade)	40	90	90	90	30
9	Indiana	Cement modified subgrade	0	60	60	60	0
10		GAB	0	30	30	30	11
11	Missouri	Subgrade	0	0	0	0	0
12		GAB	30	90	90	90	30
13	Florida	Subgrade	10	30	30	0	10
14		Base	20	60	60	0	21

Table 4-3. Material characteristics for evaluated field soils

Location and Soil Type	D30	D10	D60	Cc	Cu	Atterberg Limits			Specific Gravity
						LL	PL	PI	
Virginia, Phenix subgrade	0.21	0.09	0.48	1.01	5.49	-	-	non-plastic	2.67
MD 5, waste contaminated embankment	0.85	0.19	3.85	0.97	19.83	22.30	19.35	2.90	2.21
MD 5, subgrade	0.79	0.40	9.42	0.16	23.54	-	-	non-plastic	2.69
MD 337, deep GAB layer	0.88	0.10	3.29	2.41	33.89	-	-	non-plastic	2.71
MD 404, top subgrade	0.37	0.26	0.56	0.96	2.13	-	-	non-plastic	2.37
MD 404, local subgrade	0.57	0.30	1.42	0.76	4.70	-	-	non-plastic	2.45
MD 404, GAB	0.43	0.11	3.74	0.46	34.00	-	-	non-plastic	2.41
New York, embankment	0.24	0.14	0.36	1.19	2.56	-	-	non-plastic	2.68
Indiana, cement modified subgrade	1.90	0.19	6.00	3.17	31.58	26.90	17.74	9.16	2.55
Indiana, GAB	3.10	0.31	9.81	3.14	31.35	-	-	non-plastic	2.83
Missouri, subgrade	1.01	0.33	8.44	0.37	25.74	-	-	non-plastic	2.50
Missouri, GAB	2.09	0.34	8.15	1.59	24.17	-	-	non-plastic	2.62
Florida, Subgrade	0.20	0.15	0.26	1.01	1.80	-	-	non-plastic	2.57
Florida, Base	0.45	0.23	2.49	0.34	10.66	-	-	non-plastic	2.46

4.1. Projects Locations and Details

4.1.1. Virginia

Project: Tola road subgrade and base compaction
Address: 1603 Tola Road, Phoenix Virginia 23959, GPS: 37.074161, -78.754267
Remarks:

- Subgrade was compacted a week prior to the testing date. Subgrade surface was noticeably dry at the time of testing.
- Test site was contaminated with dried stiff clay from other parts of the roadway in some sections. Some clayey soil was carried by the trucks or compaction rollers from the other part of the road and compacted afterwards which resulted in higher variation of moduli in the field.
- Due to thunderstorm, the construction was canceled and no LWD testing was performed on the base layer.

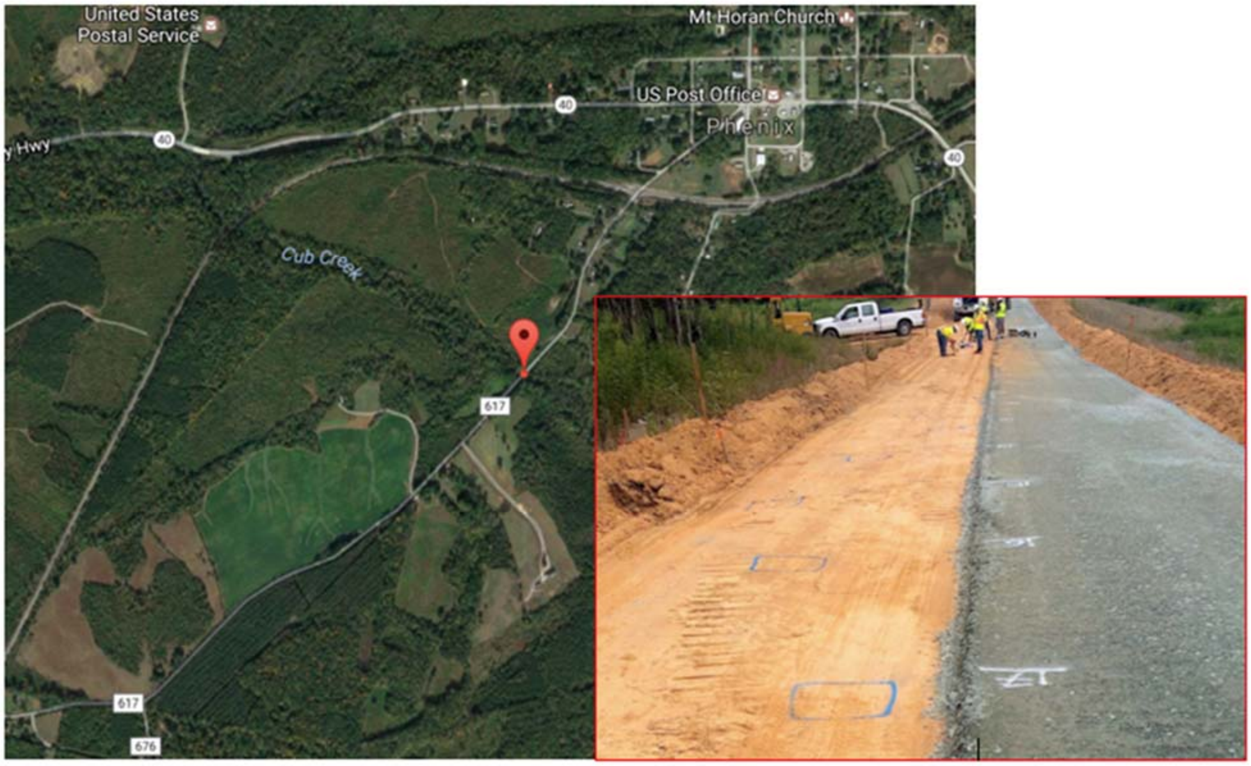
United States
Postal Service
Mt Horan Church
US Post Office
Phenix
Hwy
40
40
40
40
Cub Creek
617
617
676

Figure 4-1. Aerial view of the virgina Tola road evaluation site and test locations

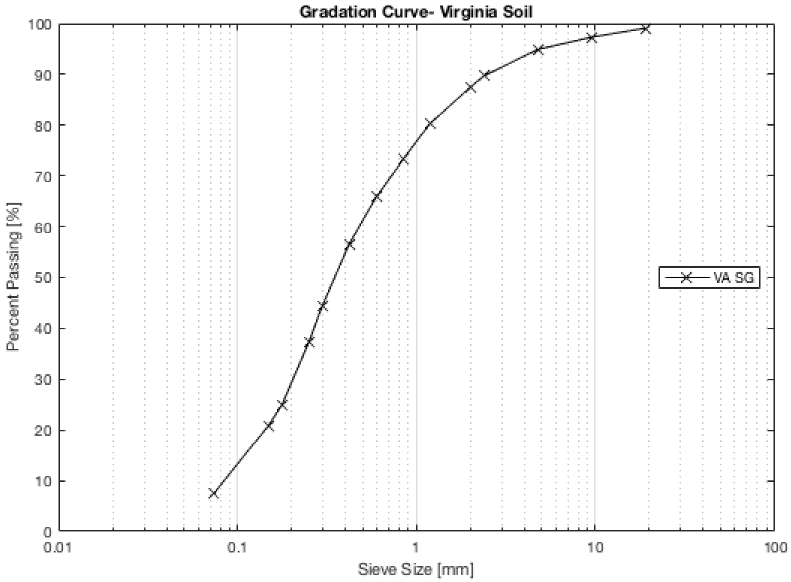

Figure 4-2. Gradation Curve of Virginia site geomaterials

4.1.2. Maryland

Project: MD 5 embankment construction and subgrade compaction on the embankment (Contract number PG494)
Address: MD 5, from Auth way to South of I-495/I-95
Remarks:

- A 2 feet deep embankment was compacted with a waste contaminated soil. The soil contained large pieces of recycled material such as glass, rubber and metal parts. Testing carried out every 1 hour on the 100 ft test section for 2 rounds.
- After a week, the subgrade material was placed over the dried embankment with a slope of about 3%.
  Testing carried out every 1 hour on the 100 ft test section for 3 rounds.

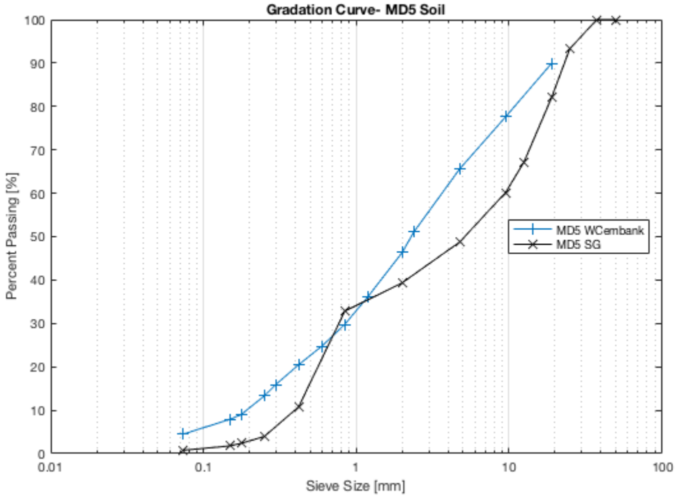

Figure 4-3. Gradation Curve of MD5 site geomaterials

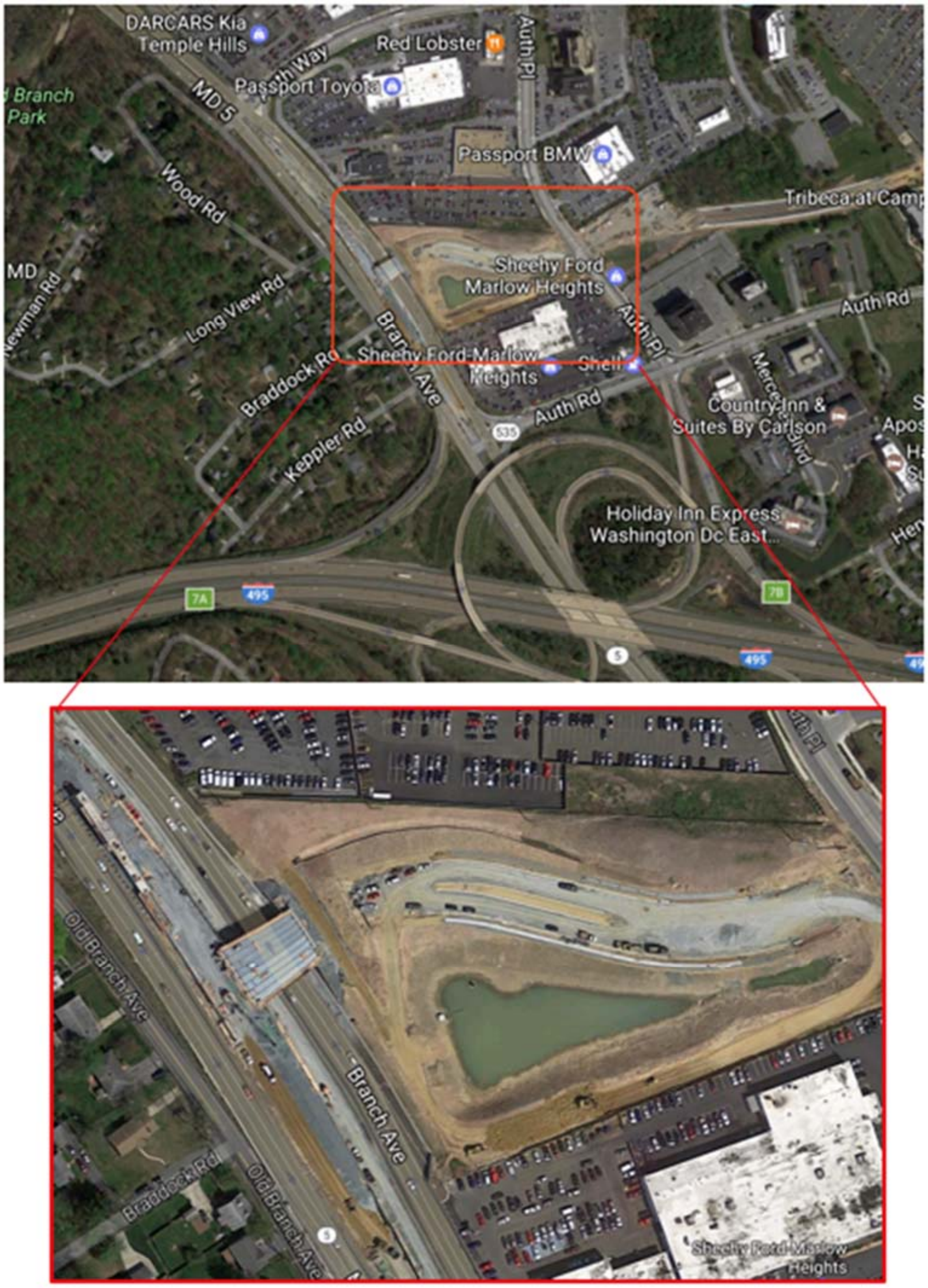
DARCARS Kia
Temple Hills
Red Lobster
Auth Pl
Auth Way
Passport Toyota
d Branch
Park
MD 5
Passport BMW
Wood Rd
Tribeca at Camp
Sheehy Ford
Marlow Heights
Auth Pl
MD
Newman Rd
Long View Rd
Branch Ave
Braddock Rd
Sheehy Ford Marlow
Heights
Shell
Auth Rd
Auth Rd
Country Inn &
Suites By Carlson
Keppler Rd
535
Holiday Inn Express
Washington Dc East...
7A
495
7B
5
495
Old Branch Ave
Branch Ave
Braddock Rd
Old Branch Ave
5
Sheehy Ford Marlow
Heights

Figure 4-4. Aerial view of the MD5 field evaluation site

Project: MD 337 lane widening
Address: 4701 Allentown road, Suitland, MD
Remarks:

- The local subgrade was a weak clay, so the lane was undercut for 3 ft. and replaced with GAB material. The initial 2 ft was compacted earlier.
- Testing was performed on top of a 6 inches GAB layer placed over the existing 2-ft layer.

- The 6-inch layer was compacted the day before testing at the end of the day. However, very little surface drying was observed on the top 0.5 inches.
- NDG was not available on site on the day of testing. Testing performed earlier on the 6-inch compacted layer reported PC of 98%.

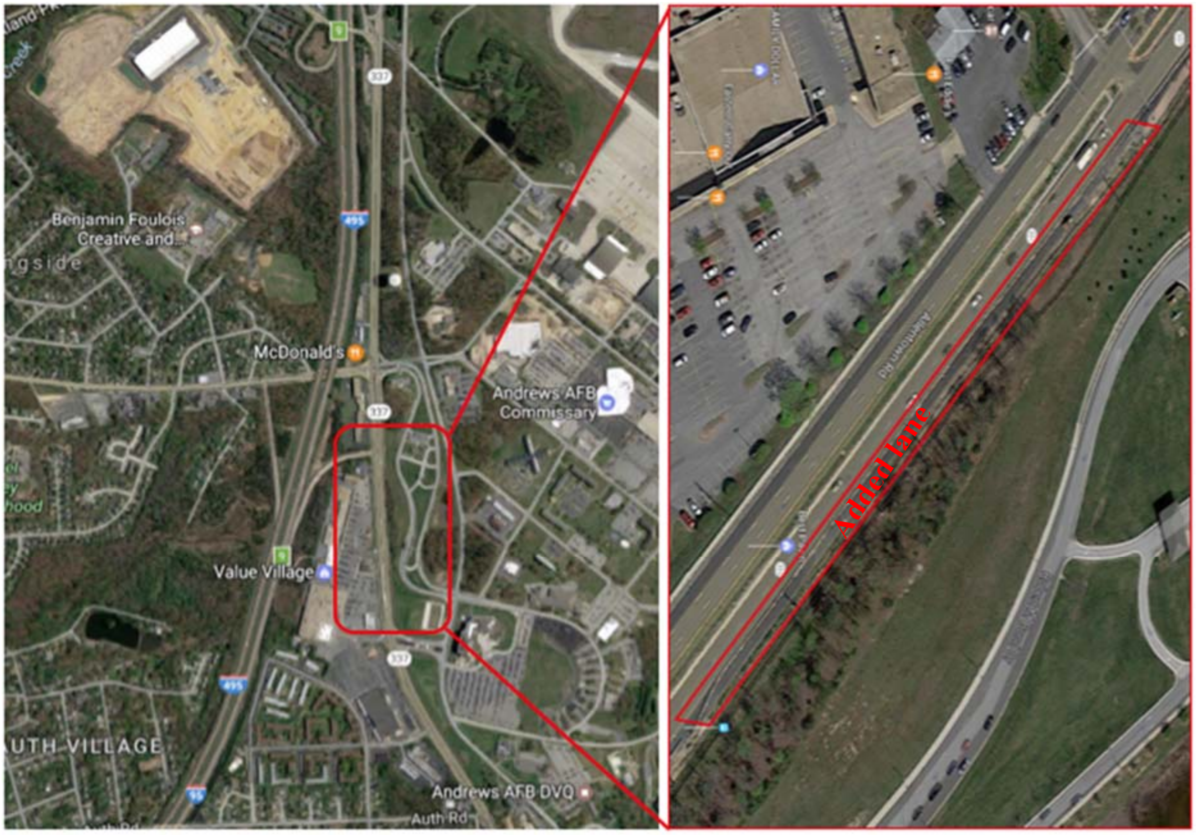
Benjamin Foulois
Creative and...
McDonald's
Andrews AFB
Commissary
Value Village
UTH VILLAGE
Andrews AFB DVQ
Auth Rd
337
495
95
Allentown Rd
Added lane

Figure 4-5. Aerial view of the MD337 field evaluation site

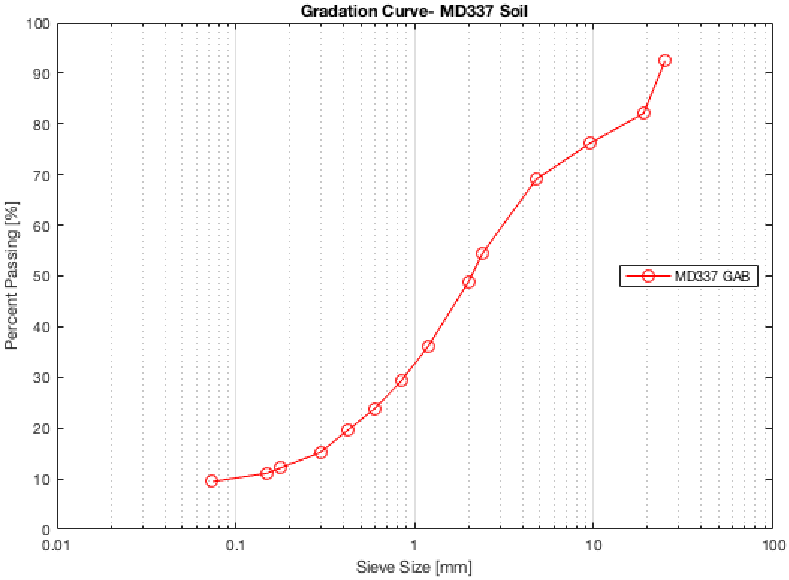

Figure 4-6. Gradation Curve of MD337 site geomaterials

Project: MD 404 dualization (Contract number AW8965270)
Address: 11419 Ridgely Rd, Ridgely, MD 21660
Remarks:

- A 5-ft embankment of local subgrade was compacted beforehand. Since the subgrade material was too wet at the time of placing the base, a 4-inch layer of uniform sand was compacted over the existing subgrade.
- Testing performed right after compaction on the sand layer.
- The GAB base layer was compacted in a layer of 6 to 8 inches.
- Testing performed right after GAB compaction.

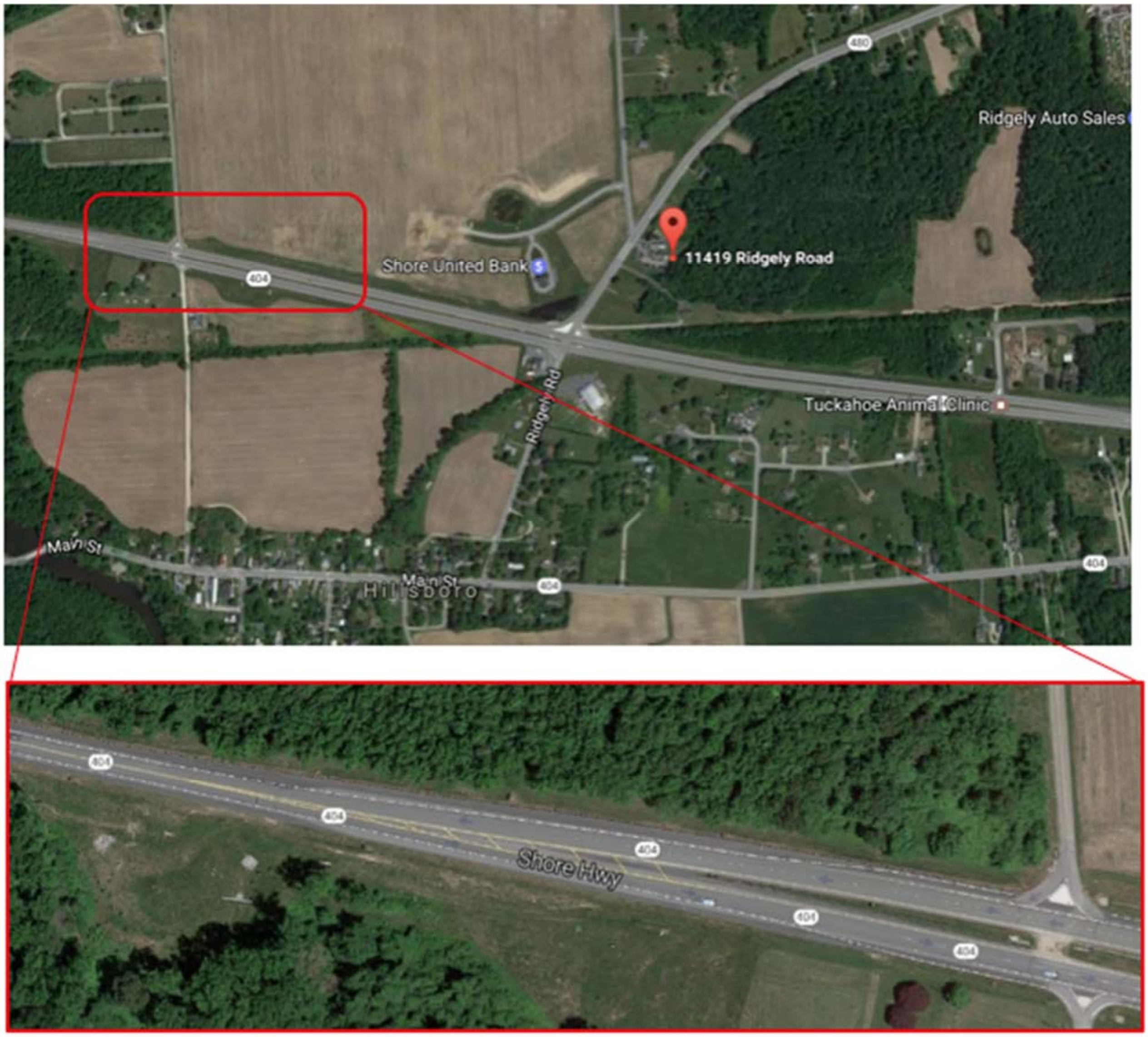
480
Ridgely Auto Sales
11419 Ridgely Road
Shore United Bank
404
Ridgely Rd
Tuckahoe Animal Clinic
Main St
Main St
Hillsboro
404
Shore Hwy

Figure 4-7. Aerial view of the MD404 field evaluation site

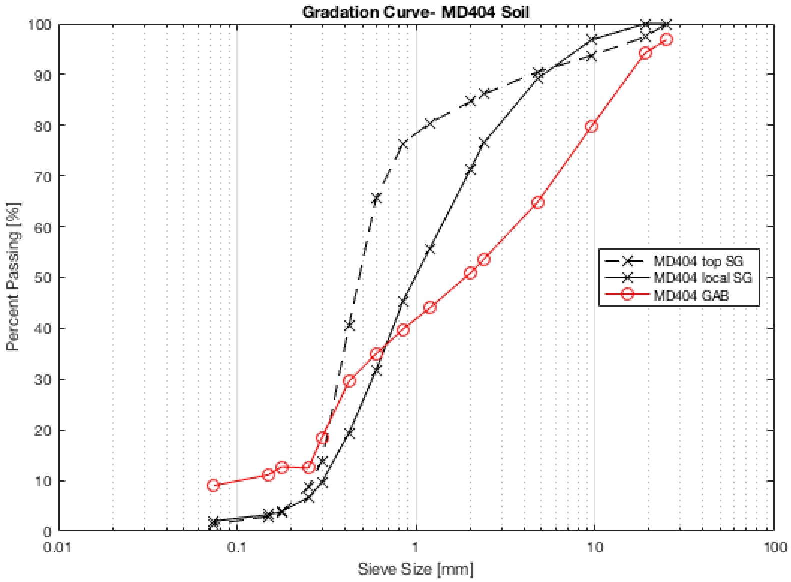

Figure 4-8. Gradation Curve of MD404 site geomaterials

4.1.3. New York

Project: Luther Forest Boulevard extension
Address: 3 Hemphill Pl Ballston Spa, NY 12020 (project office)
Remarks:

- The embankment constructed in layers of 8 inch to 1 ft thickness below the final grade.
- LWD and NDG testing performed on two lifts.
- The water content of the material was dryer than OMC at the time of compaction. Therefore, a truck was spraying water on top of the sand after placement. Spraying water was not possible on the test site as the LWD testing personnel were working.

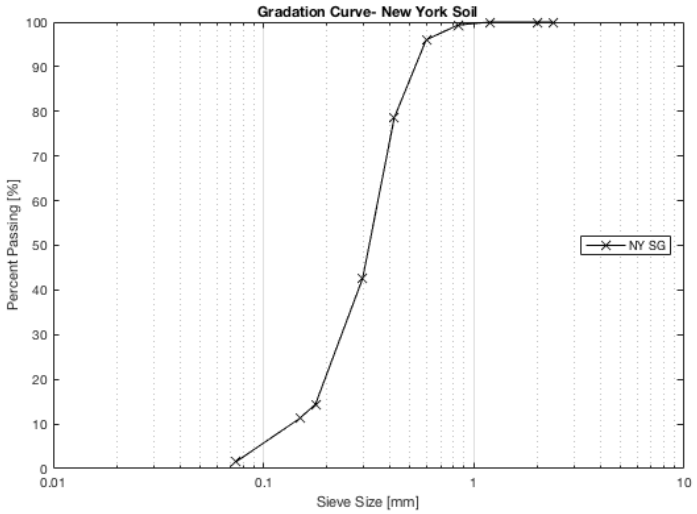

Figure 4-9. Gradation Curve of New York site geomaterials

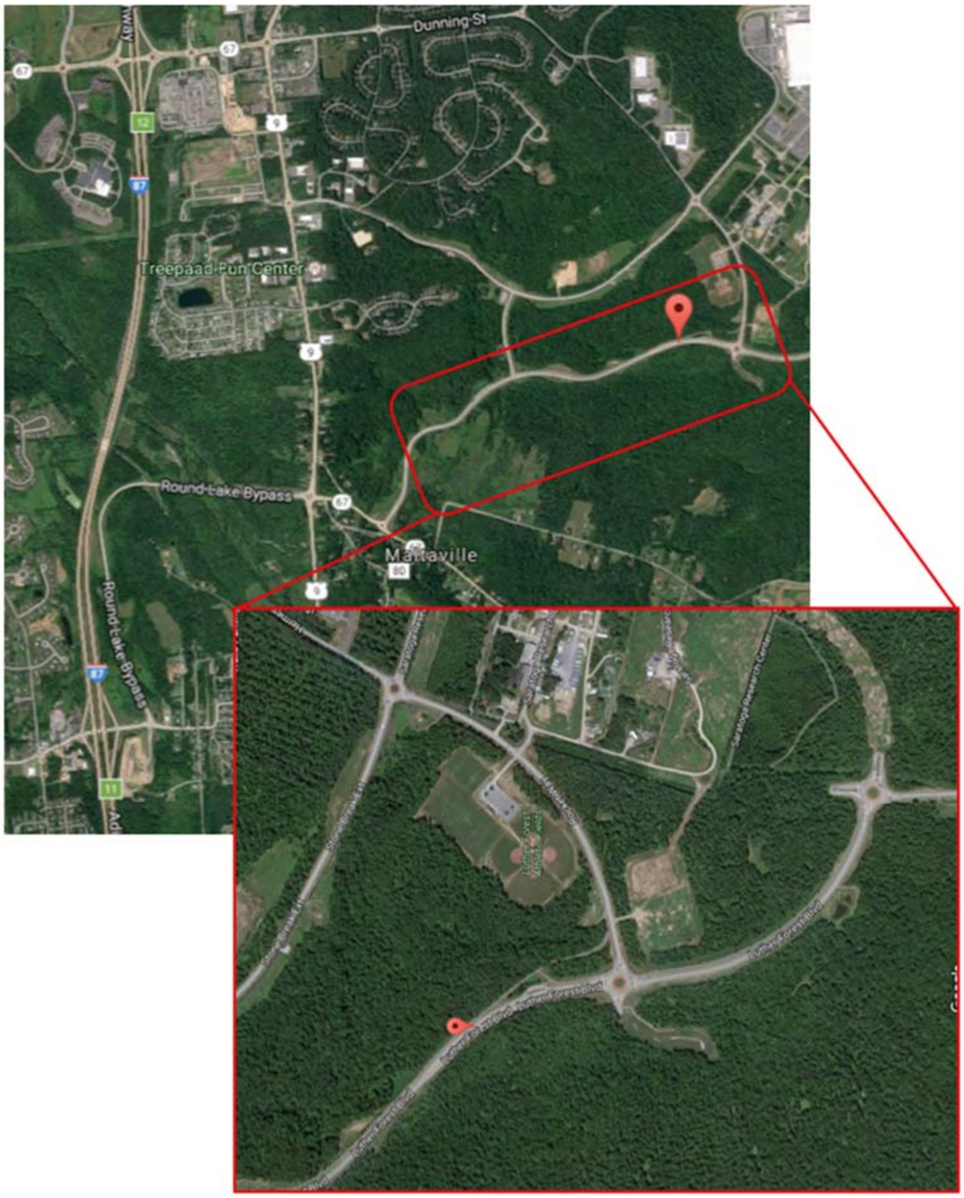
Dunning St
Treepaad Fun Center
Round Lake Bypass
Maltaville
Round Lake Bypass
67
9
87
12
11
80

Figure 4-10. Aerial view of the New York Luther Forest Boulevard evaluation site

4.1.4. Missouri

Project: I-64 lane widening and road shoulder compaction
Address: 601 Salt Mill Rd, Chesterfield, MO 63017 (project office)
Remarks:

- The concrete shoulder on the I-64 lane had been removed. The natural dirt (subgrade) below the shoulder was only compacted with 1 to 2 passes of roller compactor.
- A layer of about 4 inches of crushed lime stone (base) had been placed on top of the subgrade.
- Since the base layer had already been placed, we were unable to perform LWD testing on the subgrade. Soil samples were collected from the subgrade for lab testing.

- LWD and NDG testing on the base layer performed right after compaction in two rounds of one hour interval.

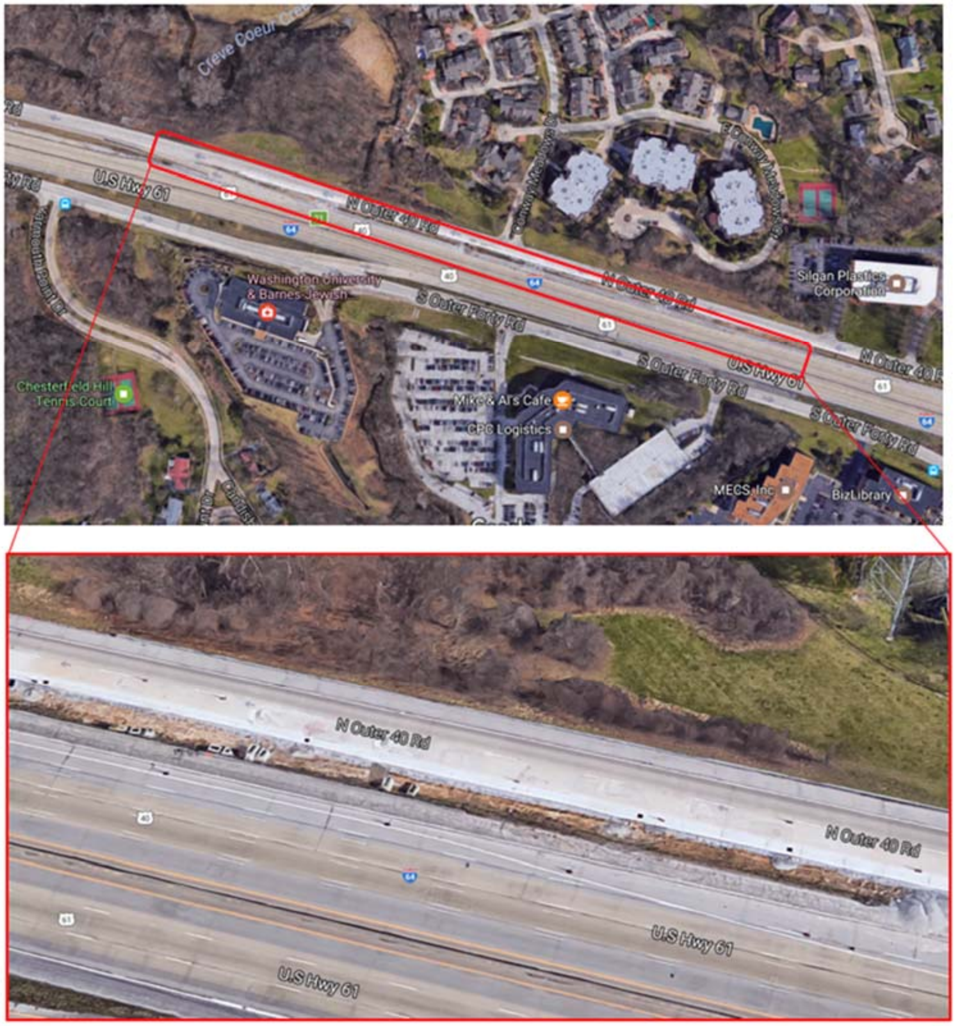
Creve Coeur Creek
U.S Hwy 61
N Outer 40 Rd
Washington University & Barnes-Jewish
S Outer Forty Rd
Silgan Plastics Corporation
Chesterfield Hill Tennis Court
Mike & Al's Cafe
CPC Logistics
MECS, Inc
BizLibrary
N Outer 40 Rd
U.S Hwy 61
U.S Hwy 61

Figure 4-11. Aerial view of the Missouri I-64 evaluation site

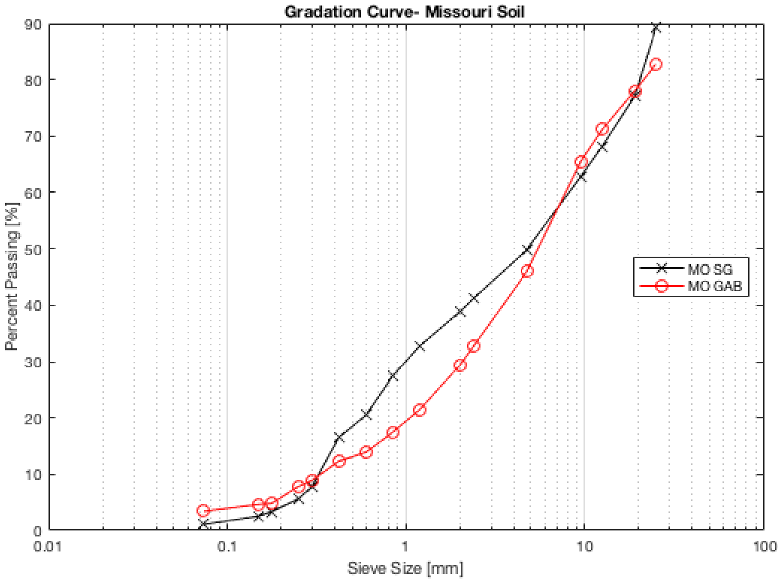

Figure 4-12. Gradation Curve of Missouri site geomaterials

4.1.5. Indiana

Project: I-65 to Worthsville road and Graham road construction (R-35187-A)
Address: 1615 S Graham Road, Greenwood, IN 46143
Remarks:

- Cement stabilized subgrade was compacted 5 days before testing. The layer's thickness was 14 inches total.
- The subgrade was cured and very stiff to excavate for moisture samples at the time of testing. Therefore, water content samples were obtained from the depth of 3 to 6 inches from the trench on the side on the road. The water content was measured using the Ohaus moisture analyzer on the site.
- INDOT does not use NDG tests for routine compaction quality control anymore. INDOT used Zorn LWD testing and proof rolling with a fully loaded tri-axle truck to evaluate the compaction.
- Base material was compacted on top of the cured cement stabilized subgrade (3 inches thickness).
- Testing on the base performed right after compaction on almost the same locations as the subgrade testing.

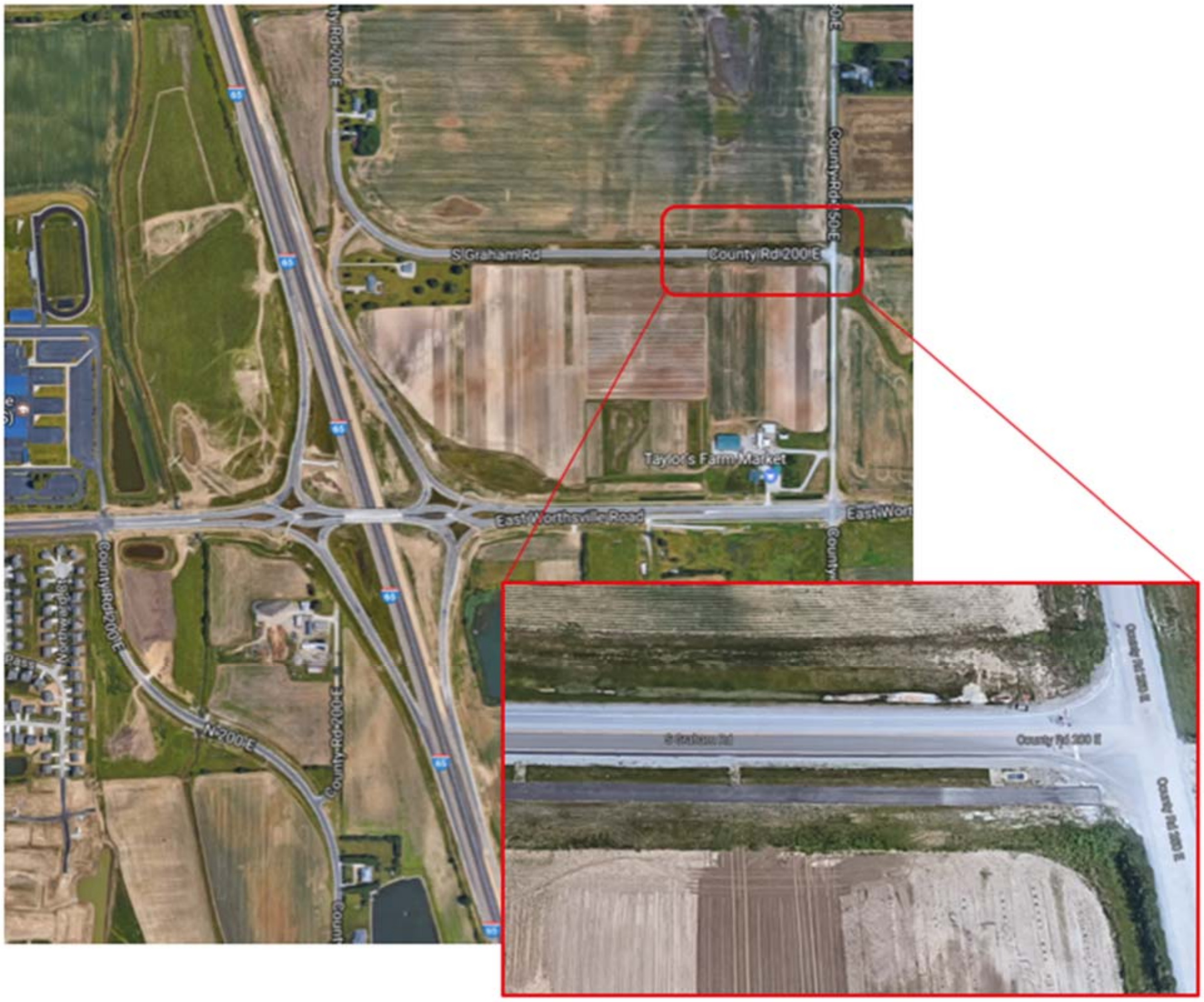
S Graham Rd
County Rd 200 E
Taylor's Farm Market
East Worthsville Road
East Wor
County Rd 200 E
N 200 E
65

Figure 4-13. Aerial view of the Indiana Graham road evaluation site

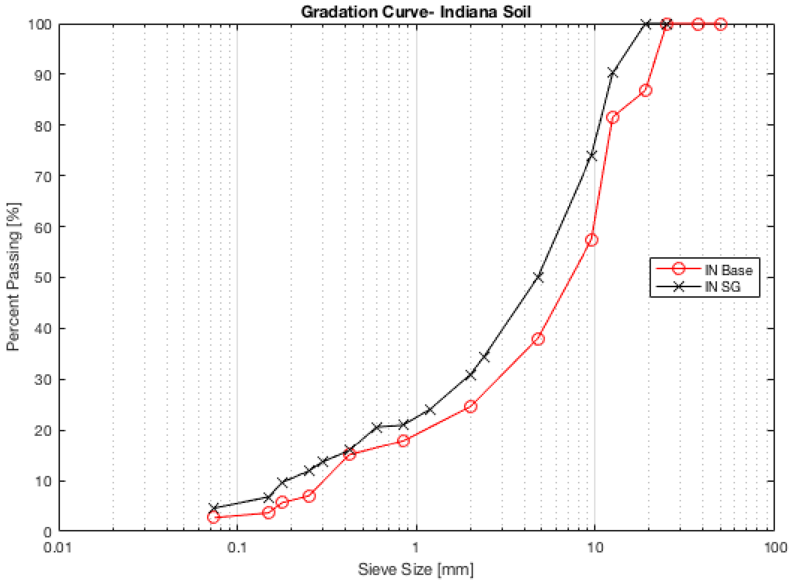

Figure 4-14. Gradation Curve of Indiana site geomaterials

4.1.6. Florida

Project: SR 23 construction, South Jacksonville, FL
From SR 21 (Blanding Blvd.) to Duval county line
Address: Branan Field Rd, Orange Park, FL 32065
Remarks:

- Subgrade was compacted a week before LWD testing in the field. LWD and NDG testing on the subgrade performed right before base placement.
- Limerock base material was compacted to a thickness of 6 to 8 inches. LWD and NDG testing on the base performed right after compaction in two rounds of one-hour interval.

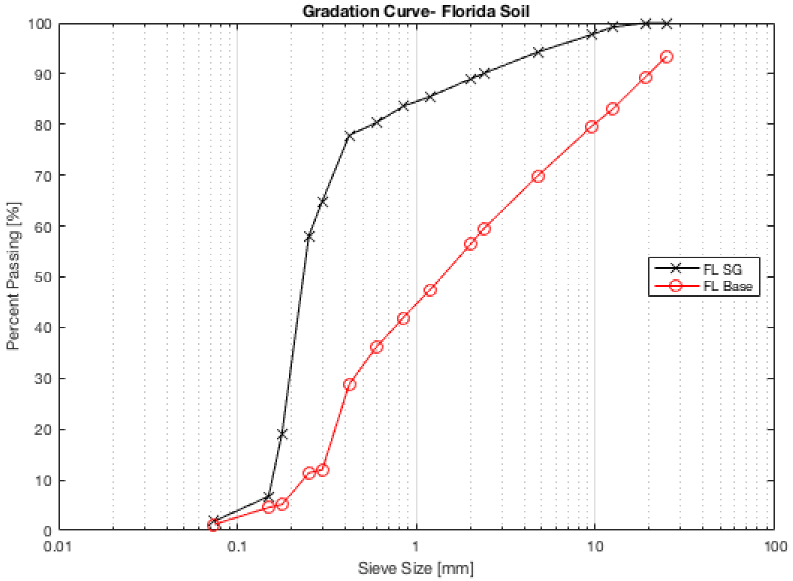

Figure 4-15. Gradation Curve of Florida site geomaterials

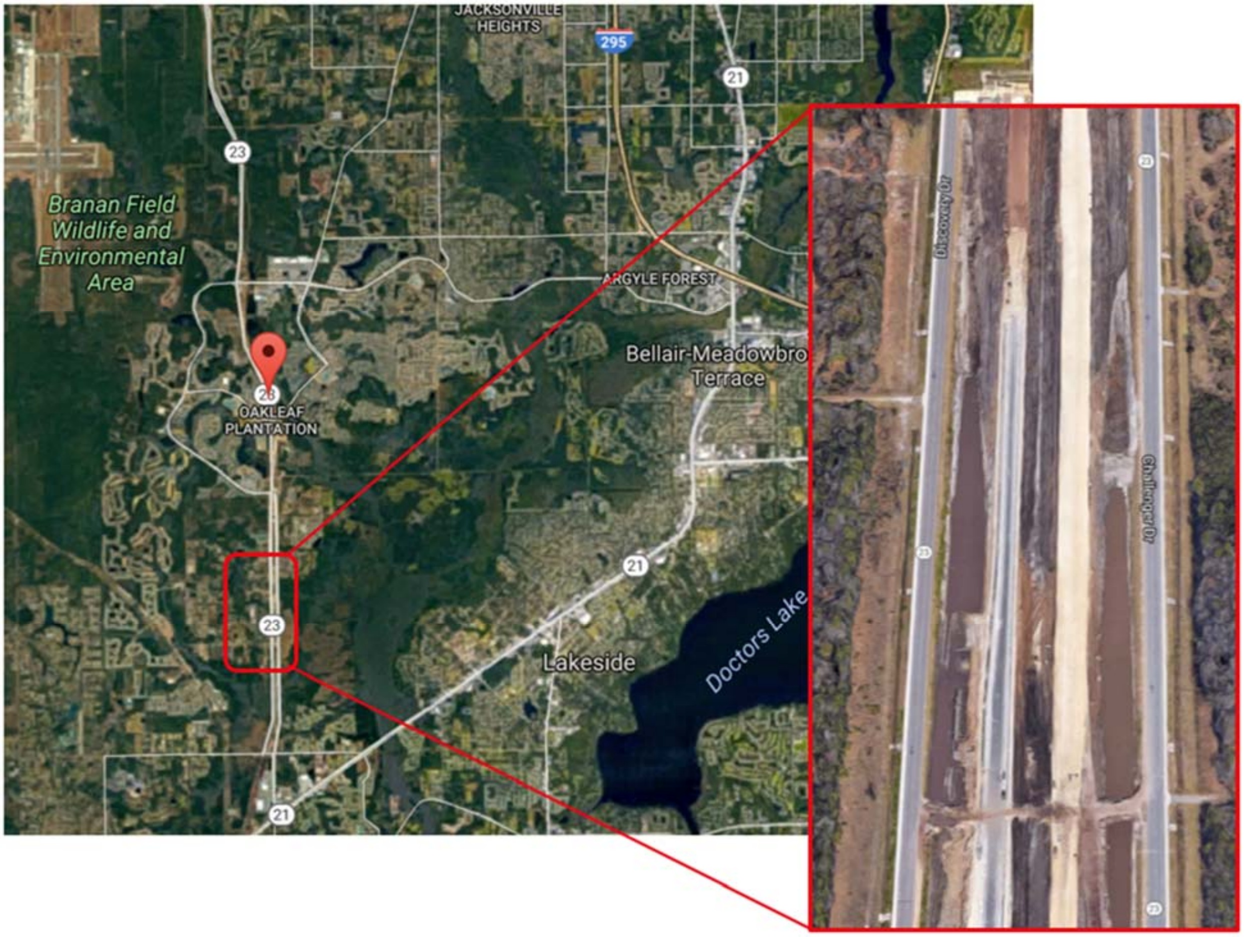
JACKSONVILLE HEIGHTS
295
21
23
Branan Field Wildlife and Environmental Area
ARGYLE FOREST
Bellair-Meadowbro
Terrace
23
OAKLEAF PLANTATION
21
23
Lakeside
Doctors Lake
21
Discovery Dr
Challenger Dr
23

Figure 4-16. Aerial view of the Florida SR23 field evaluation site

4.2. Summary of LWD Field Moduli, Measured Water Content, and NDG Results

Table 4-4. Summary of field water content measured by NDG

Location and Soil Type	Round of Testing	Average MC [%] by NDG	Standard Deviation	%COV
Virginia, Phenix subgrade	1st	12.96	5.20	40.11
MD 5 waste contaminated embankment	1st	9.94	2.60	26.19
	2nd	9.46	2.18	23.02
MD 5 subgrade	1st	4.32	0.33	7.57
	2nd	3.88	0.35	9.00
	3rd	4.22	0.78	18.38
MD 404 subgrade	1st	6.01	0.78	13.04
MD 404 GAB	1st	2.81	0.28	10.13
New York, embankment (local subgrade)	Lift 1, 1st	4.85	0.49	10.02
	Lift 1, 2st	4.72	0.58	12.26
	Lift 2, 1st	4.79	0.49	10.15
	Lift 2, 2nd	4.68	0.59	12.69
Missouri, GAB	1st	4.53	0.90	19.78
	2nd	4.31	0.69	16.07
Florida, Subgrade	1st	8.11	1.01	12.42
Florida, Base	1st	12.75	0.98	7.68
	2nd	12.12	0.53	4.35

Table 4-5. Summary of field water content obtained by oven drying method

Location and Soil Type	Round of Testing	Average MC [%] by Oven drying	Standard Deviation	%COV
Virginia, Phenix subgrade	1st	8.70	2.92	33.57
MD 5 waste contaminated embankment	1st	11.30	3.42	30.28
	2nd	10.38	2.39	23.05
MD 5 subgrade	1st	4.34	0.35	7.98
	2nd	3.37	0.40	11.76
	3rd	2.56	0.89	34.61
MD 337, deep GAB layer	1st	2.40	0.42	17.50
New York, embankment (local subgrade)	Lift 1, 1st	6.24	0.63	10.12
	Lift 1, 2st	N/A	N/A	N/A
	Lift 2, 1st	5.79	0.44	7.55
	Lift 2, 2nd	6.00	0.47	7.85
Indiana, cement modified subgrade	1st	N/A	N/A	N/A
Indiana, GAB	1st	6.44	0.32	4.98
Missouri, GAB	1st	4.77	0.92	19.27
	2nd	4.63	0.60	12.91
Florida, Subgrade	1st	8.79	0.90	10.25
Florida, Base	1st	12.95	0.64	4.91
	2nd	12.88	0.66	5.12

Table 4-6. Summary of Percent Compaction values measured by NDG in the field

Location and Soil Type	Round of Testing	Average %PC	Standard Deviation	%COV
Virginia, Phenix subgrade	1st	96.8	4.525	4.673
MD 5 waste contaminated embankment	1st	97.9	4.857	4.960
	2nd	98.3	3.977	4.042
MD 5 subgrade	1st	98.6	2.328	2.360
	2nd	98.4	1.674	1.700
	3rd	98.8	1.527	1.545
MD 337, deep GAB layer	1st	98.0	N/A	N/A
MD 404 subgrade	1st	N/A	N/A	N/A
MD 404 GAB	1st	90.2	1.214	1.345
New York, embankment (local subgrade)	Lift 1, 1st	84.8	1.565	1.845
	Lift 1, 2st	85.4	2.531	2.963
	Lift 2, 1st	83.2	2.020	2.425
	Lift 2, 2nd	83.2	1.950	2.343
Indiana, cement modified subgrade	1st	N/A	N/A	N/A
Indiana, GAB	1st	N/A	N/A	N/A
Missouri, GAB	1st	100.0	3.585	3.584
	2nd	99.6	3.339	3.354
Florida, Subgrade	1st	90.8	1.462	1.609
Florida, Base	1st	102.7	1.617	1.574
	2nd	102.4	1.327	1.295

Table 4-7. Summary of Olson LWD moduli on the field sites

Location and Soil Type	Round of Testing	Average E_{field} [MPa] Olson LWD	Standard Deviation	%COV
Virginia, Phenix subgrade	1st	19.484	13.920	71.446
MD 5 subgrade	1st	82.100	36.179	44.067
	2nd	77.571	27.815	35.858
	3rd	72.237	22.395	31.003
MD 337, deep GAB layer	1st	68.752	7.705	11.207
MD 404 subgrade	1st	36.704	6.408	17.458
MD 404 GAB	1st	35.997	5.229	14.526
New York, embankment (local subgrade)	Lift 1, 1st	22.495	4.068	18.084
	Lift 2, 1st	19.299	2.987	15.476
	Lift 2, 2st	19.366	3.517	18.159
Indiana, cement modified subgrade	1st	101.530	45.238	44.556
Indiana, GAB	1st	82.826	27.852	33.627
Missouri, GAB	1st	46.834	13.826	29.523
	2nd	55.494	16.285	29.345

Table 4-8. Summary of Zorn LWD moduli on the field sites

Location and Soil Type	Round of Testing	Average E_{field} [MPa] Zorn LWD	Standard Deviation	%COV
Virginia, Phenix subgrade	1st	27.786	22.281	80.187
MD 5 waste contaminated embankment	1st	10.401	4.019	38.641
	2nd	11.983	5.542	46.248
MD 5 subgrade	1st	65.954	25.801	39.119
	2nd	62.536	24.884	39.792
	3rd	69.263	23.889	34.491
MD 337, deep GAB layer	1st	64.713	8.059	12.454
MD 404 subgrade	1st	33.404	8.752	26.199
MD 404 GAB	1st	35.122	5.519	15.714
New York, embankment (local subgrade)	Lift 1, 1st	19.861	2.797	14.083
	Lift 1, 2st	22.338	2.752	12.321
	Lift 2, 1st	19.096	3.595	18.828
	Lift 2, 2nd	19.499	3.776	19.364
Indiana, cement modified subgrade	1st	82.240	41.411	50.354
Indiana, GAB	1st	71.105	27.580	38.787
Missouri, GAB	1st	39.209	11.040	28.156
	2nd	46.455	12.508	26.925
Florida, Subgrade	1st	71.521	7.265	10.157
Florida, Base	1st	66.411	10.155	15.292
	2nd	73.261	9.858	13.456

Table 4-9. Summary of Dynatest LWD moduli on the field sites

Location and Soil Type	Round of Testing	Average E_{field} [MPa] Dynatest LWD	Standard Deviation	%COV
Virginia, Phenix subgrade	1st	71.015	59.098	83.219
MD 5 waste contaminated embankment	1st	11.161	5.901	52.872
	2nd	16.506	9.199	55.732
MD 5 subgrade	1st	117.981	94.610	80.190
	2nd	129.931	85.468	65.779
	3rd	147.965	134.758	91.074
MD 337, deep GAB layer	1st	115.928	21.073	18.178
MD 404 subgrade	1st	44.716	13.765	30.783
MD 404 GAB	1st	45.572	9.733	21.357
New York, embankment (local subgrade)	Lift 1, 1st	28.783	4.537	15.763
	Lift 2, 1st	29.690	5.257	17.706
Indiana, cement modified subgrade	1st	355.935	338.148	95.003
Indiana, GAB	1st	152.329	130.487	85.661
Missouri, GAB	1st	71.446	29.633	41.476
	2nd	86.247	37.080	42.993
Florida, Subgrade	1st	107.789	16.347	15.166
Florida, Base	1st	95.327	26.166	27.449
	2nd	118.179	16.515	13.975

4.3. Developing Correlation Between Moduli at First and Second Half-Heights Drops

Figure 4.17, Figure 4-18, and Figure 4-19 present the moduli from second half-height drop versus moduli from first half-height drop for Zorn, Dynatest and Olson LWDs respectively. Correlation equation and coefficient of determination (R^2) are shown for each round of testing (R) and compacted lift (L) at each test site.

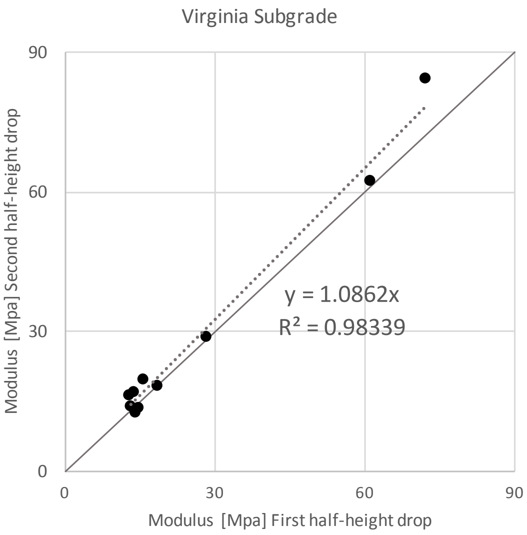
Virginia Subgrade
90
60
30
0
0
30
60
90
Modulus [Mpa] Second half-height drop
Modulus [Mpa] First half-height drop
y = 1.0862x
R² = 0.98339

A)

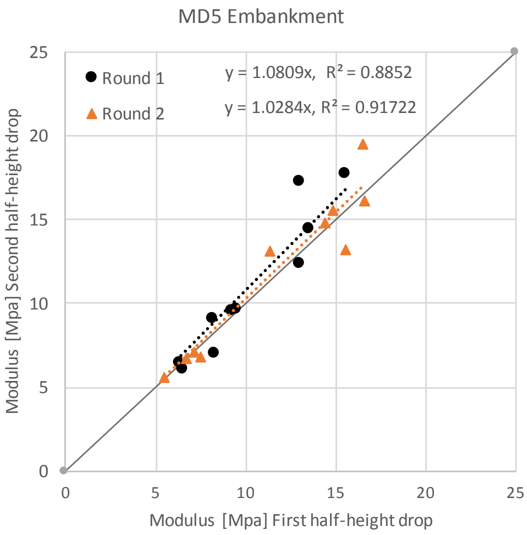
MD5 Embankment
25
20
15
10
5
0
0
5
10
15
20
25
● Round 1
▲ Round 2
y = 1.0809x, R² = 0.8852
y = 1.0284x, R² = 0.91722
Modulus [Mpa] Second half-height drop
Modulus [Mpa] First half-height drop

B)

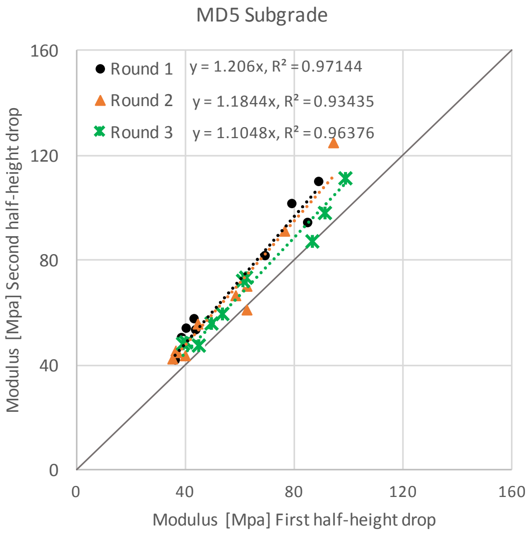
MD5 Subgrade
160
120
80
40
0
0
40
80
120
160
● Round 1
▲ Round 2
✖ Round 3
y = 1.206x, R² = 0.97144
y = 1.1844x, R² = 0.93435
y = 1.1048x, R² = 0.96376
Modulus [Mpa] Second half-height drop
Modulus [Mpa] First half-height drop

C)

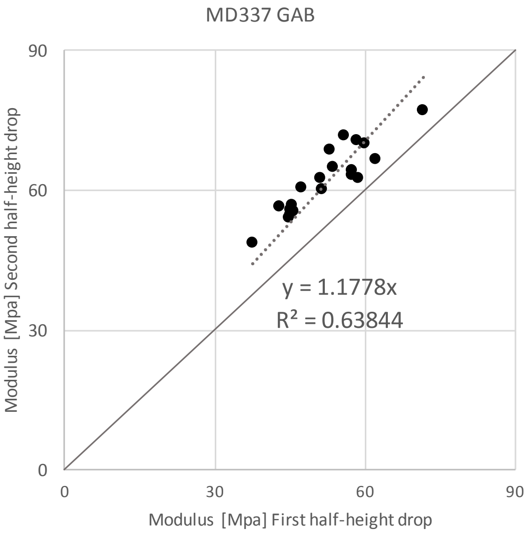
MD337 GAB
90
60
30
0
0
30
60
90
Modulus [Mpa] Second half-height drop
Modulus [Mpa] First half-height drop
y = 1.1778x
R² = 0.63844

D)

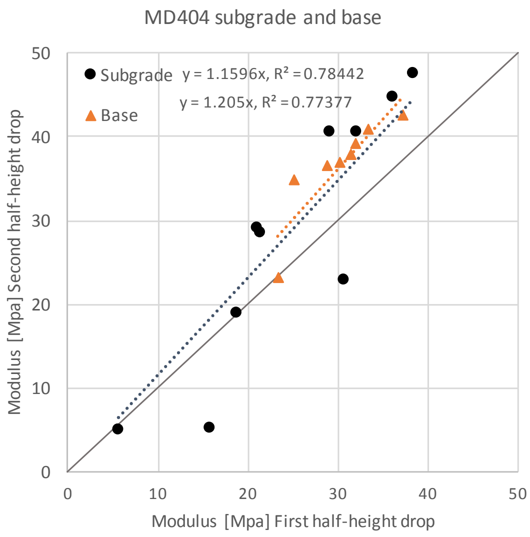

E)

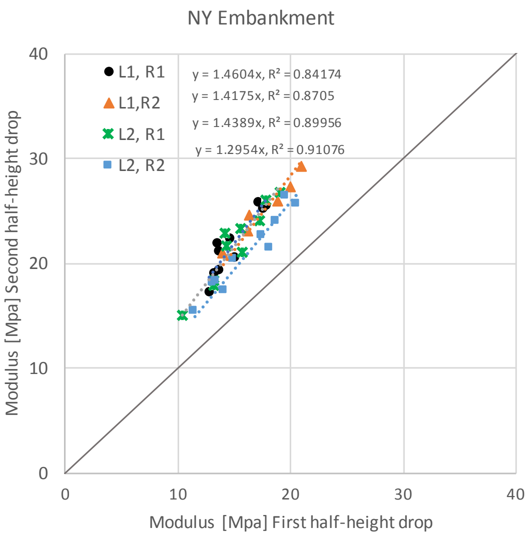

F)

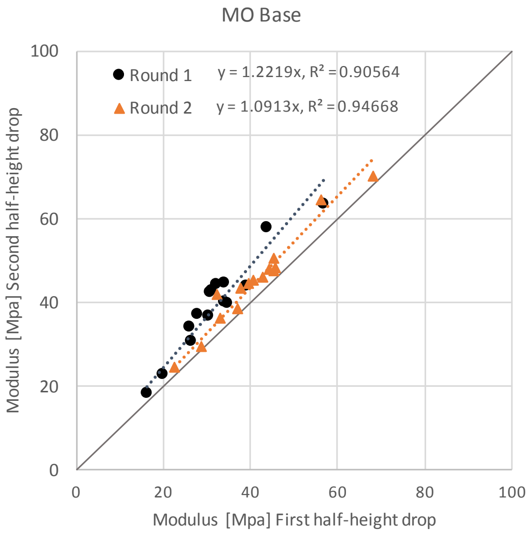

G)

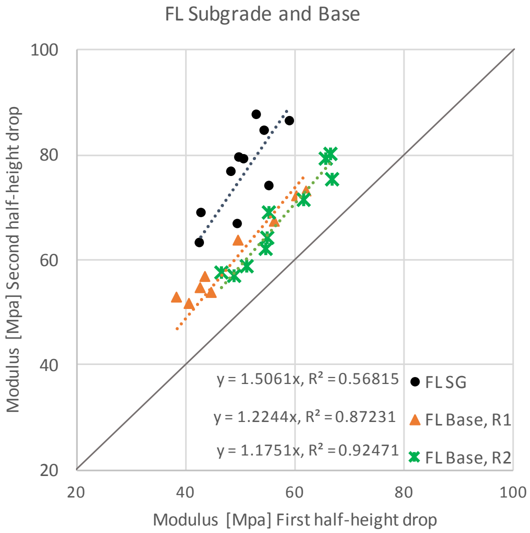

H)

I)

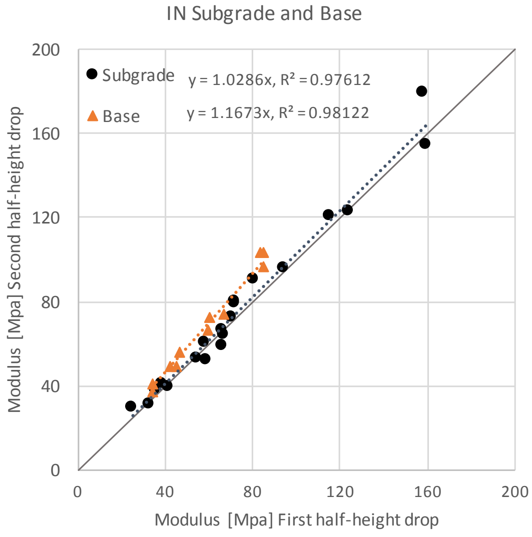

Figure 4-17. Comparison of moduli at first half-height drop and moduli at second half-height drop for Zorn LWD.

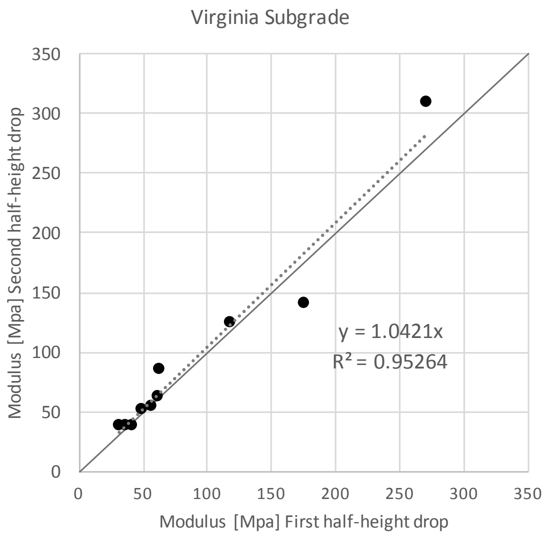
Virginia Subgrade
Modulus [Mpa] Second half-height drop
Modulus [Mpa] First half-height drop
0
50
100
150
200
250
300
350
y = 1.0421x
R² = 0.95264

A)

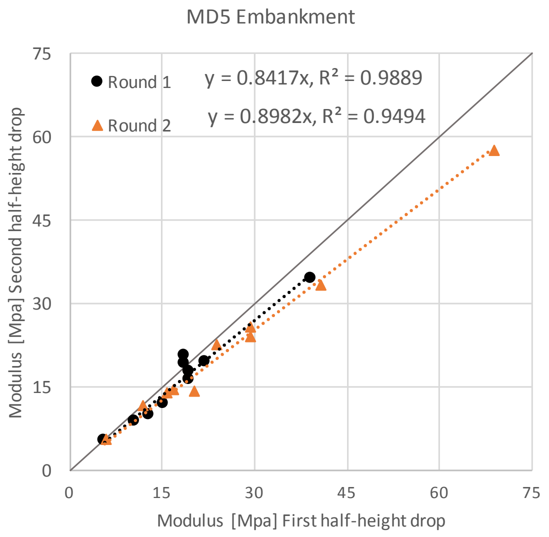
MD5 Embankment
Round 1
Round 2
y = 0.8417x, R² = 0.9889
y = 0.8982x, R² = 0.9494
Modulus [Mpa] Second half-height drop
Modulus [Mpa] First half-height drop
0
15
30
45
60
75

B)

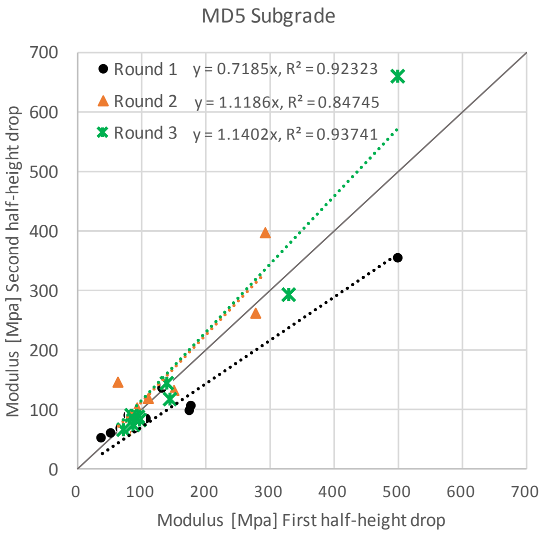
MD5 Subgrade
Round 1
y = 0.7185x, R² = 0.92323
Round 2
y = 1.1186x, R² = 0.84745
Round 3
y = 1.1402x, R² = 0.93741
Modulus [Mpa] Second half-height drop
Modulus [Mpa] First half-height drop
0
100
200
300
400
500
600
700

C)

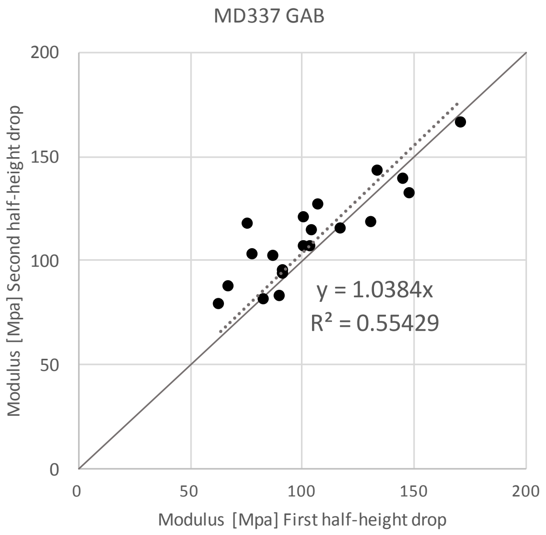
MD337 GAB
Modulus [Mpa] Second half-height drop
Modulus [Mpa] First half-height drop
0
50
100
150
200
y = 1.0384x
R² = 0.55429

D)

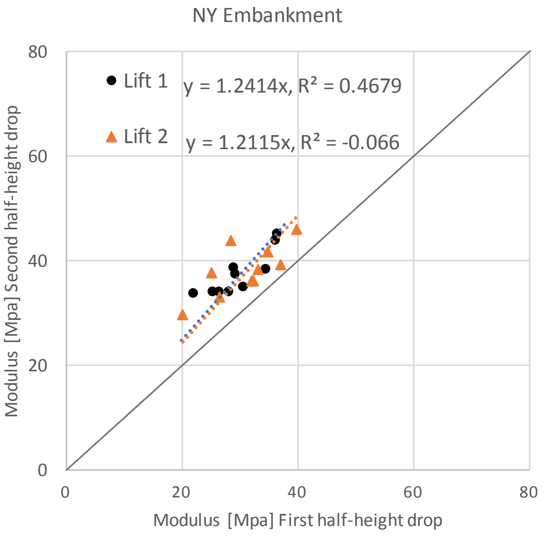
NY Embankment
Lift 1
y = 1.2414x, R² = 0.4679
Lift 2
y = 1.2115x, R² = -0.066
Modulus [Mpa] Second half-height drop
Modulus [Mpa] First half-height drop
0
20
40
60
80

E)

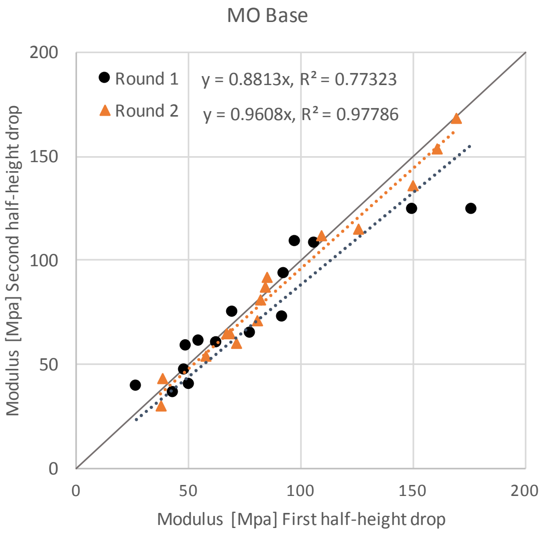
MO Base
Round 1
y = 0.8813x, R² = 0.77323
Round 2
y = 0.9608x, R² = 0.97786
Modulus [Mpa] Second half-height drop
Modulus [Mpa] First half-height drop
0
50
100
150
200

F)

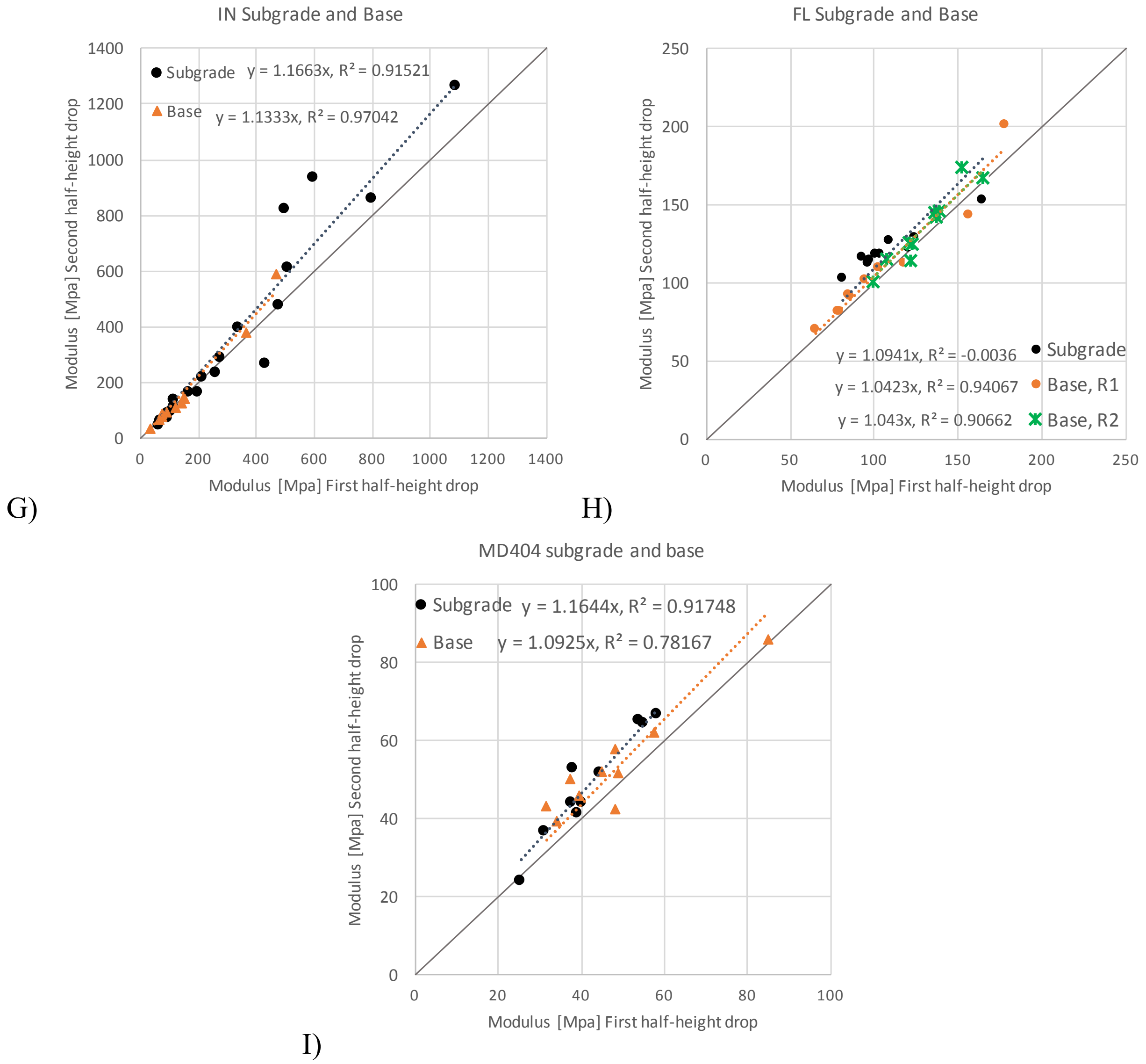

Figure 4-18. Comparison of moduli at first half-height drop and moduli at second half-height drop for Dynatest LWD.

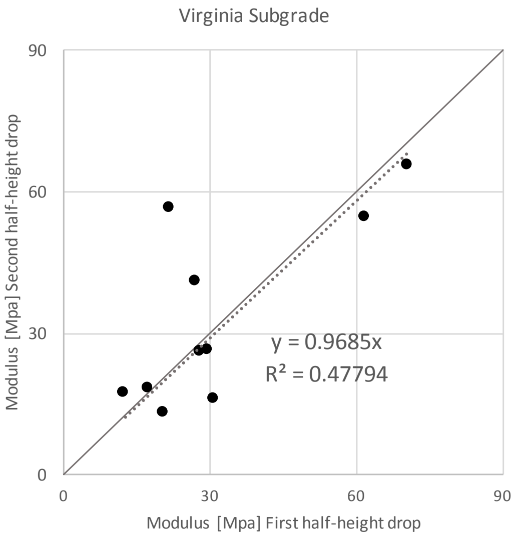
Virginia Subgrade
90
60
30
0
0
30
60
90
Modulus [Mpa] Second half-height drop
Modulus [Mpa] First half-height drop
y = 0.9685x
R² = 0.47794

A)

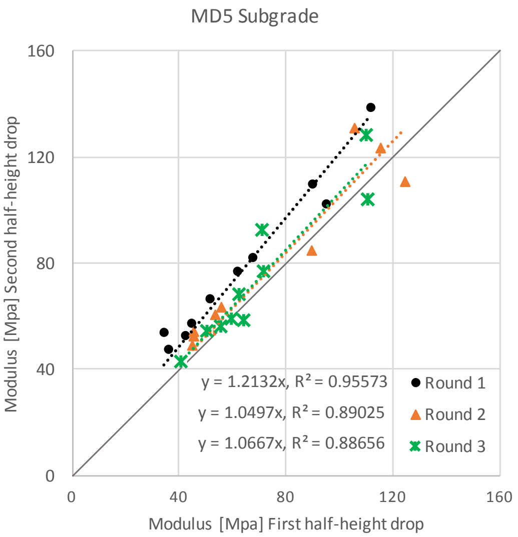
MD5 Subgrade
160
120
80
40
0
0
40
80
120
160
Modulus [Mpa] Second half-height drop
Modulus [Mpa] First half-height drop
y = 1.2132x, R² = 0.95573
y = 1.0497x, R² = 0.89025
y = 1.0667x, R² = 0.88656
● Round 1
▲ Round 2
✖ Round 3

B)

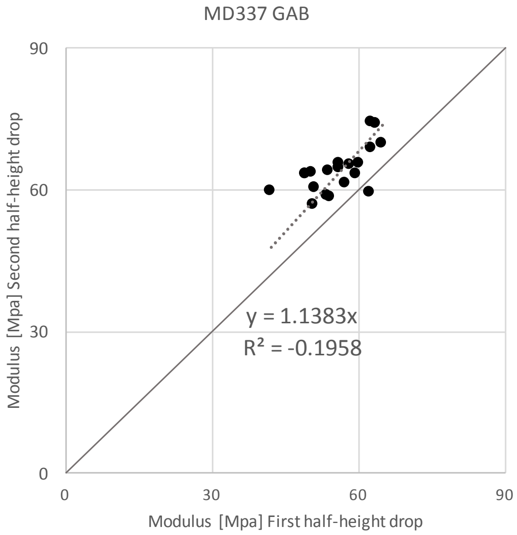
MD337 GAB
90
60
30
0
0
30
60
90
Modulus [Mpa] Second half-height drop
Modulus [Mpa] First half-height drop
y = 1.1383x
R² = -0.1958

C)

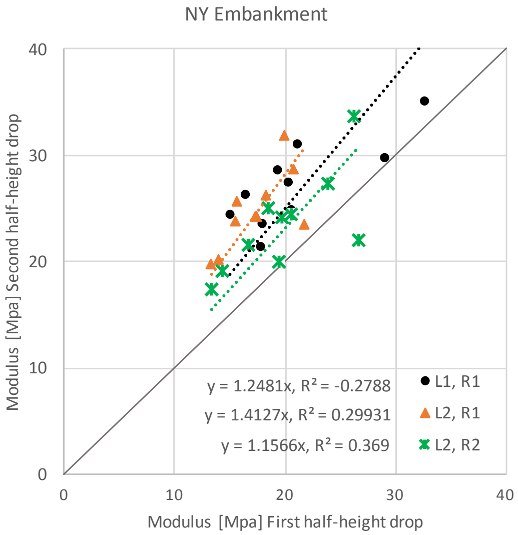
NY Embankment
40
30
20
10
0
0
10
20
30
40
Modulus [Mpa] Second half-height drop
Modulus [Mpa] First half-height drop
y = 1.2481x, R² = -0.2788
y = 1.4127x, R² = 0.29931
y = 1.1566x, R² = 0.369
● L1, R1
▲ L2, R1
✖ L2, R2

D)

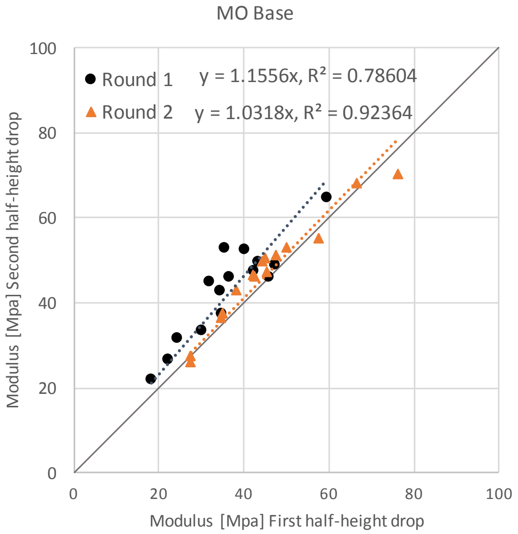
MO Base
100
80
60
40
20
0
0
20
40
60
80
100
Modulus [Mpa] Second half-height drop
Modulus [Mpa] First half-height drop
● Round 1 y = 1.1556x, R² = 0.78604
▲ Round 2 y = 1.0318x, R² = 0.92364

E)

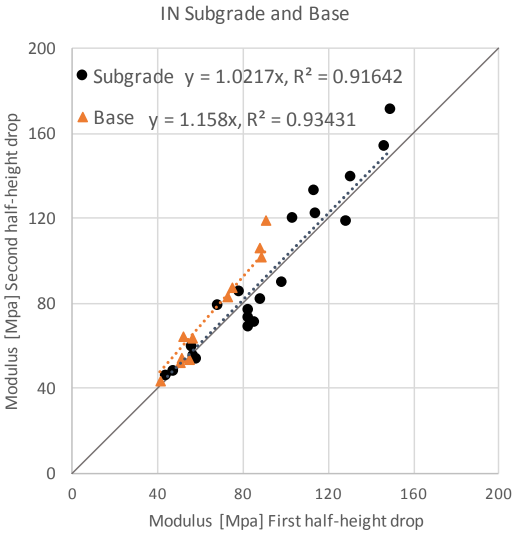
IN Subgrade and Base
200
160
120
80
40
0
0
40
80
120
160
200
Modulus [Mpa] Second half-height drop
Modulus [Mpa] First half-height drop
● Subgrade y = 1.0217x, R² = 0.91642
▲ Base y = 1.158x, R² = 0.93431

F)

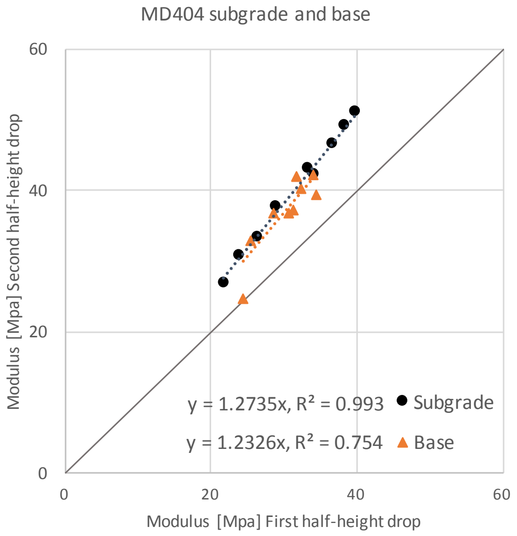

G)

Figure 4-19. Comparison of moduli at first half-height drop and moduli at second half-height drop for Olson LWD.

4.4. Regression Analysis

Table 4-10 to Table 4-14 present the regression coefficient and statistics for evaluated soils in Section 4.6 final report. Target values were then calculated by inputting the field GWC and P/Pa using the coefficients below. Regression statistics tables present the square root of R^2 (Multiple R), the R^2 (R Square), the adjusted R^2 used when more than on variable applied, the sample estimate of the standard deviation of the error as the standard error, and the number of observations used in the regression for each LWD.

Table 4-10. Regression coefficients and statistics for MD 5 subgrade

MD 5 subgrade	Regression Coefficients		
	Zorn LWD	Dynatest LWD	Olson LWD
Intercept	203.96	73.17	210.15
GWC	-269.41	0.00	-219.99
GWC^2	135.45	-84.21	87.27
GWC^3	-29.80	44.30	-13.61
GWC^4	2.94	-7.81	0.72
GWC^5	-0.11	0.45	0.00
P/Pa	9.18	208.41	6.79
P/Pa^2	-0.87	-285.03	1.01
P/Pa^3	0.00	122.00	0.00

MD 5 subgrade	Regression Statistics		
	Zorn LWD	Dynatest LWD	Olson LWD
Multiple R	0.9489	0.7574	0.9866
R Square	0.9003	0.5736	0.9733
Adjusted R Square	0.8798	0.3925	0.9664
Standard Error	4.1649	36.5916	2.7220
Observations	42	30	30

Table 4-11. Regression coefficients and statistics for NY embankment soil

NY Embankment	Regression Coefficients		
	Zorn LWD	Dynatest LWD	Olson LWD
Intercept	53.15	1724.25	-407.05
GWC	-5.48	-57.80	0.00
GWC^2	-0.76	6.98	83.89
GWC^3	0.08	-0.28	-20.81
GWC^4	0.00	0.00	1.88
GWC^5	0.00	0.00	-0.06
P/Pa	20.01	-3476.59	12.57
P/Pa^2	-2.67	2669.25	-2.87
P/Pa^3	0.00	-676.92	0.37

NY Embankment	Regression Statistics		
	Zorn LWD	Dynatest LWD	Olson LWD
Multiple R	0.9362	0.9572	0.8105
R Square	0.8765	0.9163	0.6569
Adjusted R Square	0.8507	0.8777	0.5023
Standard Error	4.1907	4.9758	16.7743
Observations	30	20	30

Table 4-12. Regression coefficients and statistics for MD 337 GAB

MD 337 GAB	Regression Coefficients		
	Zorn LWD	Dynatest LWD	Olson LWD
Intercept	34.72	8.63	343.18
GWC	0.00	0.00	-275.21
GWC^2	-16.42	1.22	79.59
GWC^3	3.52	-0.03	-7.47
GWC^4	0.00	0.00	0.00
GWC^5	0.00	0.00	0.00
P/Pa	48.03	102.28	-1.39
P/Pa^2	-13.27	-75.42	4.82
P/Pa^3	1.54	21.15	-0.33

MD 337 GAB	Regression Statistics		
	Zorn LWD	Dynatest LWD	Olson LWD
Multiple R	0.9598	0.9597	0.9442
R Square	0.9212	0.9209	0.8915
Adjusted R Square	0.8050	0.8047	0.8532
Standard Error	4.6596	3.4683	6.7559
Observations	18	18	24

Table 4-13. Regression coefficients and statistics for MD 404 GAB

MD 404 GAB	Regression Coefficients		
	Zorn LWD	Dynatest LWD	Olson LWD
Intercept	41.66	2064.44	-337.98
GWC	-4.88	1192.86	189.31
GWC^2	0.19	-197.11	-30.35
GWC^3	0.00	10.78	1.60
GWC^4	0.00	0.00	0.00
GWC^5	0.00	0.00	0.00
P/Pa	40.57	-10163.89	-1.54
P/Pa^2	-6.97	7860.82	5.93
P/Pa^3	0.00	-2012.39	-1.35

MD 404 GAB	Regression Statistics		
	Zorn LWD	Dynatest LWD	Olson LWD
Multiple R	0.9829	0.9284	0.5648
R Square	0.9660	0.8619	0.3190
Adjusted R Square	0.9556	0.7982	0.0921
Standard Error	2.2850	26.8883	8.0510
Observations	18	20	25

Table 4-14. Regression coefficients and statistics for FL base material

FL Base	Regression Coefficients	
	Zorn LWD	Dynatest LWD
Intercept	460.80	-2829.00
GWC	0.00	979.38
GWC^2	-11.83	-84.64
GWC^3	0.69	2.36
GWC^4	0.00	0.00
GWC^5	0.00	0.00
P/Pa	102.10	-1866.55
P/Pa^2	-31.29	1677.53
P/Pa^3	0.00	-509.43

FL Base	Regression Statistics	
	Zorn LWD	Dynatest LWD
Multiple R	0.9852	0.9433
R Square	0.9706	0.8899
Adjusted R Square	0.8589	0.8611
Standard Error	4.2806	32.7026
Observations	15	30